



<https://theses.gla.ac.uk/>

Theses Digitisation:

<https://www.gla.ac.uk/myglasgow/research/enlighten/theses/digitisation/>

This is a digitised version of the original print thesis.

Copyright and moral rights for this work are retained by the author

A copy can be downloaded for personal non-commercial research or study,  
without prior permission or charge

This work cannot be reproduced or quoted extensively from without first  
obtaining permission in writing from the author

The content must not be changed in any way or sold commercially in any  
format or medium without the formal permission of the author

When referring to this work, full bibliographic details including the author,  
title, awarding institution and date of the thesis must be given

Enlighten: Theses

<https://theses.gla.ac.uk/>  
[research-enlighten@glasgow.ac.uk](mailto:research-enlighten@glasgow.ac.uk)

FLUX PENETRATION AND A.C. LOSSES  
IN SUPERCONDUCTING NIOBIUM  
AND TANTALUM FILMS

A Thesis

presented to the Faculty of Engineering  
of the University of Glasgow  
for the degree of

Doctor of Philosophy

by

Kenneth A.M. Arton, B.Sc.

May, 1970

ProQuest Number: 10760474

All rights reserved

INFORMATION TO ALL USERS

The quality of this reproduction is dependent upon the quality of the copy submitted.

In the unlikely event that the author did not send a complete manuscript and there are missing pages, these will be noted. Also, if material had to be removed, a note will indicate the deletion.



ProQuest 10760474

Published by ProQuest LLC (2018). Copyright of the Dissertation is held by the Author.

All rights reserved.

This work is protected against unauthorized copying under Title 17, United States Code  
Microform Edition © ProQuest LLC.

ProQuest LLC.  
789 East Eisenhower Parkway  
P.O. Box 1346  
Ann Arbor, MI 48106 – 1346

## ACKNOWLEDGEMENTS

The investigations reported in this thesis were carried out as part of a co-operative research project supported by the Ministry of Technology.

I wish to express my gratitude to Professor J. Lamb for the provision of the excellent research facilities of the Department of Electronics and Electrical Engineering. I am indebted to Mr. P. Hlawiczka for his supervision, advice and encouragement throughout the project. I should like also to thank my colleagues Mr. W. I. Dunn, Mr. I. M. Green, and latterly Mr. M. J. Witcomb, for many fruitful discussions. Thanks are due especially to Mr. M. J. Witcomb for his help in the microscopic examination of film specimens. I am grateful to Mr. W. McGill who assisted with the preparation of many of the films, and to members of the workshop staff for the construction of equipment, in particular Mr. C. Proudfoot who prepared a number of the film substrates.

The Talysurf profile traces were generously provided by the Department of Production Engineering at the University of Strathclyde.

I wish to record my indebtedness to the Science Research Council for the award of a research studentship, and to the Ministry of Technology for providing financial support during the latter

stages of the work.

Finally, I wish to thank my parents, without whose continual support and encouragement this work would not have been completed.

K.A.M.A.

May, 1970.

CONTENTS

Acknowledgements		1	
Summary		v	
List of principal symbols		viii	
CHAPTER	1	<u>Introduction</u>	1
	1.1	Some basic properties of superconductors	2
	1.2	Superconductivity under time varying conditions	9
	1.3	A.C. superconductive properties of niobium	11
	1.4	Relation to a practical cable system	12
CHAPTER	2	<u>Theory of flux penetration into a superconductor</u>	16
	2.1	BCS Theory	16
	2.2	GLAG Theory	18
	2.3	Numerical values of some parameters	29
	2.4	Non-ideal type II superconductivity	30
	2.5	Critical state models	38
CHAPTER	3	<u>Film preparation</u>	47
	3.1	Possible methods of film preparation	47
	3.2	Deposition of tantalum films by evaporation	48
	3.3	Deposition of niobium and tantalum films by sputtering	53
	3.4	Choice of substrate material	62
CHAPTER	4	<u>Some properties of the films</u>	67
	4.1	Film thickness	69
	4.2	Macrodefects and grain size	71
	4.3	Surface topography	79

4.4	Impurities and cold work	81
4.4.1	Cryogenic system	84
4.4.2	Measurement of critical temperature	85
4.4.3	Measurement of upper critical field	89
CHAPTER 5	<u>Flux penetration and losses</u>	93
5.1	Preliminary measurements of screening field of short tantalum cylinders	93
5.2	Flux penetration and losses — experimental methods	96
5.3	The loss measuring system	101
5.4	Penetration waveforms and compensation	107
5.5	Results of loss and flux penetration measurements	112
5.6	Discussion of results	120
CHAPTER 6	<u>Localized flux penetration</u>	126
6.1	Variation of flux penetration with respect to axial direction	126
6.2	Variation of flux penetration with respect to circumferential direction	127
6.3	Non-uniform penetration and macrodefects	133
CHAPTER 7	<u>Discussion and conclusions</u>	138
7.1	Effect of surface on penetration and losses	138
7.2	Surface effects and sputtered films	143
7.3	Relation of results to a practical cable system	147
7.4	Suggestions for further work	148
REFERENCES		152

SUMMARY

The penetration of magnetic flux into superconducting niobium and tantalum films, deposited by sputtering on the inside of cylindrical substrates, has been monitored under conditions of an a.c. magnetic field applied parallel to the film surface. The energy dissipation associated with irreversible flux motion in the film has been measured, and an attempt has been made to explain results on the basis of critical state models.

Niobium and tantalum films were prepared by sputtering with a d.c. glow discharge in an argon atmosphere. A cylindrical geometry was adopted to deposit films on the inner surface of cylindrical substrates, and the gettering action of the sputtered niobium or tantalum was utilized to obtain a pure deposit at the substrate. Films up to 1  $\mu\text{m}$  thick were deposited on quartz cylinders, and films from 3  $\mu\text{m}$  to 25  $\mu\text{m}$  thick were sputtered onto copper or stainless steel. To obtain a measure of purity the critical temperatures of tantalum films have been obtained,  $T_c$  values indicating a gaseous impurity content of typically 0.2 at.%.  $H_{c2}$  has been measured approximately for some thick niobium films, the results indicating kappa values of about 5, corresponding to about 1 at.% of dissolved gaseous impurities.

A 50 Hz a.c. field was applied to one side only of the film cylinders by means of a solenoid positioned co-axially inside, the solenoid being shorter than the cylinder to reduce the effects of field fringing at the ends. Flux penetration into the film was monitored with a pickup coil in close proximity to the film surface in conjunction with a compensation system to remove unwanted pickup. Losses in the film were measured by means of an electronic wattmeter technique. Mean power loss and peak flux penetration for niobium films from 16  $\mu\text{m}$  to 25  $\mu\text{m}$  thick have been obtained at 4.2 K as a function of peak applied field, and comparative measurements have been made on a thick sputtered tantalum film and on a specimen machined from bulk niobium. The results have been compared with other work on a.c. losses in niobium.

It was found that flux penetration and loss results cannot be readily explained by any critical state model. More detailed study of the manner of flux penetration revealed that the magnetic field penetrates preferentially at localized areas on the film surface, and that this behaviour dominates to such an extent that critical state concepts are not applicable. Examination of the films under optical microscope revealed the presence of relatively large scale defects (macrodefects) having a size of the order of several microns and being similar in structure to pinholes. It is concluded that such defects cause localized non-uniform flux penetration by acting as sites for flux line nucleation and penetration into the film.

Causes of macrodefects and means of eliminating them are discussed, and the work has been related to a possible practical superconducting a.c. power cable system.

List of Principal Symbols

In the following list no distinction has been made between scalar and vector quantities. Many of the symbols are more fully defined in the text, and any symbols not included in this list are defined in the text.

b	specimen circumference
B	magnetic induction
c	velocity of light
e	electronic charge
e(t) e <sub>1</sub> e <sub>2</sub>	pickup voltage
E	electric field
f	frequency
F <sub>b</sub> F <sub>m</sub> F <sub>p</sub>	force acting on unit length of flux line
h ( ħ = h/2π )	Planck's constant
H H <sub>0</sub>	magnetic field
H <sub>c</sub> H <sub>co</sub>	thermodynamic critical field
H <sub>c1</sub>	lower critical field
H <sub>c2</sub> H <sub>c3</sub>	upper critical field
ΔH	surface shielding field
J	current density
J <sub>c</sub>	critical current density
k <sub>B</sub>	Boltzmann's constant
<u>l</u>	electronic mean free path
M	magnetization

$n_s$	density of superelectrons
$\bar{P}$	mean power loss per unit surface area
$t$	time
$T$	temperature
$T_c$	critical temperature
$w$	film thickness
$\Delta$	energy gap
$\kappa \quad \kappa_0 \quad \kappa_1 \quad \kappa_2 \quad \kappa_3$	kappa parameter
$\lambda \quad \lambda_L$	penetration depth
$\xi \quad \xi_0$	coherence length
$\phi$	magnetic flux
$\phi_m$	peak magnetic flux
$\phi_0$	magnetic flux quantum
$\Psi$	Ginzburg-Landau order parameter
$\omega$	angular frequency

## CHAPTER 1

### INTRODUCTION

Although the phenomenon of superconductivity was first discovered nearly seventy years ago, it is only in the past twenty years that interest in the effect has flourished. Broadly speaking, there are two aspects of superconductivity which provide motivation for the very intensive research which has been, and still is being, carried out. First is its significance as a physical phenomenon. Apart from superfluidity in liquid helium, it is the only effect known in which quantization occurs on a large scale ; in fact it is macroscopic quantization which gives rise to the unique properties. Superconductivity has therefore been the subject of much fundamental theoretical and experimental work.

The second reason for the interest in superconductivity is its practical significance. A material which can carry current without loss is obviously of great potential in many applications. A great deal of work has gone into developing the possibilities, to such effect that superconducting solenoids and other devices based on superconductivity are now standard equipment in many laboratories, and commercial uses are rapidly becoming feasible. This thesis is chiefly concerned with one aspect of the practical applications,

namely the possibility of developing a superconducting cable for a.c. power transmission. I have confined my studies almost entirely to the a.c. properties of the superconducting material and have not considered any of the many other important aspects of a superconducting cable system.

The thesis is arranged as follows : In this chapter I shall introduce some basic properties of superconductors and explain the reasons for studying particular materials and for carrying out experiments in a particular way. In the next chapter the theory of superconductivity is developed, particular emphasis being placed on the aspects which are most relevant to present work. Chapter 3 describes the preparation of specimens in the form of sputtered films, and experiments to determine some preliminary properties of these are dealt with in chapter 4. Then follows the main experimental work of the project, which is concerned with field screening by, and magnetic flux penetration into, the films when they are subjected to an a.c. magnetic field applied parallel to the film surface. This part of the work and the results are presented in chapter 5. Chapter 6 deals with experiments to determine in more detail the manner of magnetic field penetration into the sputtered layers. Finally, findings are discussed and conclusions are drawn in the last chapter.

### 1.1 Some basic properties of superconductors

This section is a simplified account of some superconductive

phenomena, the theory being developed more fully in chapter 2. It must be kept in mind that statements made here may be subject to certain qualifications which will become clear later. In addition to references quoted at the beginning of chapter 2, the book by Newhouse (1964) provides useful introductory material.

### Critical temperature

The resistivity of a normal metal such as copper decreases with decreasing temperature, tending to reach a residual value as temperature approaches absolute zero. With a superconductor (which in fact includes the majority of elemental metals) the resistivity falls abruptly to zero at a temperature known as the critical temperature,  $T_c$ , which is typically a few degrees above absolute zero. If a small magnetic field is applied to a superconductor below  $T_c$  no magnetic flux penetrates into the body of the specimen, i.e. it behaves as a perfect diamagnet as well as a perfect conductor. Circulating screening currents flow without loss in a thin surface layer to screen the interior from the applied field.

### Critical field

Now consider a superconductor such as tin, which is known as a type I superconductor (the significance of this designation will be explained shortly). It will be assumed that the specimen geometry is such that the presence of the superconducting specimen does not distort an applied magnetic field and thus cause localized

field enhancement, i.e. the demagnetizing factor is zero. An infinitely long cylinder or infinite slab in a parallel magnetic field has zero demagnetizing factor, and such a geometry will be assumed in the discussion that follows. On increasing the magnetic field complete flux exclusion persists until at a certain field, called the critical field,  $H_c$ , superconductivity is destroyed, normal resistivity is restored and flux penetrates completely into the specimen. The critical field is a function of temperature. As illustrated in fig. 1.1 it varies approximately parabolically with temperature, thus

$$H_c \cong H_{c0} \left[ 1 - (T/T_c)^2 \right] \quad (1.1)$$

### Magnetization curve and reversibility

There is no magnetic flux inside a superconductor below  $H_c$ , that is, inside the specimen  $\underline{B} = 0$ . In the c.g.s. system magnetic quantities are related by

$$\underline{B} = \underline{H} + 4 \pi \underline{M}$$

Therefore, for the specimen, below  $H_c$

$$- 4 \pi \underline{M} = \underline{H}$$

Since the specimen is diamagnetic  $\underline{M}$  is negative. A magnetization curve for the tin sample with zero demagnetizing factor can thus be

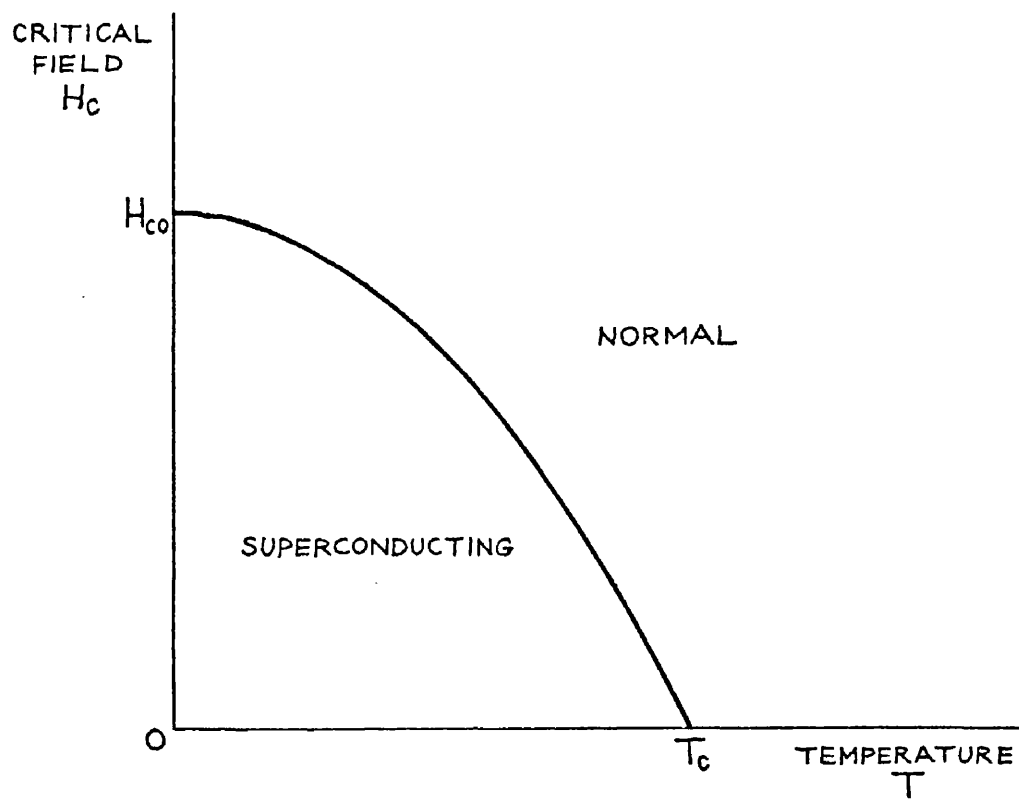


Fig. 1.1 Variation of critical field with temperature.

drawn either as a B-H curve or as an M-H curve as shown in fig. 1.2. In dealing with superconductivity it is generally more convenient to plot specimen magnetization M as a function of field as at (b). The magnetization curve of an ideal specimen is completely reversible, so that when applied field is reduced from a level above  $H_c$  all flux in the specimen is abruptly expelled on passing through  $H_c$ . This is called the Meissner effect. It can be shown thermodynamically (Lynton, 1964) that because the process is reversible the difference between the Gibbs free energy in the normal state and the Gibbs free energy at zero field in the superconducting state is equal to the stored magnetic energy at  $H_c$  due to the exclusion of flux from the specimen. The stored energy per unit volume when the applied field is equal to the critical field is given simply by the area under the magnetization curve, i.e.

$$G_n - G_s(0) = - \int_0^{H_c} \tilde{M} d\tilde{H} = \frac{H_c^2}{8\pi} \quad (1.2)$$

per unit vol.

$H_c$  is therefore referred to as the thermodynamic critical field.

### Penetration depth

When a field less than  $H_c$  is applied to type I material it is not in fact completely excluded, but penetrates a small distance into the surface. To be more precise the field inside a superconductor

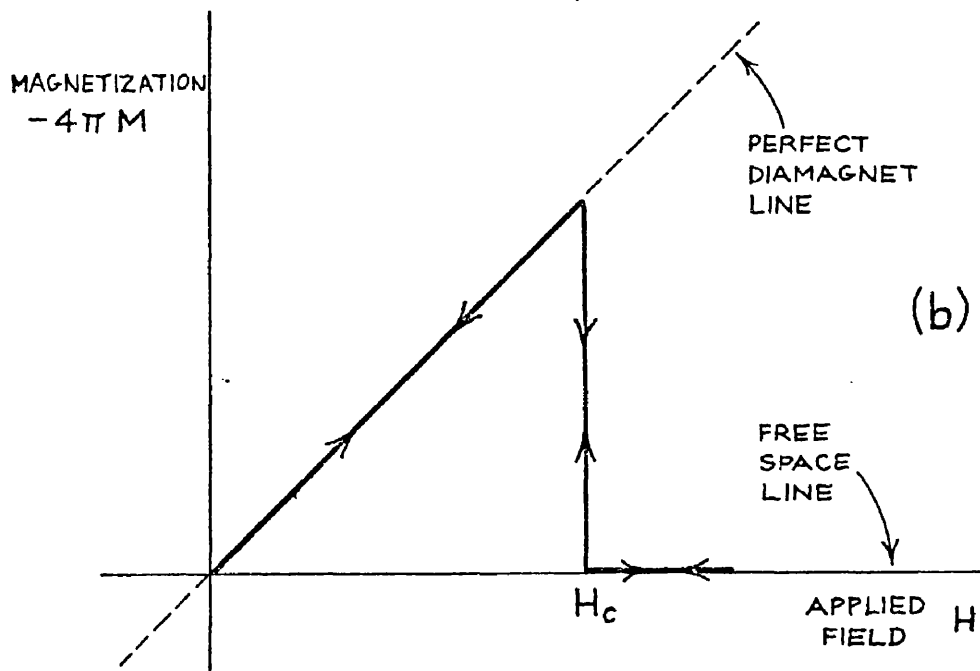
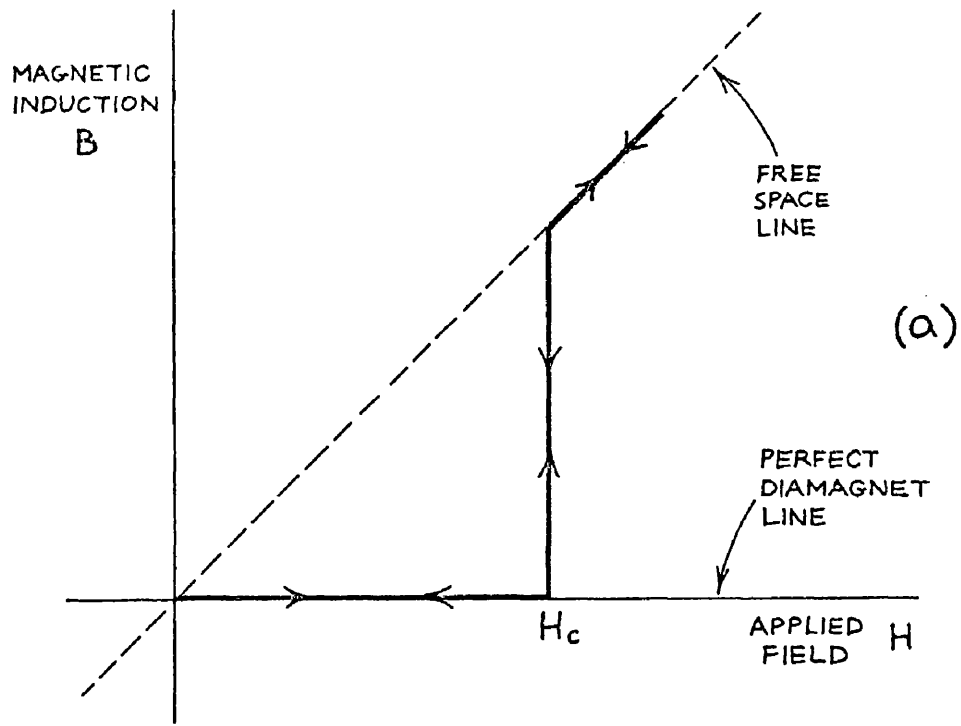


Fig. 1.2 Magnetization curve for an ideal type I superconducting specimen with zero demagnetizing factor.

decays exponentially from its value  $H_0$  at the surface, i.e.

$$\tilde{H}(x) = \tilde{H}_0 \exp(-x/\lambda_L) \quad (1.3)$$

The distance  $\lambda_L$  is known as the London penetration depth, and in a type I superconductor well below  $T_c$  is typically of the order of 100 Å. The penetration depth is a function of temperature, tending to infinity as the temperature approaches  $T_c$ . A formula defining  $\lambda_L$  in terms of basic quantities is given in section 2.2. The circulating currents which screen the interior also decay exponentially with distance in from the surface in the same manner, being related to field by Ampere's Law.

### Type I and type II

All superconductors can be placed in one of two categories. Those which exhibit behaviour of the kind just described are designated type I, this class including most of the elemental superconducting metals. Type I superconductors characteristically have a rather low critical field, e.g. for tin  $H_{c0} = 306$  Oe. There is a second class of superconductors, known as type II, which includes a great many alloys, and whose magnetic properties may differ radically from those of type I. When subjected to a magnetic field a type II superconductor behaves exactly as type I up to a field  $H_{c1}$ , called the lower critical field. Above  $H_{c1}$  flux penetrates into the body of the specimen but superconductivity is not destroyed,

9

persisting instead until the applied field reaches a value  $H_{c2}$ , known as the upper critical field. Beyond  $H_{c2}$  superconductivity is destroyed in the bulk of the specimen, but can persist on the surface to a field  $H_{c3}$ . Like the thermodynamic critical field,  $H_{c1}$ ,  $H_{c2}$  and  $H_{c3}$  vary approximately parabolically with temperature. The upper critical field of some alloys can be very large — 100,000 Oe or even higher.

By suitable metallurgical treatment such alloys can be made to support very high d.c. current densities within their bulk, in contrast with the surface currents which flow in type I materials. Such high-field alloys — sometimes termed "hard" superconductor — are used in the windings of solenoids to generate very high d.c. fields.

## 1.2 Superconductivity under time-varying conditions

Hard superconductors can carry very high d.c. currents without loss, but their dynamic properties are poor. When subjected to time varying fields or transport currents large losses occur, the reason for this being their inherent irreversibility, a concept which will be dealt with fully in chapter 2. Therefore for a.c. applications we are limited to areas where superconductive properties are more or less reversible, which means type I superconductors below  $H_c$  or type II below  $H_{c1}$ . Below  $H_c$  or  $H_{c1}$  losses may still occur

under a.c. conditions, and it is with the investigation of the nature of such losses that this thesis is concerned.

From a practical point of view it is clearly desirable to study the metal which has the highest  $H_c$  or  $H_{c1}$  at the temperature of interest, which for present purposes will be assumed to be 4.2 K, the boiling point of liquid helium at atmospheric pressure. The material which fulfils this criterion is niobium; it is type II, has  $T_c$  of 9.2 K and  $H_{c1}$  of 1400 Oe at 4.2 K. Therefore the majority of studies of a.c. losses in superconductors have been concerned with niobium. In this work I likewise have concentrated chiefly on niobium. I have, however, carried out a limited amount of experimental work on tantalum since it provides useful comparisons, some of the properties of tantalum and niobium being very similar. Tantalum has the advantage that it is easier to deal with from the point of view of experimental work. Because its critical temperature is approximately 4.5 K it is a simple matter to perform experiments over the whole temperature range from  $T_c$  down to about  $0.3 T_c$  in a liquid helium bath, whereas with niobium the temperature range between  $T_c$  and  $\sim 0.5 T_c$  is only accessible with rather complex low temperature equipment. It should be noted that tantalum differs from niobium in one important respect in that, when pure, it is a type I superconductor.

### 1.3 A.C. superconductive properties of niobium

The properties of niobium under a.c. conditions have been studied extensively. A list of references to work on a.c. losses in superconductors in general is given by Seebold (1969). As the superconductive properties of most metals and alloys, and of niobium and tantalum in particular, are very sensitive to metallurgical structure (Livingston and Schadler, 1964), studies have been mainly concerned with the relation between structural factors such as purity, presence of dislocations, etc., and the a.c. loss properties. Much of the work on losses in niobium has been on material in the form of wire with an a.c. transport current. However, as the next section will show, this is not a very realistic experimental technique to adopt if one wishes to apply results to high capacity a.c. cable systems. It is more useful to study losses with an applied a.c. field parallel to the specimen surface instead of an applied transport current ; in this way the experimental arrangement can be made to resemble more closely the geometry of a cable system. Reports of loss measurements on niobium under such conditions are rather limited in number, and much of the work reported uses the technique of superimposing a relatively small a.c. field on a large d.c. field.

The experimental method used here consists of applying an a.c. field only, parallel to the surface of sputtered niobium specimens. The work is an extension of investigations carried out

by Easson and Hlawiczka (1967, 68) on a.c. losses in niobium, and uses some of the measurement techniques which they developed. The results on sputtered niobium are compared with results from Easson and Hlawiczka in chapter 5, and also some limited comparisons are made with work by Rocher and Septfonds (1967) and Buchhold and Rhodenizer (1969) whose experimental methods are sufficiently similar to enable comparisons to be drawn.

#### 1.4 Relation to a practical cable system

Designs for superconducting a.c. transmission cables are invariably based on a symmetrical arrangement of tubes (Cairns et al, 1969). A number of different arrangements are possible, such as a twin tube conductor assembly, or a multi-tube assembly, or an arrangement in which all the conductor tubes are co-axial. The twin tube system is one of the simplest, and is illustrated by the cross-sectional diagram in fig. 1.3. The superconductor takes the form of a layer on the outside of each inner phase conductor tube and on the inside of each outer tube. The current flows only on the surface of the superconducting layers within a depth of the order of the penetration depth  $\lambda$ , and the associated magnetic and electric fields are confined to the annular space between inner and outer tubes. It follows that the superconducting current carrying layer need not be more than a few penetration depths in thickness.

An experimental arrangement which is reasonably representative

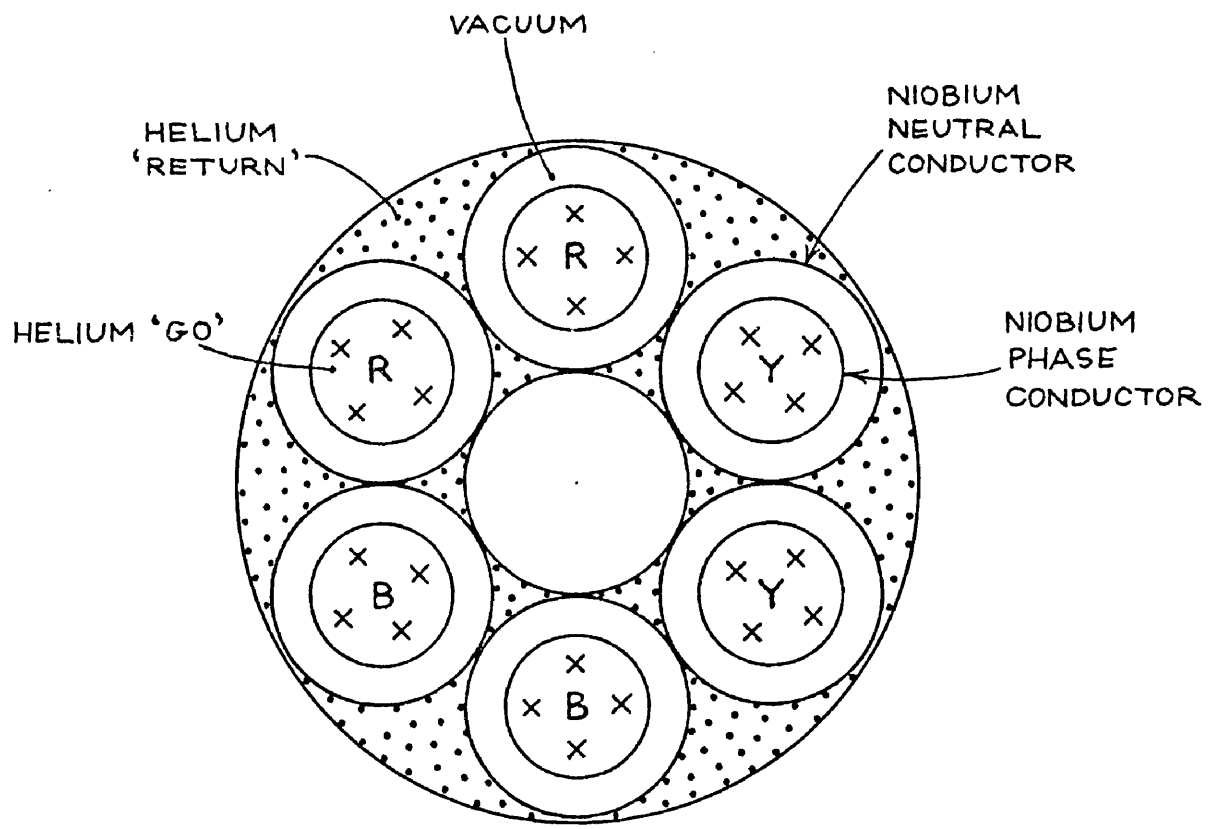


Fig. 1.3 Twin tube conductor assembly for a superconducting cable.  
(From Cairns et al, 1969)

of conditions in a cable should consist of a thin layer of niobium with an a.c. field applied parallel to one side only of the layer, and without end effects which would cause unwanted field distortion. Such a set-up can be achieved by using either of the cylindrical geometries shown in fig. 1.4. As long as the solenoid is shorter than the film cylinder the degree of field fringing round the ends of the cylinder will be small, and can be arranged not to interfere with measurements. The system at (b) in the figure was the one used for work presented in this thesis, the geometry being dictated (as will be explained in chapter 3) by the method of film preparation. Niobium layers were deposited by sputtering and all investigations were made with a.c. field only at 50 Hz.

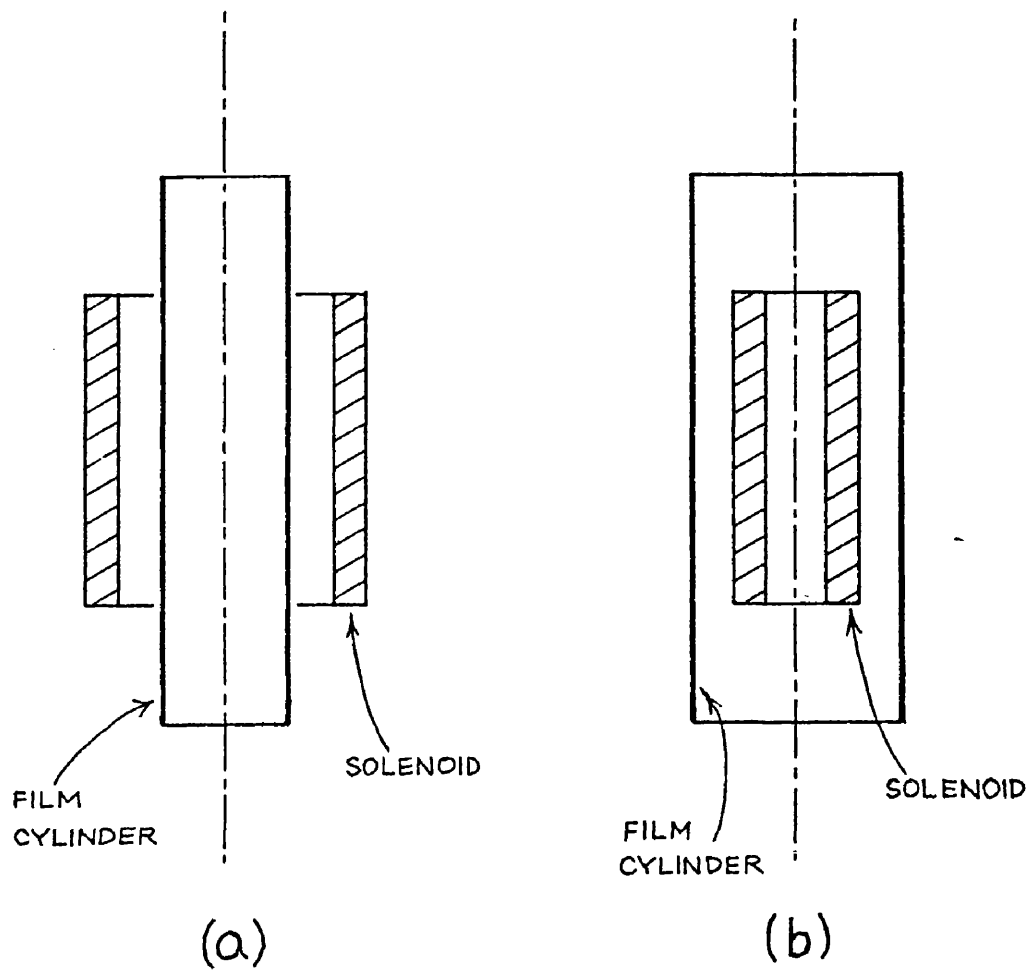


Fig. 1.4 Arrangements to apply a.c. field to one side of superconducting film.

## CHAPTER 2

### THEORY OF FLUX PENETRATION INTO A SUPERCONDUCTOR

This chapter deals in some detail with the processes by which flux penetrates into and moves within a superconductor. The BCS theory is considered briefly, followed by a more detailed explanation of GLAG theory, which gives an adequate description of properties of ideal materials. This section follows mainly the books of de Gennes (1966), Lynton (1964) and reviews by Lowell (1965) and Livingston and Schadler (1964). A particularly comprehensive recent work is that edited by Parks (1969) of which chapters 6 and 14 are relevant to GLAG theory. Very few references have been quoted in sections 2.1 and 2.2 as original papers are listed fully in the above textbooks and reviews. Non-ideal behaviour is dealt with in section 2.4, leading on to critical state models in section 2.5. References in sections 2.4 and 2.5 are given more fully, although the review by Livingston and Schadler and chapter 19 from Parks contain very comprehensive lists of references on non-ideal properties.

#### 2.1 BCS Theory

In 1957 Bardeen, Cooper and Schrieffer developed a microscopic theory of superconductivity which became known as the BCS theory. According to this theory the wavefunctions of two electrons in a superconductor can become coupled via the interaction

of electrons with lattice vibrations (phonons). The coupling of electron wavefunctions is equivalent to an attractive force which binds the electrons together in pairs, known as Cooper pairs. To break up a correlated electron pair requires a finite energy, and there is therefore an energy gap between Cooper pairs (which are said to be in a condensed energy state) and normal electrons. The electrons in a Cooper pair behave as a single particle which cannot transfer any energy to the lattice unless it exceeds the binding energy of a pair. The pair must move through the lattice in a loss-free manner, thus carrying current without resistance.

The binding energy, or energy gap,  $\Delta$ , is given by  $\Delta = 3.52 k_B T_c$ . Gor'kov (1959) has shown that the energy gap is proportional to the G-L order parameter  $\Psi$ , introduced below. The distance of separation between two electrons in a Cooper pair can be quite large, of the order of several hundred atomic spacings, this distance being termed the coherence length. The BCS coherence length is given by

$$\xi_0 = \frac{2 \hbar V_0}{\pi} \quad (2.1)$$

where  $V_0$  is mean electron velocity at the Fermi level.

This thesis is concerned chiefly with the magnetic properties of superconductors for which the BCS theory does not provide a convenient approach. We will therefore not pursue the BCS theory further, but turn our attention instead to a simpler theory which still

gives an adequate description of all the important properties of ideal superconductors.

## 2.2 GLAG Theory

In 1950 Ginzburg and Landau introduced a phenomenological theory which allowed for spatial variations in the order parameter or superconducting electron density. Gor'kov (1959) has shown that the G-L theory can be derived from BCS theory, (it is therefore no longer strictly phenomenological), and in 1957 Abrikosov determined the detailed form of flux penetration in a type II superconductor from analysis of the G-L equations. The Ginzburg-Landau-Abrikosov-Gor'kov theory will be outlined briefly.

### G-L equations

According to G-L theory the free energy of a superconductor close to  $T_c$  is given by

$$F = F_n + \alpha |\psi|^2 + \frac{\beta}{2} |\psi|^4 + \frac{1}{2m^*} \left| \left( -j \hbar \nabla - \frac{e^* \mathbf{A}}{c} \right) \psi \right|^2 + \frac{\hbar^2}{8\pi} \quad (2.2)$$

where  $F_n$  is free energy in the normal state,

$\psi(r)$  is the complex order parameter, which has the physical significance that when normalised

$|\psi|^2 = n_s$ , the density of superconducting electrons,

$e^*$  is the effective charge, equal to  $2e$ ,

$\hbar$  is the microscopic magnetic field,

$\alpha$ ,  $\beta$  and  $m^*$  are phenomenological constants.

Any system tends to adopt a state of minimum free energy ; we therefore minimize the above expression for free energy with respect to the spatial distribution of order parameter and magnetic field. On so doing we obtain the conditions

$$\alpha\psi + \beta\psi|\psi|^2 + \frac{1}{2m^*} \left( -j\hbar\nabla - \frac{2e\mathbf{A}}{c} \right)^2 \psi = 0 \quad (2.3)$$

$$\mathbf{J} = - \frac{e\hbar}{jm^*} (\psi^* \nabla \psi - \psi \nabla \psi^*) - \frac{4e^2}{m^*c} \psi^* \psi \mathbf{A} \quad (2.4)$$

These are the fundamental G-L equations. The first gives the order parameter or superconducting electron density, and the second gives the current or magnetic field, as a function of position.

### Characteristic lengths

On solution of equations 2.3 and 2.4 we find each has associated with it a characteristic length. The characteristic length associated with equation 2.3 is called the coherence length,  $\xi$ , and defines the distance over which the order parameter decays from the boundary of a superconducting region. It is also the typical separation of the two electrons in a Cooper pair. In a pure metal at zero temperature the G-L coherence length equals the BCS value, being given in terms of basic parameters by

$$\xi_0 = \frac{0.18\hbar v_0}{k_B T_c} \quad (2.5)$$

$\xi_0$  is of the order of 50-1000 Å.

Similarly upon solution of equation 2.4 we find a characteristic length which defines the distance from a N-S boundary over which magnetic field decays to zero. This distance, called the penetration depth, is the same as the distance of field penetration into a type I superconductor according to London's theory. The London penetration depth at 0 K is

$$\lambda_L(0) = \left[ \frac{mc^2}{4\pi n_s(0)e} \right]^{\frac{1}{2}} \quad (2.6)$$

Both  $\xi$  and  $\lambda$  are temperature dependent, but their ratio is approximately temperature independent. This ratio defines a dimensionless quantity known as the G-L kappa parameter,

$$\kappa = \frac{\lambda}{\xi} \quad (2.7)$$

### Superconducting - Normal interface

Consider now the boundary between a superconducting and a normal phase within some material. In the superconducting region the order parameter or density of superelectrons will have some finite value  $n_s$  and the field will be zero, while in the normal region the order parameter will be zero and the magnetic field will equal the thermodynamic critical field  $H_c$ . Fig. 2.1 shows the variation of order parameter and field along a line perpendicular to the phase boundary for the case of  $\kappa \ll 1$  and  $\kappa \gg 1$ . There is a certain surface energy

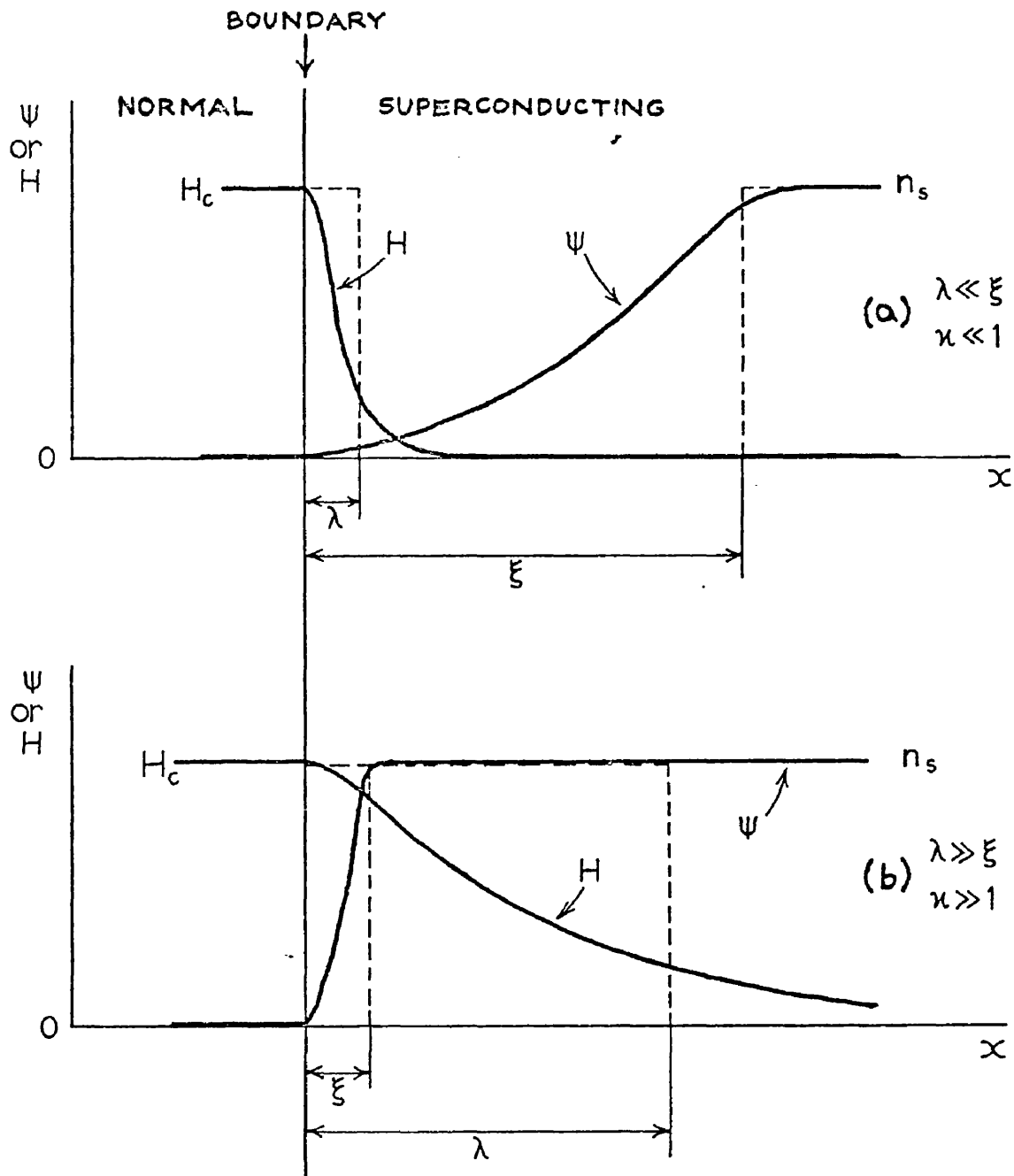


Fig. 2.1 Variation of field and order parameter at a superconducting-normal phase boundary.

associated with the phase boundary. Both magnetic field and superelectron pairs in the boundary region contribute to this energy, the contribution from each being given roughly by the area under the field curve within the boundary region, as indicated by broken lines in the figure. In the case  $\kappa \ll 1$  the surface energy is  $\sim \xi H_c^2 / 8\pi$  per unit area, and is positive; for  $\kappa \gg 1$  the surface energy is  $\sim \lambda H_c^2 / 8\pi$  per unit area, and is negative. Whether the S-N boundary energy is positive or negative is critical in determining how the material behaves.

Let us first look at the situation when  $\kappa \ll 1$ . Because the boundary energy is positive it is energetically unfavourable for there to be a S-N interface within the bulk of the material at any field below  $H_c$  (zero demagnetizing factor being assumed), therefore complete flux exclusion occurs right up to  $H_c$ . The material is driven completely normal when the applied field exceeds  $H_c$ . This is type I behaviour. However, when  $\kappa \gg 1$  the boundary energy is negative. In this case the free energy is minimized by flux entering the bulk of the material when applied field exceeds a critical value which is lower than  $H_c$ . This is type II behaviour. It is found that the precise value of  $\kappa$  which determines the change-over from type I to type II behaviour is

$$\kappa = 1/\sqrt{2}. \quad \text{Hence}$$

$$\kappa < 1/\sqrt{2} \quad - \quad \text{type I}$$

$$\kappa > 1/\sqrt{2} \quad - \quad \text{type II}$$

For the moment I shall only discuss type II superconductivity.

### Ideal type II superconductivity

A detailed solution of the G-L equations in the case  $\kappa > 1/\sqrt{2}$  was first carried out by Abrikosov(1957). He shows that the magnetization curve for an ideal type II superconductor is as shown by the solid curve in fig. 2.2. At low applied fields there is complete flux exclusion, the material behaving as type I. At some field  $H_{c1}$ , the lower critical field, it becomes energetically favourable for flux to penetrate the bulk in order to establish S-N interfaces within the material. Flux penetration takes place in the form of flux lines or vortices which are threads or tubes of normal phase with their axes parallel to the field and surrounded by circulating screening currents. Superconductivity is not destroyed at  $H_{c1}$  but persists to an upper critical field  $H_{c2}$  which is greater than  $H_c$ . The region between  $H_{c1}$  and  $H_{c2}$  where vortices are present is known as the mixed state. The area under the curve defines the thermodynamic critical field  $H_c$  as the critical field of a type I M-H curve having the same area, as shown by broken lines, i.e.

$$\frac{H_c^2}{8\pi} = - \int_0^{H_{c2}} M dH \quad (2.8)$$

### Flux lines

A flux line or vortex consists of a core of normal material with a radius of the order of the coherence length, surrounded by circulating currents which screen the rest of the superconductor from the field

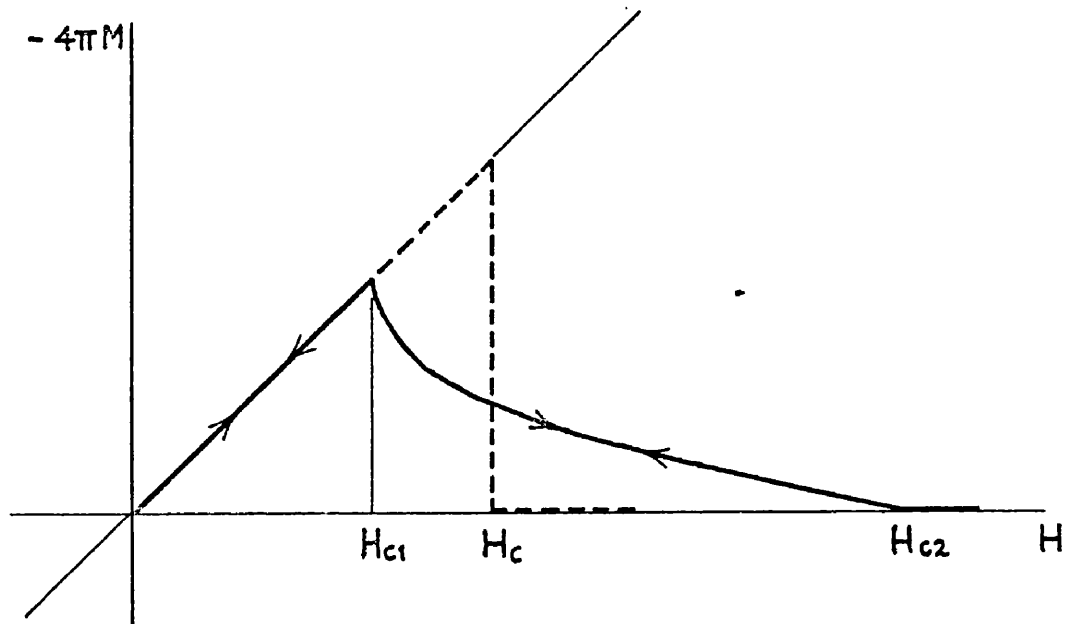


Fig. 2.2 Ideal type.II magnetization curve.

in the core. The field or screening current extends to a radius of the order of the penetration depth. Fig. 2.3 illustrates the variation of order parameter and field along a diameter of a flux line. In order that the free energy is minimized the system of flux lines will tend to maximize the S-N surface area, hence each line will carry the minimum possible amount of flux. Now it is known from theory and experiment that the flux enclosed by a superconducting ring must take on discrete values  $\phi = n \phi_0$ , where  $n$  is an integer and  $\phi_0$  is given by

$$\phi_0 = \frac{ch}{2e} = 2 \times 10^{-7} \text{ Maxwell.}$$

So each flux line carries one quantum of flux,  $\phi_0$ .

At low applied fields, just above  $H_{c1}$ , the flux lines are widely spaced, the spacing decreasing as field is increased. The upper critical field  $H_{c2}$  is determined by the point at which vortices are so close together that the cores begin to overlap. Under equilibrium conditions in the mixed state flux lines arrange themselves in a uniform triangular lattice.

#### Some formulae defining the magnetization curve

The lower critical field, the upper critical field and the slope of the M-H curve at  $H_{c2}$  can all be expressed, for an ideal specimen, in terms of  $\kappa$  and  $H_c$  as follows :

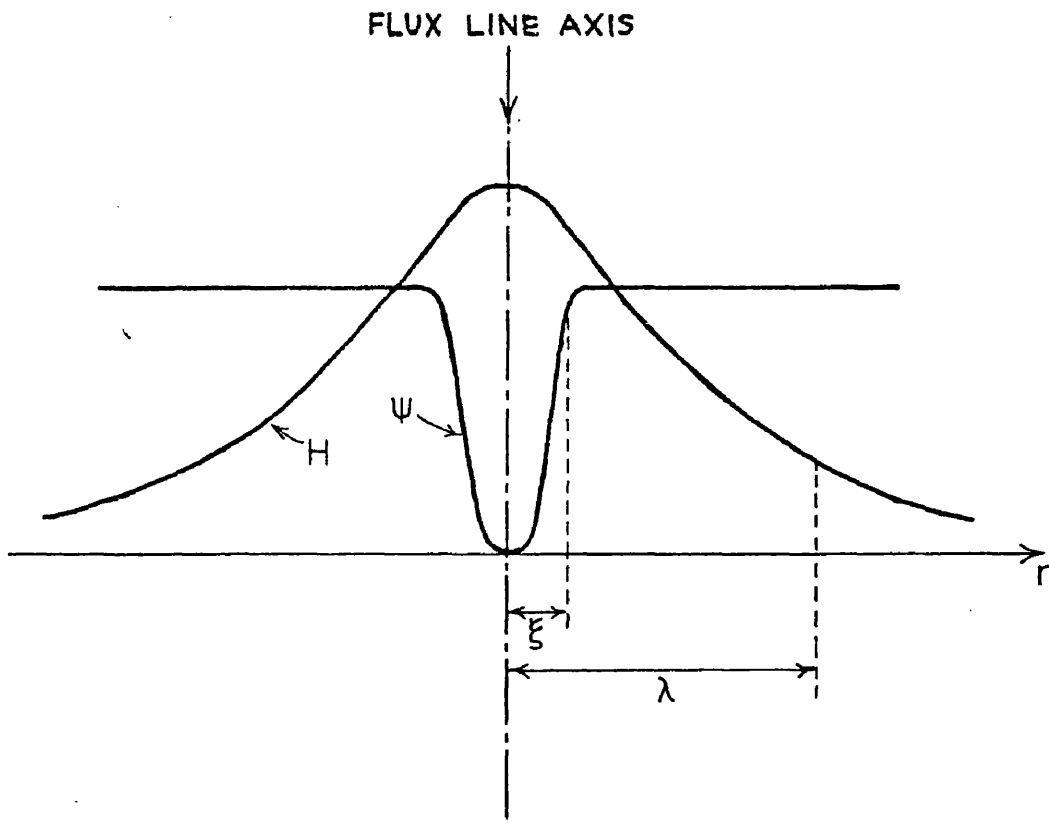


Fig. 2.3 Structure of a flux line.

$$H_{c1} = \frac{H_c}{\sqrt{2\kappa}} (\ln \kappa + 0.08) \quad (\text{only for } \kappa \gg 1) \quad (2.9)$$

$$H_{c2} = \sqrt{2\kappa} H_c \quad (2.10)$$

$$4\pi \left[ \frac{dM}{dH} \right]_{H=H_{c2}} = \frac{1}{1.16(2\kappa^2 - 1)} \quad (2.11)$$

The G-L theory outlined above is applicable only near the critical temperature. If the theory is extended to take into account slight variation of  $\kappa$  with temperature it is found that the values of  $\kappa$  defined by the above three equations are not in general identical. It is therefore necessary to introduce three kappa parameters (known as Maki parameters),  $\kappa_1, \kappa_2, \kappa_3$ , all of which are functions of temperature. (Maki, 1964,66). These are defined respectively by equations 2.10, 2.11 and 2.9. At the critical temperature

$$\kappa_1 = \kappa_2 = \kappa_3 = \kappa = 0.96 \frac{\lambda_L(0)}{\xi_0}$$

In chapter 4 measured values of  $H_{c2}$  for sputtered niobium and tantalum will be used in conjunction with the above equations (equation 2.9 being modified to allow for low kappa) to derive values of  $H_{c1}$ .

#### The effect of electronic mean free path

The properties of all type II superconductors are critically dependent on metallurgical structure, both macroscopic and microscopic.

Some of the effects of microstructure are expressed through the mean free path,  $\underline{l}$ , of electrons in the normal state. The effect of m.f.p. is taken into account by considering how it influences the coherence length, the penetration depth and thus the  $\kappa$  value. Reducing m.f.p. results in decreased  $\xi$ , in increased  $\lambda$ , and therefore in increased  $\kappa$  (Livingston and Schadler, 1964). This can be expressed quantitatively in the limit of  $\underline{l} \ll \xi_0$  thus

$$\xi = \sqrt{(\xi_0 \underline{l})} \quad (2.12)$$

$$\lambda = \lambda_L \sqrt{(\xi_0 / \underline{l})} \quad (2.13)$$

$$\kappa = \kappa_0 \lambda_L / \underline{l} \quad (2.14)$$

where  $\kappa_0$  is the value for  $\underline{l} \gg \xi_0$

For a given material reducing the m.f.p., e.g. by introducing scattering centres in some form, results in increased  $\kappa$  and thus in a lower value of  $H_{c1}$ . As will be explained more fully in chapter 4 it is particularly important to consider this when dealing with niobium. Note that scattering centres which limit m.f.p. should not be confused with the flux line pinning centres which will be discussed below. A material with short m.f.p. can show ideal type II behaviour.

### Surface superconductivity

The G-L equations 2.3 and 2.4 take no account of boundary conditions which may be present at the surface of a superconductor. Solutions of the G-L equations which allowed for special conditions at the surface were first derived by St.-James and de Gennes (1963), who showed that superconductivity should persist on a thin surface

layer for applied field in excess of  $H_{c2}$ . They found that superconductivity should persist on a surface parallel to the applied field up to a field  $H_{c3}$  where  $H_{c3} = 1.69 H_{c2}$ .  $H_{c3}$  depends on the angle between field and surface, falling from  $1.69 H_{c2}$  for field parallel to surface, to  $H_{c2}$  when field is at right angles to the surface. The superconducting layer above  $H_{c2}$ , termed a surface sheath, has a thickness of the order of the coherence length and can carry appreciable transport current. The surface sheath may also be present in the mixed state when it can have a significant effect on the hysteretic behaviour of non-ideal material. Surface superconductivity is destroyed when a superconductor is plated with a normal metal.

### 2.3 Numerical values of some parameters

To put the above theory into perspective I have listed in Table 2.1 numerical values of the basic parameters for pure, defect-free niobium and tantalum. The figures for niobium are from experimental work by French (1968) and those for tantalum are based on experiments by McEvoy et al (1969), except for the value of  $H_{c0}$  which is from Budnick (1960).

	$T_c$	$\xi_0$	$\lambda_L(0)$	$\kappa_0$	$H_{c0}$
	(K)	(Å)	(Å)		(Oe)
Niobium (type II)	9.20	390	330	0.82	1980
Tantalum (type I)	4.482	925	330	0.34	830

Table 2.1

Also, from French (1968) for niobium at 4.14 K:

$$H_{c1} = 1460 \text{ Oe}, \quad H_c = 1550 \text{ Oe}, \quad H_{c2} = 2670 \text{ Oe}, \quad H_{c3} = 4520 \text{ Oe}.$$

#### 2.4 Non-ideal type II superconductivity

The GLAG theory is based on the minimization of free energy, which means that the superconducting system must always be in a state of equilibrium. This implies that magnetization curves are reversible and that there is no energy dissipation associated with any process ; materials which behave this way are described as ideal superconductors. I shall now consider non-ideal properties. Non-equilibrium behaviour can manifest itself in two ways : (a) An ideal superconductor can show non-ideal properties if there is not sufficient time for it to attain its equilibrium state. In this case energy dissipation occurs due to the viscous motion of flux lines or S-N phase boundaries through the specimen. (b) A superconductor will be non-ideal if inhomogeneities are present which have a size of the order of or larger than the coherence length. Such inhomogeneities may act as "pinning centres" which inhibit the motion of flux lines, thus enabling a flux line gradient to be established. These two effects will first be discussed separately, although in general they both contribute to non-ideal behaviour.

##### Viscous flow of flux lines

Many theories of flux motion in ideal type II material have been developed with varying degrees of success. Among some of the more useful studies are those of van Vijfeijken and Niessen (1965),

Bardeen and Stephen (1965) and Tinkham (1964). These, and other work on flux line motion, are reviewed in a paper by Vinen and Warren (1967).

Consider an ideal type II superconductor in the mixed state and subjected to a steadily increasing applied field. As flux lines penetrate from the surface they set up a flux line gradient or magnetic pressure due to the finite speed at which they move. The magnetic pressure tends to push further in flux lines which are already in the bulk. A line will experience a force which is proportional to the gradient of flux line density. Friedel et al (1963) has shown that the force acting on one flux line is

$$F_m = - \frac{\phi_0}{4\pi} \cdot \frac{\partial}{\partial x} H(B) \quad \text{per unit length} \quad (2.15)$$

This equation applies to a simple slab geometry where  $x$  is distance normal to the slab surface and field is in the  $z$ -direction.  $H(B)$  is the applied external field which would produce induction  $B$  under equilibrium conditions. According to Bardeen and Stephen (1965) the vortex motion which the field gradient causes is accompanied by an electric field which is large in the region of the normal core and gives rise to a normal current through the core. Therefore when a flux line moves dissipation occurs and the line experiences a force tending to oppose its motion. This force is a viscous force, being proportional to the vortex velocity (Tinkham, 1964); the line will therefore tend to reach a velocity such that viscous drag balances the driving force  $F_m$  defined above. Dissipation in the mixed state of

an ideal material is clearly dependent on rate of change of field.

It is helpful to look at the effect of viscous flow of vortices on an ideal type II M-H curve (fig. 2.4 a). The solid line is the ideal magnetization curve which is followed when rate of change of field is very low. If the applied field is swept up and down at a constant rate which is comparable with or greater than the relaxation time associated with viscous vortex flow, then magnetization will follow a path something like that shown by broken lines, i.e. hysteresis appears. As with all hysteretic processes the energy dissipated in one cycle is given by loop area, regardless of the actual mechanism of dissipation.

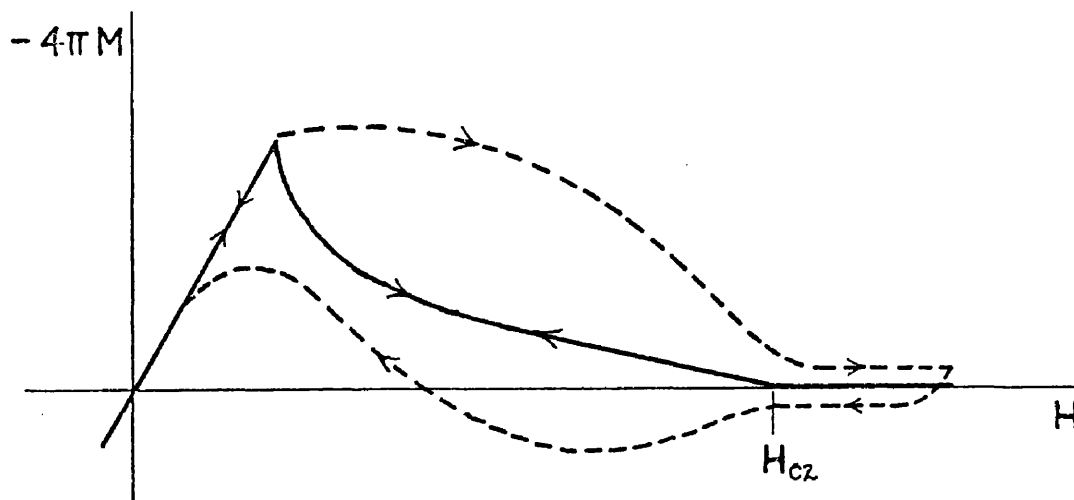
The presence of a flux line density gradient implies the existence of a macroscopic current density in accordance with Ampere's Law :

$$4\pi \underline{J} = \underline{\nabla} \cdot \underline{x} \quad \underline{H} \quad \text{in c.g.s. units.}$$

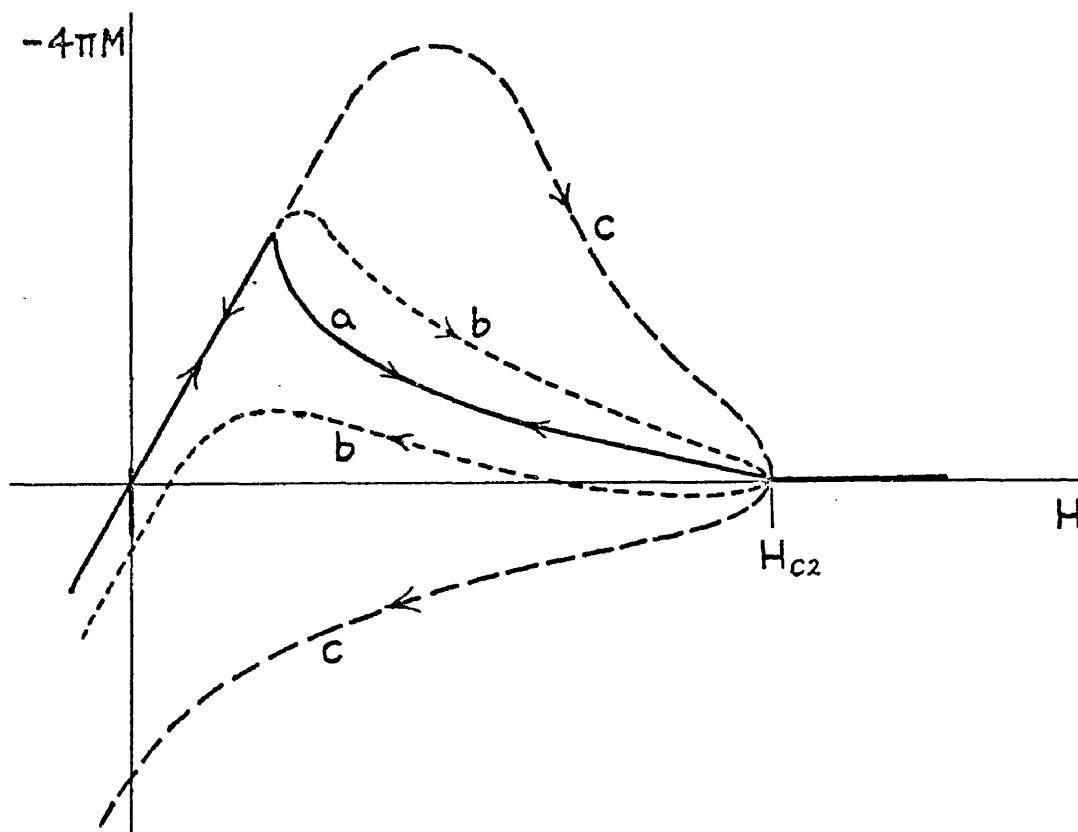
For the one dimensional case of a slab

$$J(x) = \frac{1}{4\pi} \cdot \frac{\partial H}{\partial x} \quad (2.16)$$

The converse also applies, namely, an ideal superconductor in the mixed state cannot carry a bulk transport current without dissipation, since the presence of a current requires a flux line gradient, hence viscous flux line motion and energy loss. It should be noted that the motion of a S-N phase boundary in a type I material is subject to similar viscous flow, which in this case can be pictured as due to eddy currents in the normal phase.



- (a) Effect of viscous flow of flux lines on ideal type II magnetization curve when field is swept up and down at constant rate.



- (b) Effect of pinning of flux lines on type II magnetization curve (static); (a) defect free, (b) cold worked, (c) severely cold worked.

Fig. 2.4 Non-ideal behaviour in type II superconductors.

### Flux pinning

So far it has been assumed that flux lines can move relatively freely through a specimen. In the vast majority of practical type II superconductors this is not so. Structural defects, through local changes in superconducting parameters, produce localized areas where flux lines may have higher or lower free energy, and so can cause flux lines to become "pinned" at the defect. When a flux line is pinned it is in a local free energy minimum. Among defects which may cause pinning are lattice vacancies, interstitial impurities, dislocations and grain boundaries. The effectiveness of a defect as a pinning centre depends, among other factors, on its spatial extent, and in this respect it should be noted that defects which cause superconducting parameter fluctuations on a scale much smaller than a coherence length will not act as pinning sites (Livingston and Schadler, 1964). The most significant defects are dislocations, especially in groups, and large clusters of a second phase. The degree of cold work of a specimen is thus critical in determining its behaviour in the mixed state. This is illustrated in fig. 2.4(b) which shows the effects of cold work on the magnetization curve of an originally defect free specimen. The non-ideal curves B and C in this case are static M-H loops. Again loop area gives the loss per cycle.

A great deal of work has been reported in the literature on different types of pinning centres with the associated parameter variations and pinning forces. Recent theories by Japanese groups

(Irie and Yamafuji 1967 , Kusayanagi and Yamafuji 1969, and others ) are possibly the most comprehensive and useful studies to date. Nevertheless, the mechanism of flux pinning is still not properly understood.

### Flux creep and the critical state

As mentioned above, when a gradient of flux line density is established in the mixed state between  $H_{c1}$  and  $H_{c2}$  then a flux thread experiences a force given by Friedel's equation (2.15). Suppose now that the flux line is pinned. At absolute zero the line cannot be unpinned until the force  $F_m$  is sufficient to overcome the pinning force  $F_p$  ; therefore the condition  $F_m = F_p$  defines a static critical flux gradient

$$\left| \frac{\partial}{\partial x} H(B) \right| = \frac{4\pi}{\phi_0} F_m = \frac{4\pi}{\phi_0} F_p \quad (2.17)$$

$F_p$  is pinning force per unit length of one line. If a time varying field is applied flux lines will move in such a way as to maintain the critical gradient everywhere within the specimen.

However, this account is an over-simplification. The critical flux gradient is not, in fact, static, except perhaps at zero temperature. At a finite temperature thermal activation may unpin a flux line when  $F_m < F_p$  by raising it above the local energy barrier. This phenomenon, termed flux creep, was first proposed, analysed and studied experimentally by Anderson (1962), Anderson and Kim (1964), Kim et al (1962, 63, 64, 65). These authors show, first, that local perturbations of flux line density are very unfavourable

energetically and that lines therefore become pinned and move as groups having a size of the order of the penetration depth, such a group being described as a "flux bundle". Fig. 2.5, from Kim et al (1963b) illustrates how thermal activation can unpin a flux bundle. The figure shows the spatial variation of free energy with flux bundles situated at minima associated with pinning centres, and subjected to a flux density gradient. A flux bundle will move if thermal activation is sufficient to overcome the barrier  $F_b$ .  $F_b$  is directly related to  $F_p - F_m$ , and it can be shown by statistical analysis that the rate of motion of flux is proportional to  $\exp(-F_b/k_B T)$ .

According to flux creep theory the flux gradient will decay logarithmically with time, and this has in fact been observed by Kim et al (1963). The term "flux creep" is generally used to describe the very slow decay of gradient which continues once a more-or-less stable gradient has been established. As long as the time scale of the process being studied is short compared with the rate of decay due to flux creep (as is certainly the case at 50 Hz), we are justified in assuming the gradient to be critical.

The current flow which maintains a critical flux gradient is called the critical current,  $J_c$ . A superconductor in which flux gradients and currents within the bulk are maintained by the mechanism of flux pinning is said to be in the critical state.

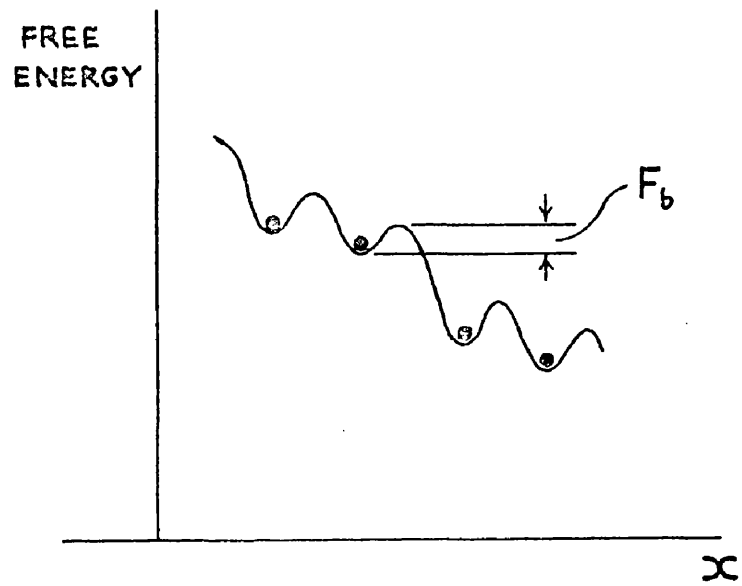


Fig. 2.5 Flux bundles pinned at free energy minima, illustrating flux creep.

## 2.5 Critical state models

The critical state can be a very useful concept for analysing the behaviour of "hard" superconductors, a hard superconductor being one in which flux pinning causes extreme irreversibility. For this purpose it must be embodied in a critical state model. It is first necessary to define the effective pinning force  $F_p$  and its variation with magnetic field ;  $F_p$  is taken to be the pinning force which maintains the flux gradient after flux creep has reached a stage where it is negligible. In all that follows the geometry is that of a semi-infinite superconductor with surface on the  $y - z$  plane at  $x = 0$ , and field parallel to the surface in the  $z$ -direction. Therefore current flows in the  $y$ -direction, pinning forces act in the  $x$ -direction and quantities vary only in the  $x$ -direction.

Now in general the pinning force is a function of the local magnetic field, i.e.  $F_p = f(H)$ . From equation 2.17 flux gradient is related to pinning force by

$$\left| \frac{\partial}{\partial x} H(B) \right| = \frac{4\pi}{\phi_0} F_p.$$

$H(B)$  is the applied field which causes induction  $B$  under equilibrium conditions. We now make the approximation that local field gradient  $\partial H(x)/\partial x$  equals  $\partial H(B)/\partial x$ ; the difference is a factor  $\partial H(B)/\partial B$ , so the approximation is valid except near  $H_{c1}$  (Friedel et al, 1963). By Ampère's law the local field is related to local current density by

$$\frac{\partial H}{\partial x} = 4\pi J$$

$$\text{Hence } |J| = \frac{F_p}{\phi_0} = \frac{f(H)}{\phi_0} . \quad (2.18)$$

So the critical current density and pinning force are both related to local field in the same manner. Defining critical current density,  $J_c$ , as a function of field is equivalent to defining the variation of  $F_p$  with field.

In all critical state models to date no serious attempt has been made to relate the variation of  $F_p$  with field to forces which pin a flux line, since the mechanism of pinning is not yet sufficiently well understood. Rather, the various proposed functions  $F_p(H)$  (or  $J_c(H)$ ) are purely empirical in that they are chosen to give models which agree with experiments. Once a form has been chosen for  $J_c(H)$  one can proceed to evaluate the distribution of flux and its density gradient within the specimen, and the total flux penetration and associated energy dissipation.

One of the first models was proposed by London (1963) and Bean (1964) who assume  $J_c$  to be independent of field. The Bean-London model therefore gives constant flux gradient within the superconductor. The Kim-Anderson model (Kim et al 1962, 63a, Anderson 1962) assumes a relationship  $J_c = \alpha/(H + H_0)$  where  $\alpha$  and  $H_0$  are constants. A generalized critical state model was then proposed by Green and Hlawiczka (1967) in which critical current is defined by the more general expression

$$J_c = \alpha |H|^n \quad \text{where } \alpha \text{ is a constant.}$$

This model has the advantage that it embodies both the Bean-London model ( $n = 0$ ) and a simplified version of the Kim-Anderson model ( $n = -1$ ). Fig. 2.6(a, b) shows the form of flux distribution inside the superconductor for  $n = 0$  and  $n = -1$  when a field  $H_0$  is applied at the surface.

#### Effect of $H_{c1}$ and surface sheath

These models have the serious shortcoming that they take no account of the lower critical field and of surface screening currents which flow in the surface sheath. Neglecting  $H_{c1}$  limits the experimental situations to which a model can be applied since it is a valid approximation only for applied fields much greater than  $H_{c1}$ . The presence of a surface sheath is important because it can have considerable effect on hysteretic properties through flux trapping. An extension of the generalized model, allowing for both  $H_{c1}$  and surface screening,  $\Delta H$ , has recently been proposed by Dunn and Hlawiczka (1968). Fig. 2.6(c) illustrates the predicted form of flux penetration. Their model is based on a hysteresis loop of the form shown in fig. 2.7. At turning points of the applied field ( $> H_{c1}$ ) surface sheath currents screen the bulk and cause flux to be completely trapped as  $H$  decreases over a range  $2\Delta H$ . For applied fields roughly in the range  $-H_{c1} < H < H_{c1}$  complete flux trapping also takes place. Screening currents on the surface layer cause the effective applied field seen by the bulk of the material to be different from the externally applied field.

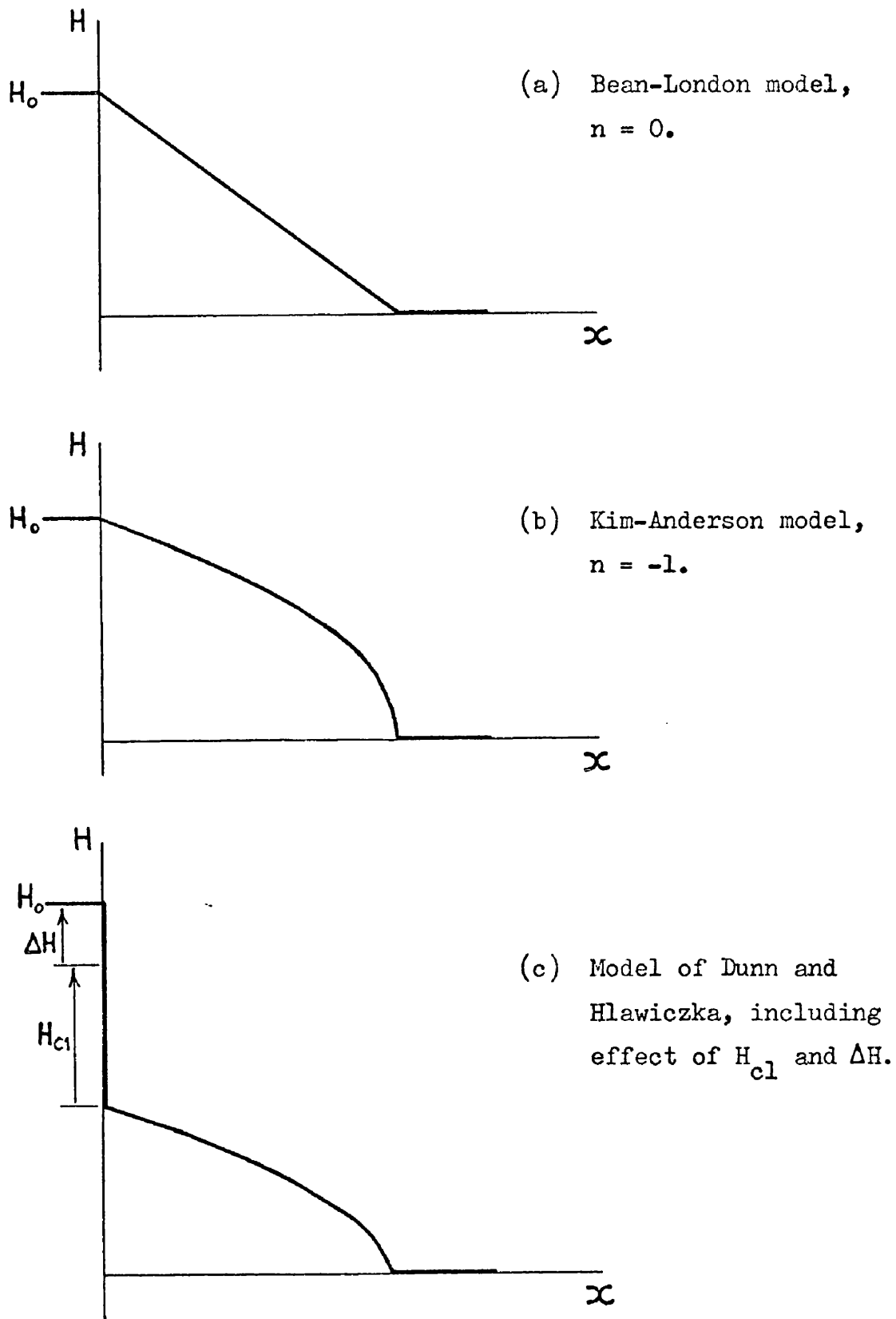


Fig. 2.6 Flux distribution inside a superconductor according to various critical state models.

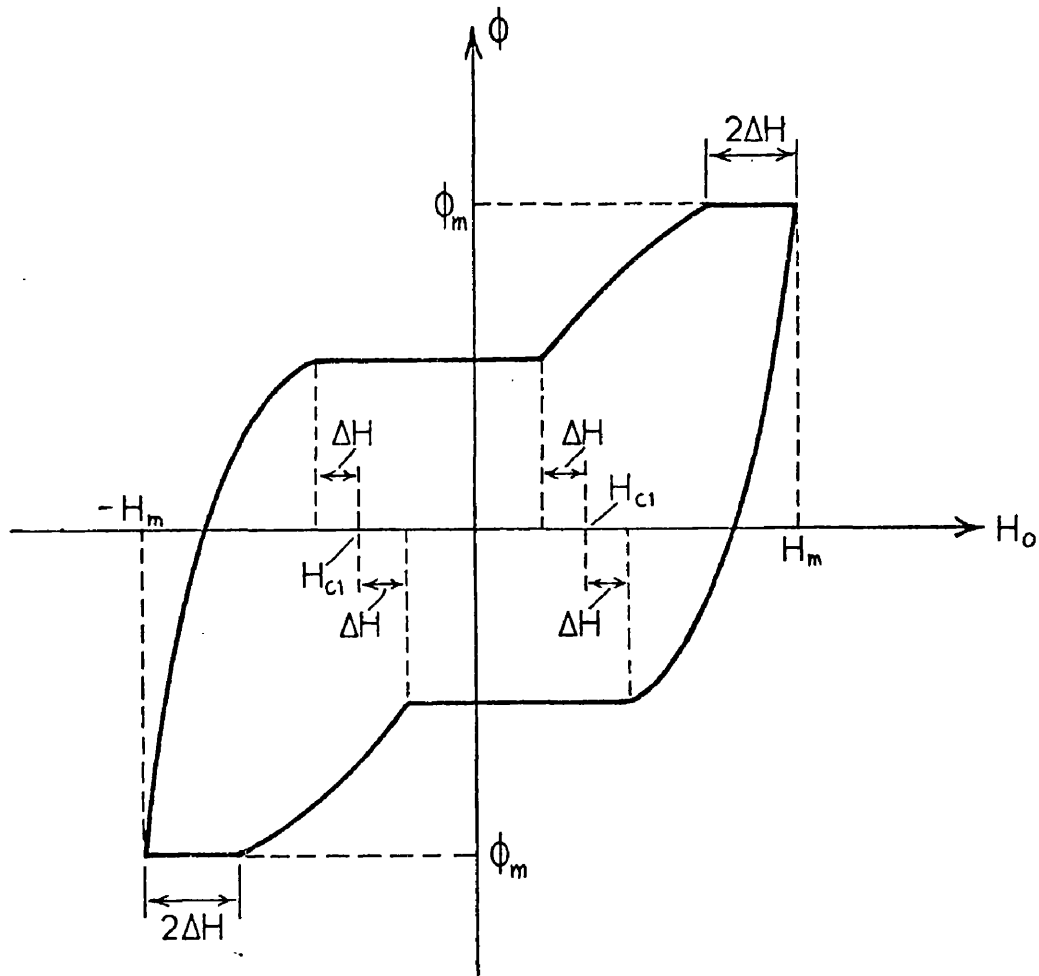


Fig. 2.7 Form of hysteresis loop assumed as a basis of the generalized critical state model. (From Dunn and Hlawiczka, 1968.)

Dunn and Hlawiczka analysed in detail the flux distribution and losses predicted by their model when the applied field is sinusoidal with peak value  $H_m$ . Their critical state model has been used by Easson and Hlawiczka (1967, 68) for analysis of and comparison with extensive experimental results on bulk niobium. For their experiments Easson and Hlawiczka used a flat slab geometry with parallel a.c. field applied to both sides of the slab, an arrangement which permits direct comparison of results with predictions of the model. Measured values of flux penetration and losses in sputtered niobium films will be compared with the results of Easson and Hlawiczka in chapter 5. For this reason, and because the model of Dunn and Hlawiczka allows for  $H_{c1}$  and  $\Delta H$ , it is the most useful description of the critical state in the context of present work.

#### Effect of viscous flow

The mechanism of viscous flux flow outlined above implies that a finite amount of time is required for a critical state to be established, i.e. for flux motion to proceed to a stage where the effect of flux flow is negligible. If the rate of change of applied field is great enough flux line density gradients steeper than the critical state gradient may be established within the specimen, resulting in dissipation by viscous flow (Kim et al 1964, 65). This can be tested experimentally by observing hysteresis as a function of frequency of applied a.c. field, an experiment which permits separation of dissipation due to unimpeded flux flow from dissipation due to flux

flow between pinning sites. Easson (1967) points out that there is ample experimental evidence that loss per cycle is independent of frequency for many materials, including niobium, in the range 20 Hz to 40 kHz ; so viscous flow effects are not present. From this point of view the assumption of a critical state is valid.

#### A criticism of the critical state concept

On the other hand, in a series of paper by Schweitzer (1967,68), Schweitzer and Bertman (1966 a,b,c) and Schweitzer and Garber (1967 a,b) the concept of critical state is called in question. These papers describe a series of experiments on high and low kappa hysteretic superconductors which yielded many results that were incompatible with the Bean-London and Kim-Anderson models being used at the time. Schweitzer and Garber (1967 b) conclude that critical state and pinning concepts do not explain hysteresis in low kappa type II superconductors, but that surface currents play the major role in determining hysteresis. Their experiments show, further, that surface currents do not originate from pinning properties of a thin outer shell. It seems that we must conclude that the surface sheath plays a major role in hysteretic behaviour although, as Bertman et al (1966) point out, there is in general no necessary or unique correspondance between the St.-James-de Gennes surface currents and hysteresis. At the time of publication of the papers by Schweitzer et al no critical state model took surface superconductivity into account. As the model since proposed by Dunne and Hlawiczka does allow for a surface sheath, it is perhaps not subject to the above criticisms.

### Initial flux penetration

From the point of view of this thesis we are particularly interested in the initial stages of flux penetration into a relatively low kappa material ; so we would like to know what kind of behaviour to expect near  $H_{c1}$ . The lower critical field  $H_{c1}$  is the field at which the presence of a flux thread in the bulk becomes energetically favourable. But in order to penetrate, the external field must overcome a surface energy barrier (Bean and Livingston, 1964) which resists flux penetration or escape, with the result that penetration may be delayed until the applied field is considerably in excess of  $H_{c1}$ . Now the critical state model of Dunn and Hlawiczka does in fact predict that there is no flux penetration until  $H_m = H_{c1} + \Delta H$ , thus allowing for surface barrier.

The most important point, however, is that the nature of flux line nucleation and entry is strongly dependent on surface topography (De Blois and De Sorbo 1964, Joseph and Tomasch 1964). Surface defects, such as scratches, are expected to provide spots of easy flux entry. In this case initial flux penetration will not occur uniformly over the whole surface area of the superconducting slab, but will instead begin to penetrate at "patches" where the barrier is weakened by surface defects. Clearly no critical state model can be applied to such a situation. This point, the possibility of non-uniform initial penetration of flux into a type II superconducting slab, is central to the thesis, and I shall return to it in chapter 6. A detailed discussion of various effects associated specifically with the surface

is given in chapter 7, where the problems of surface phenomena and non-uniform flux penetration are dealt with in the context of experimental results.

CHAPTER 3FILM PREPARATION

In order to be able to apply field to one side of the film only, and to eliminate end effects completely, niobium and tantalum films are required in cylindrical form. Since we are mainly interested in the initial stages of flux penetration it appears that it should not be necessary to investigate films more than several penetration depths in thickness, i.e. up to about 3  $\mu\text{m}$  thick. However, as we shall see, I required in practice to perform experiments on films much thicker than this, up to 25  $\mu\text{m}$  thick in fact. The problem therefore was to deposit niobium and tantalum films up to 25  $\mu\text{m}$  thick on cylindrical substrates.

### 3.1 Possible methods of film preparation

Various methods of preparing metal films are reviewed in an article by Campbell (1966) in which is summarized the applicability of each method to the uses for which the film is intended. According to Campbell superconducting films are best prepared by evaporation or by deposition from a compound in the vapour phase ; but his conclusions are only intended to apply to "soft" (type I) superconductors such as tin, lead, or aluminium which are not difficult to prepare in pure form. On the other hand the preparation of both niobium and tantalum films is difficult for two reasons: (a) Both metals have a very strong affinity for oxygen, nitrogen and hydrogen, thus films

become contaminated very readily on deposition. (b) The superconducting properties of both metals are very strongly dependent on their purity.

Partly because of the difficulties a great deal of work has been done on the deposition of niobium and tantalum films, tantalum having been the subject of particularly intensive study (Berry et al 1968). The techniques used have been chiefly high vacuum evaporation and sputtering. It was therefore decided to try both these methods to prepare cylindrical films ; the evaporation and sputtering methods are described in sections 3.2 and 3.3 respectively. It should be mentioned at this point that more recently electrolytic deposition has been used to produce extremely high quality niobium films which could be of considerable technological importance (Mellors and Senderoff 1965, Meyerhoff 1969). Due to lack of time I have not been able to do any work on electrodeposition for this thesis. I shall refer to the work of Mellors et al again in the concluding chapter, when its significance will be more apparent.

### 3.2 Deposition of tantalum films by evaporation

Evaporation of refractory metals is usually carried out under ultra high vacuum by electron-beam melting a small area in a piece of the metal to be deposited, as used for example by Asada and Nose (1969). Neugebauer and Ekvall (1964) prepared tantalum films by this method with conventional high vacuum equipment by relying on the gettering action of the deposited metal to reduce the partial pressure of

contaminating gases. Niobium films have been produced by London and Clarke (1964) by evaporation under ultra high vacuum from an electrically heated niobium wire.

It was decided to try to prepare tantalum films by a combination of these two methods — evaporation from a heated wire in a conventional vacuum unit while utilising the gettering action of tantalum to ensure a pure deposit on the substrate. Just below its melting point of  $3000^{\circ}\text{C}$ , the rate of evaporation of tantalum from the solid phase is quite high. For example, at  $2900^{\circ}\text{C}$  the rate of evaporation is  $2.8 \times 10^{-5} \text{ g cm}^{-2} \text{ s}^{-1}$  (Miller, 1959). This fact suggests the possibility of preparing cylindrical films by evaporation from a resistively heated Ta wire placed axially inside the substrate cylinder. It was expected that the gettering action of the continuously deposited tantalum film at the ends of the substrate cylinder would result in a pure film at the centre.

#### The evaporation unit

Considerable effort was spent on developing this possibility, the arrangement which was finally arrived at being illustrated in fig. 3.1. The apparatus, constructed as far as possible of stainless steel, is under high vacuum in a conventional Edwards 12E3 coating unit. Such a unit uses an oil diffusion pump with liquid nitrogen cold trap, backed by a rotary pump, and is capable of an ultimate vacuum of  $5 \times 10^{-6}$  torr without bakeout. The tantalum wire, 1.8 mm diameter, is high purity material (99.7%) supplied by Imperial Metal Industries. At a temperature  $100^{\circ}\text{C}$  below its melting point, where

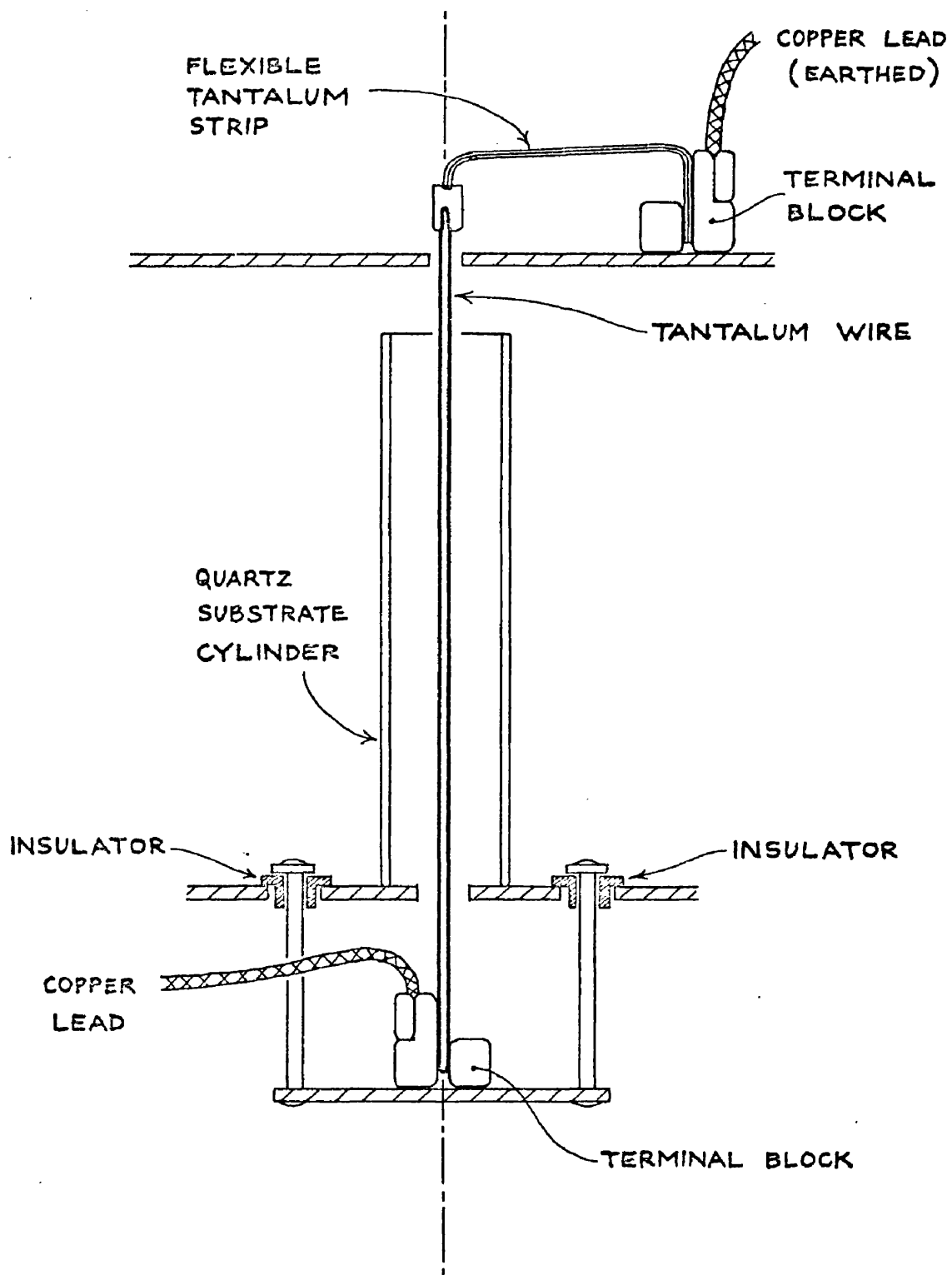


Fig. 3.1 The evaporation unit — sectional diagram.

the evaporation rate has the value quoted above, and assuming a substrate inside diameter of 24 mm, the rate of deposition will be  $12.5 \text{ \AA/s}$ . The flexible tantalum strip connection to the upper end of the wire allows expansion to take place freely. To maintain a wire 1.8 mm diameter at  $2900^{\circ}\text{C}$  under high vacuum requires a current of about 135 amps, this current being drawn from a welding transformer with Variac control in the primary circuit. The tantalum wire is 18 cm long, the voltage drop across this length when carrying 135 amps being 13 volts, so that during evaporation about 1.75 kW is dissipated as heat inside the vacuum chamber. The substrate cylinder is fused quartz.

#### Evaporation procedure

To deposit a film the following procedure was used. The substrate cylinder and tantalum wire were carefully cleaned and mounted in the vacuum chamber which was then pumped down to an ultimate vacuum of about  $5 \times 10^{-6}$  torr. The current through the wire was slowly increased to the required level, the exact current for a given evaporation rate having been previously determined by trial and error. After about 2 minutes it was no longer possible to see the white-hot wire through the quartz substrate, this serving as an indication that a film was being deposited, and when evaporation had taken place for a sufficient length of time the current was switched off and the apparatus left to cool under high vacuum. In this way several tantalum films were deposited inside fused quartz cylinders of various diameters.

Disadvantages of evaporation method

In spite of its apparent simplicity the method suffers from several serious drawbacks.

- (a) As evaporation proceeds the wire becomes thinner, so that to maintain the correct evaporation rate current must be reduced; therefore, control of evaporation rate by controlling the current is very difficult. To overcome this problem the temperature of the wire could be measured with an optical pyrometer. This, however, would not be very satisfactory as it could only indicate the wire temperature near one end and not at the centre of the substrate cylinder where thermal conditions are different.
- (b) Dissipation of 1.75 kW in the vacuum chamber during evaporation causes the apparatus to become hot, the substrate in particular reaching a high temperature. As a result, outgassing causes the pressure to rise to between  $10^{-5}$  and  $10^{-4}$  torr during deposition, leading to high impurity concentration in the film. Gettering action at the cylinder ends is not effective enough to handle such contamination. To improve the vacuum during deposition it would be necessary to use a bakeable unit, possibly capable of ultra high vacuum and having fast pumping speed at low pressures. Even this might not solve the problem of film contamination by substrate outgassing.

- (c) Because of the high substrate temperature during deposition the evaporated films are very granular. They also have many macroscopic defects in the form of "pinholes" which could be seen during deposition.

Because of these difficulties, preparation of films by evaporation was abandoned in favour of the sputtering method.

### 3.3 Deposition of niobium and tantalum films by sputtering

Sputtering is very widely employed to prepare thin films of nearly all materials (Berry et al 1968, Maissel 1966). The basic principle of sputtering is as follows. When a glow discharge is established between a pair of electrodes the cathode is subjected to bombardment by positively charged particles created by the ionization of gas molecules in the space between the electrodes. This bombardment causes atoms of cathode material to be ejected from the surface and diffuse away from the cathode. Such sputtered atoms can deposit to form a film on a suitably placed substrate. A complete account of the theory of the sputtering mechanism is given in a review by Maissel (1966), where he also discusses sputtering technology and applications.

The simplest sputtering system consists of a d.c. glow discharge in an inert atmosphere with the anode at earth potential and the substrate placed on or near the anode. There are many variations of the basic system, such as asymmetric a.c. sputtering, d.c. sputtering with a biased substrate, radio frequency sputtering, and special methods for sputtering at very low pressures. The

purpose of these different systems is to reduce film contamination or achieve faster deposition rate or both. Simple d.c. sputtering has been used to prepare tantalum films by Altman (1962) and Maissel (1962) and for niobium films by Sosniak and Hull (1967), who also used substrate bias sputtering (Sosniak, 1968). Asymmetric a.c. sputtering and r.f. sputtering have been used by Vratny and Harrington (1965) and Vratny (1967) for tantalum films.

It was decided that the best method for cylindrical films would be a d.c. glow discharge in a cylindrical geometry with substrate at anode (earth) potential. From the point of view of simplicity in performing the experiments to be described in later chapters it would be best to have the film on the outside of the substrate cylinder. However, attempts to deposit sputtered films on the outside of cylinders met with very little success ; the deposition rate was low and the apparatus unreliable in operation. So it was decided to use a sputtering geometry which deposited a film on the inside of cylinders, this being the system used successfully by Hlawiczka and Ross (1968) to prepare niobium film cylinders. There is the advantage that it can easily be arranged to utilize gettering action to achieve a pure deposit on the substrate, hence ultra high vacuum is not necessary. Getter sputtering, as it is called, was originally developed by Theuerer and Hauser (1964).

#### The sputtering unit

A sectional view of the sputtering unit is given in fig. 3.2. It is used in the vacuum chamber of an Edwards 12E3 coating unit. All

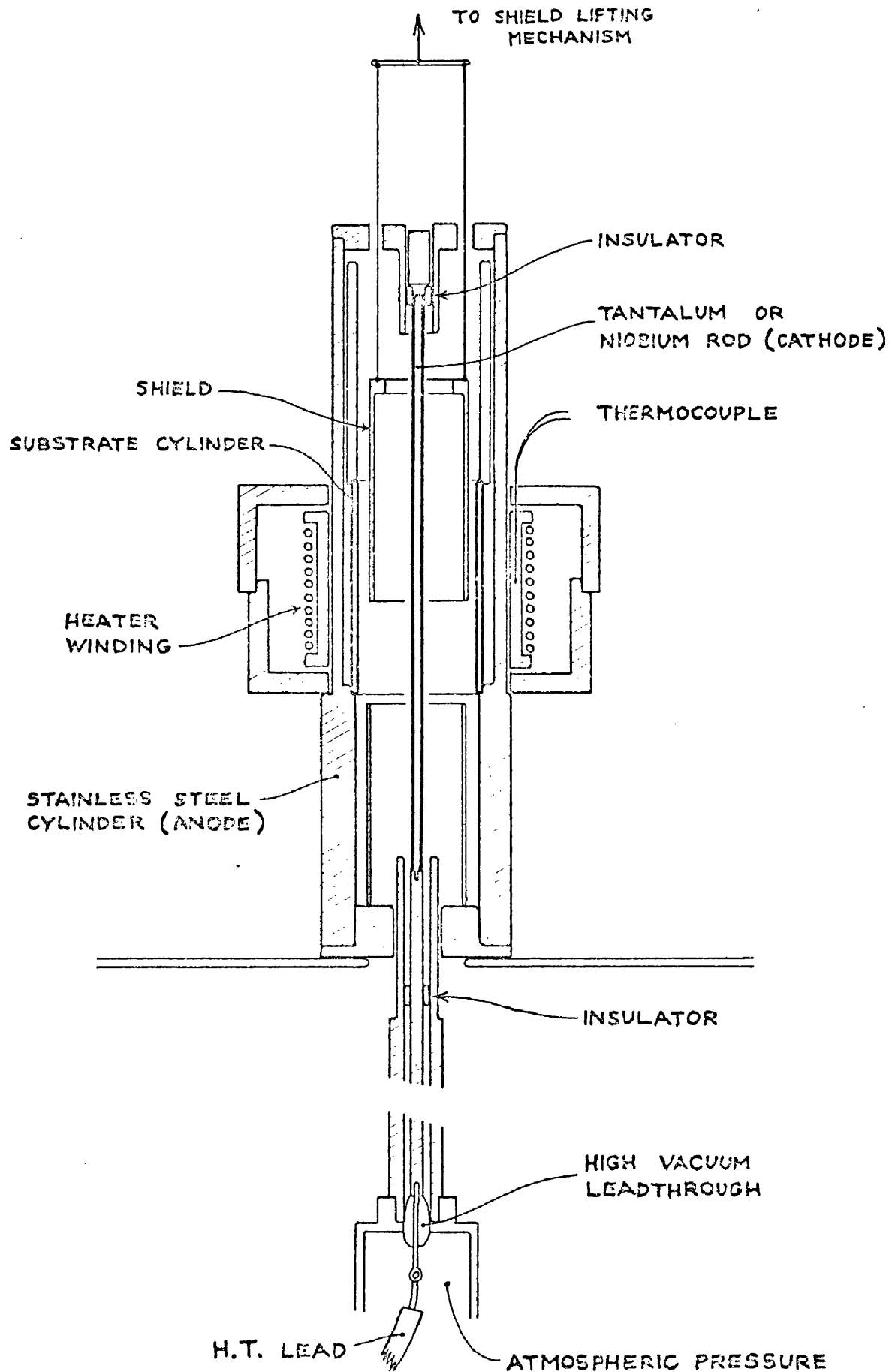


Fig. 3.2 The sputtering unit — sectional diagram.

parts shown hatched in fig. 3.2 are stainless steel. The stainless steel cylinder and the tantalum or niobium rod act as anode and cathode respectively for a glow discharge which is set up in the long annular space between them. The anode is earthed, the rod being raised to a high negative potential. The substrate cylinder (copper or stainless steel) is positioned as shown at the centre of the glow discharge region to receive tantalum or niobium sputtered from the rod. Sputtering takes place in an atmosphere of high purity argon (impurity content not more than 15 p.p.m.) at a pressure which gives suitable glow discharge conditions, typically 0.4 torr. Any impurity gas entering the sputtering unit will tend to be removed by the gettering action of the continuously deposited film near the ends of the glow discharge region. This is shown more clearly in fig. 3.4(a) which is a simplified diagram indicating the glow discharge and gettering regions. The sputtered film will, therefore, be impure at the ends and pure at the centre where the substrate is placed. A shield, shown half raised in fig. 3.2 is provided to prevent an initial deposit of impure film when sputtering is started. The photograph in fig. 3.3 shows the complete sputtering unit mounted on its vacuum chamber baseplate. The baseplate is 33 cm in diameter.

In the deposition of thin films it is possible to define a "sticking coefficient" (Berry et al 1968, Neugebauer and Ekvall 1964) as the mean length of time for which an atom or molecule of the material being deposited remains on the surface of the substrate

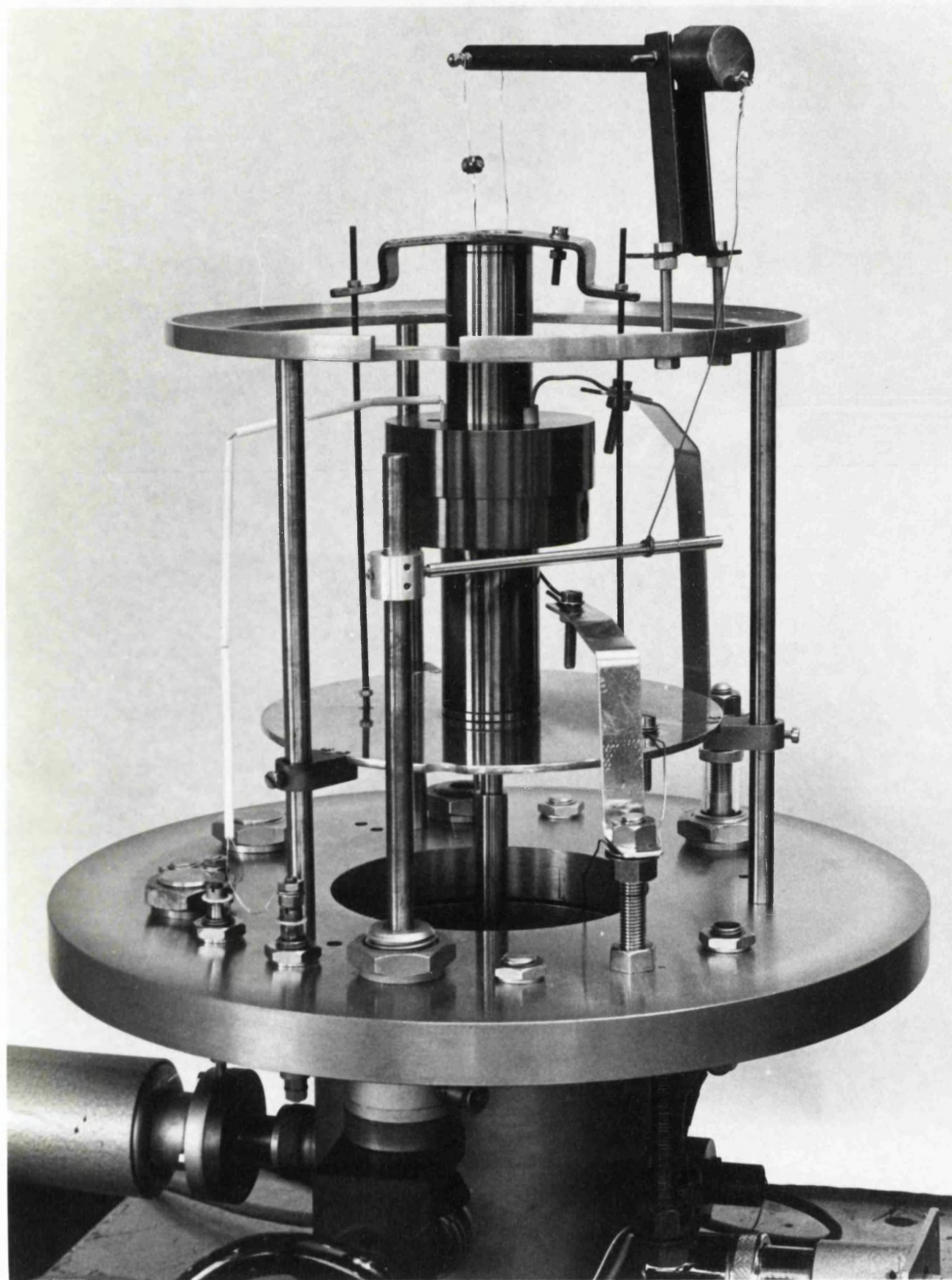


FIG. 3.3 SPUTTERING UNIT MOUNTED ON  
VACUUM CHAMBER BASEPLATE.

before becoming detached again, assuming it is not buried by subsequent incident particles in the interval. The ratio of the sticking coefficients of tantalum or niobium to the sticking coefficients of impurity gases, such as oxygen, nitrogen and hydrogen, will determine the film purity ; the higher this ratio, the purer the film. The sticking coefficient of impurity gases is a function of temperature, decreasing as the temperature is increased to about 600°C, whereas the sticking coefficient of tantalum or niobium is approximately constant up to such temperatures ; therefore purer films will be obtained if the substrate is heated (Sosniak, 1968). As shown in fig. 3.2 a heater winding is used to do this. A platinum/ 10% rhodium-platinum thermocouple in the heater winding former serves to indicate temperature.

The sputtering unit is 17.5 cm long, the anode cylinder having an effective inside diameter of 20.6 mm. The cathode rod is 2.5 mm. diameter initially although, of course, its diameter decreases gradually as it is used. Tantalum and niobium rods are supplied by Murex Metals Limited. The tantalum is 99.9225% pure material, the chief impurity being niobium, of concentration 0.05%, followed by nitrogen and carbon. The niobium cathode rod is 99.57% pure, the major impurity in this case being 0.31% of tantalum.

#### Sputtering procedure

Before depositing a film the substrate cylinder was subjected to a rigorous cleaning process which included ultrasonic agitation

in a proprietary de-contaminant solution and prolonged rinsing in a continuous flow of hot de-ionised water. After substrate cleaning the sputtering unit was assembled in the vacuum chamber, precautions generally used for high vacuum work being observed, for example vacuum chamber parts were handled with tweezers or polythene gloves. The chamber was then pumped out. Using the heater shown in fig. 3.2 the unit was heated until the temperature, as indicated by a thermocouple in the heater winding former, stabilized at  $680^{\circ}\text{C}$ . This served to bake out the whole vacuum chamber, the system being left to bake out for 4 hours, after which time pressure as indicated by a gauge head in the pumping manifold had fallen to  $\sim 4 \times 10^{-6}$  torr. The chamber was then flushed out with high purity argon by closing the pumping valve and admitting argon through a needle valve until atmospheric pressure was reached. The chamber was then pumped down to a pressure of  $5 \times 10^{-6}$  torr, flushed out a second time with argon and pumped down once more. Heater current was then reduced until the thermocouple temperature stabilized at  $575^{\circ}\text{C}$ .

When this stage had been reached the needle valve was opened carefully to admit argon, the pumping valve being kept fully open, until a state of dynamic equilibrium was reached with an argon pressure in the chamber of 0.4 torr. The H. T. supply, full-wave rectified unsmoothed, was switched on and increased to establish the glow discharge. The H.T. supply and argon pressure were adjusted until a mean discharge current of 50 mA at a mean voltage of 2.5 kV was obtained. After 10 minutes the shield was raised to expose the substrate and film

deposition began. Once conditions had been established it was not difficult to deposit a film over a period of several hours if desired.

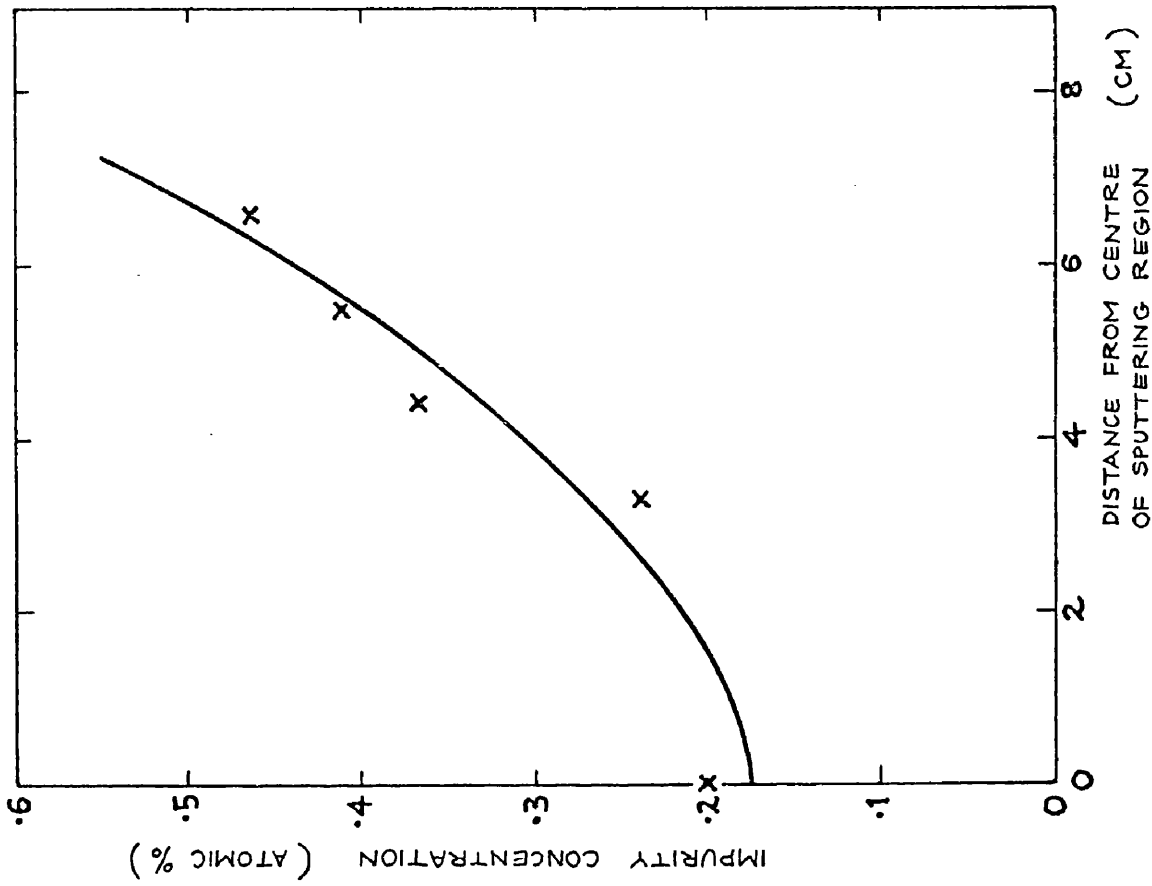
Typical deposition parameters were :

Discharge voltage	-	2.5 kV
Discharge current		50 mA
Temperature (by thermocouple)		575°C
Argon pressure		0.4 torr
Deposition rate - tantalum		11 Å/s
- niobium		9.5 Å/s

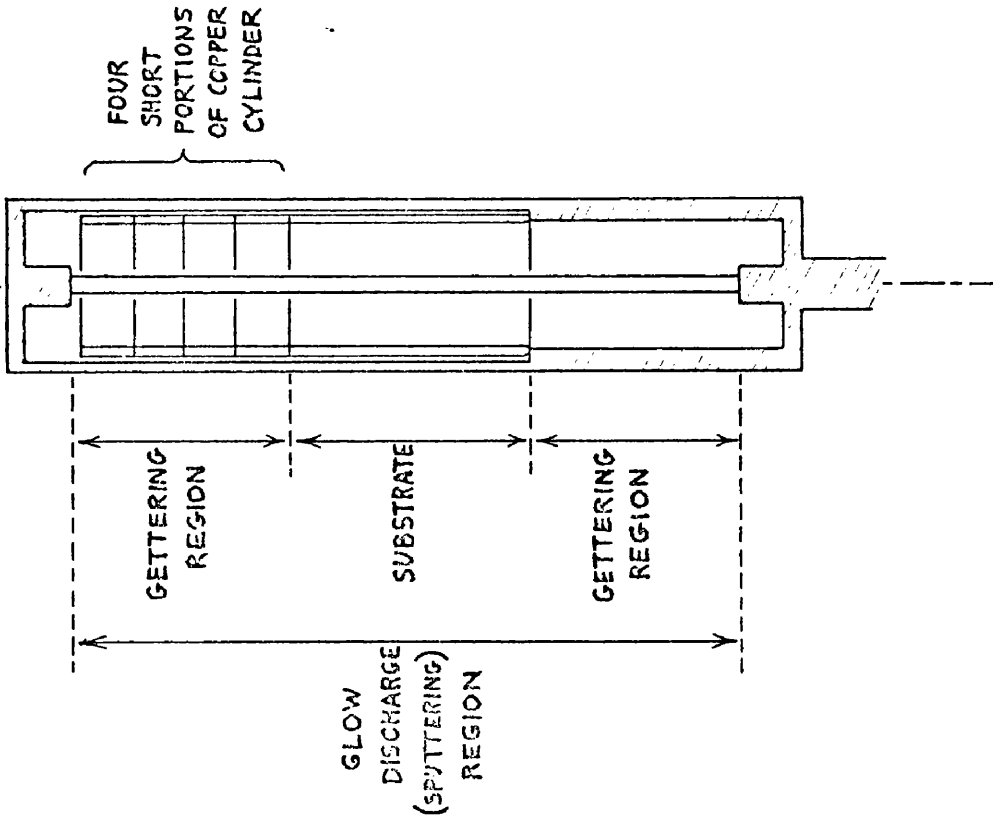
The deposition rate was calculated from film thickness, measured as described in chapter 4. When the required length of time had elapsed, determined by previous knowledge of deposition rate, the H.T. was switched off, the argon inlet needle valve closed, and the unit left to cool under vacuum.

#### Effectiveness of gettering

A simple experiment was carried out to check that gettering action was effective in reducing contamination at the substrate. A copper cylinder was prepared in the form of four short portions which were placed in the gettering region in the sputtering unit as shown in fig. 3.4(a). A substrate cylinder 55 mm long occupied the centre region as it normally would and the shield was removed. A tantalum film about 3 µm thick was sputtered following the normal procedure outlined above. Now, as will be explained in the next chapter the critical temperature of tantalum can be related directly to the interstitial



(b) Impurity content of sputtered tantalum film.



(a) Simplified diagram of sputtering unit showing gettering regions.

Fig. 3.4 Arrangement used to test effectiveness of gettering.

gaseous impurity content. Therefore  $T_c$  for the film deposited on each portion of cylinder was measured by methods to be described in chapter 4, the value so obtained being used to estimate the percentage of gaseous impurity in each part. The results are shown in fig. 3.4(b) where impurity content has been plotted as a function of distance from centre of sputtering region. It appears that gettering action plays a part in improving film purity. It should be noted, however, that the film will tend to be purer at the centre in any case because the temperature is higher near the centrally placed heater winding.

#### 3.4 Choice of substrate material

For reasons given above the substrate is heated to about  $680^{\circ}\text{C}$  before deposition, and to  $575^{\circ}\text{C}$  during deposition. We are therefore limited in choice of substrate to materials which can withstand such temperatures without decomposing or outgassing severely, and which have a suitable coefficient of expansion. If the latter condition is not satisfied then upon cooling the substrate with its film to room temperature and subsequently to liquid helium temperature, the differential coefficient of expansion between film and substrate may cause high stresses in the film. Table 3.1 lists the melting point, maximum working temperature and coefficient of expansion for tantalum, niobium and four possible substrate materials, two ceramic and two metallic.

Material	Melting point °C	Approximate max. working temp. °C	Linear coeffic. of expansion* x 10 <sup>6</sup> per C°
Niobium	2470	—	7.6
Tantalum	3000	—	6.6
Fused silica glass, SiO <sub>2</sub> (quartz)	1730	1500	0.5
Alumina, Al <sub>2</sub> O <sub>3</sub> (Degussit Al23)	2030	1900	7.7
Copper	1080	900	20
Stainless steel	~1460	1000	13

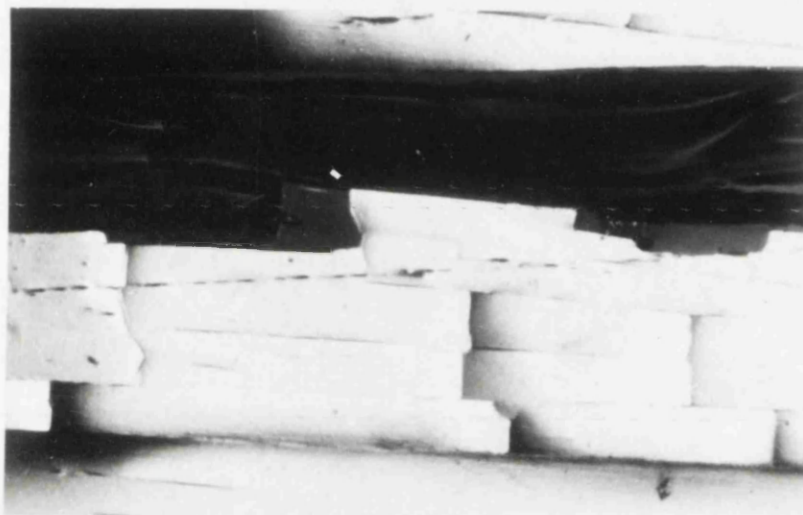
\*Approximate mean value over temperature range 20 - 600°C.

Table 3.1 Properties of tantalum, niobium and  
substrate materials.

Quartz: Fused silica glass (quartz) was used as a substrate for all the earlier attempts to prepare films. It has a very low coefficient of expansion, so that when it cools after deposition the niobium or tantalum film contracts more than the substrate. Films on quartz are therefore under tensile stress at room temperature. If the film is greater than about 1  $\mu\text{m}$  thick the stress causes it to craze and even peel off the substrate altogether, as shown in fig 3.5. Fused quartz is therefore unsuitable as a substrate for thick films.

Alumina: The coefficient of expansion of sintered aluminium oxide is a close match to that of niobium or tantalum so in this respect alumina is ideal. It suffers from the serious drawback, however, that it must be glazed to give a smooth enough surface. Because of the glazing process tubular substrates cannot be made to a sufficiently close tolerance on the inside diameter. In addition the manufacture of alumina tubes glazed on the inside is difficult and costly.

Metallic substrates: The possibility of using a normal metal as substrate was not considered at first because it was thought that the substrate would interfere with measurements of the superconductive properties of the film. However, the experiments described in chapters 5 and 6 are concerned with flux penetration from one side of the film only, and can be



┌───┐  
0.1 mm

FIG. 3-5 2.3  $\mu\text{m}$  THICK SPUTTERED Ta FILM ON QUARTZ, ILLUSTRATING PEELING OF A THICK FILM WHEN DEPOSITED ON QUARTZ

so arranged that measurements are not affected by a metallic substrate. Copper and stainless steel are the most likely candidates, their relevant properties being given in the table. In both cases the coefficient of expansion is considerably larger than for niobium and tantalum. When the substrate with its film cools to room temperature the substrate contracts more than the film, placing the film under compressive stress which does not cause the film to peel off or break up in any way. Copper and stainless steel substrates have, therefore, been used successfully for all work on thick films. It should be noted that the compression of the film on cooling must inevitably result in a degree of cold working, a factor which I shall discuss more fully in chapter 4.

Substrate surface finish and its effect on the film is discussed in the next chapter. It is sufficient to mention here that it is difficult to put a very smooth finish on copper substrates as copper, being relatively soft, is difficult to polish. Stainless steel is more satisfactory because it is hard and can be polished easily. For this reason stainless steel has been used as substrate for most of the thick films.

CHAPTER 4SOME PROPERTIES OF THE FILMS

This chapter is concerned with those properties of the films which have been studied and which are most conveniently considered separately from the flux penetration experiments in chapters 5 and 6. I have examined films under an optical microscope to assess macroscopic structure, studied the surface topography, and made measurements of critical temperature and upper critical field in order to get some idea of the effects of impurities. Measured and calculated parameters for a number of films are summarized for convenience in table 4.1. During earlier stages of the work many films were prepared on quartz substrates, such films being of little use because of peeling or crazing. Therefore only some films, those deposited on metallic substrates when the sputtering technique had been perfected, are listed in the table ; nearly all the experimental work presented in chapters 5 and 6 relates to these specimens.

To provide a comparison with sputtered niobium films most of the experiments have also been performed on a cylinder machined from bulk niobium supplied by Murex Metals Ltd. (impurity content 0.4 wt% of which 0.3 wt% is tantalum). The cylinder is 55 mm long and 23 mm inside diameter, these dimensions being the same as for

Film no.	Substrate	Thickness $\mu\text{m}$	$T_c$ K	Impurity content (from $T_c$ ) at.%	$H_{c2}$ at $0.8T_c$ Oe	$\kappa_1$
41	Cu	3.4	4.34	0.18	-	-
43	Cu	4.1	4.32	0.22	-	-
44	Cu	8.2	4.37	0.14	900	2.1
48	s.s.	23.6	4.32	0.22	1020	2.4
Pure $T_a$	-	-	4.482	0	$H_c=300$	$\kappa_0=0.34$

(a) Tantalum

Film no.	Substrate	Thickness $\mu\text{m}$	Impurity content (from $H_{c2}$ ) at.%	$H_{c2}$ at $0.45T_c$ Oe	$\kappa_1$	$\kappa_3$	$H_{c1}$ at $0.45T_c$ Oe
45	Cu	6.5	1.4	12900	5.9	6.8	410
49	s.s.	10.3	0.8	8200	3.75	4.3	540
50	s.s.	16.1	1.2	11400	5.2	6.0	450
47	s.s.	19.4	0.9	9400	4.3	4.95	500
51	s.s.	24.7	1.0	10200	4.65	5.35	480
machined Nb cyl.	-	$\sim 250$	1.5	13500	6.2	7.1	400
Pure Nb	-	-	0	2670	1.22	-	1460

(b) Niobium

Table 4.1 Measured and calculated parameters for sputtered tantalum and niobium films and machined niobium cylinder.

Some figures for the pure metals are included for comparison.

films, and has a wall thickness of 0.25 mm, this being the minimum thickness that could be achieved with conventional machining. The cylinder was in the as-machined state for all measurements. Results for the bulk cylinder will be presented and compared with the films when appropriate. Some parameters are included in table 4.1 (b).

#### 4.1 Film thickness

The thicknesses of all films have been determined by weighing substrates before and after deposition, the difference being the weight of film deposited. In calculating thickness it is assumed that the film has the density of bulk material and that it is deposited uniformly over the length of the substrate cylinder. A check on thickness was made on film 44 — an 8.2  $\mu\text{m}$  thick (by weight) tantalum film on an as-machined copper substrate — in the manner illustrated in fig. 4.1. The substrate cylinder carrying film 44 was cut at  $2^\circ$  to the axis as indicated by line AA. One extremity of the ellipse-shaped section was polished and a microphoto taken, the result being as shown in the figure. The apparent thickness  $x$  of the film at the extremity of the ellipse, when multiplied by  $\sin 2^\circ$ , gives the actual thickness. Thickness determined in this way is 9.8  $\mu\text{m}$ , compared with 8.2  $\mu\text{m}$  by weight. The discrepancy can be accounted for by the difficulty of determining  $x$  accurately, the film surface and film-substrate interface being blurred by machining

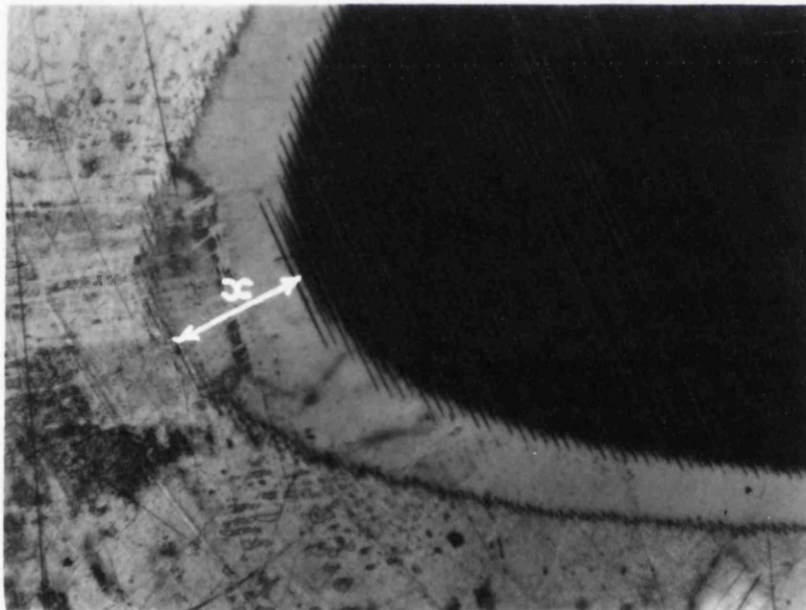
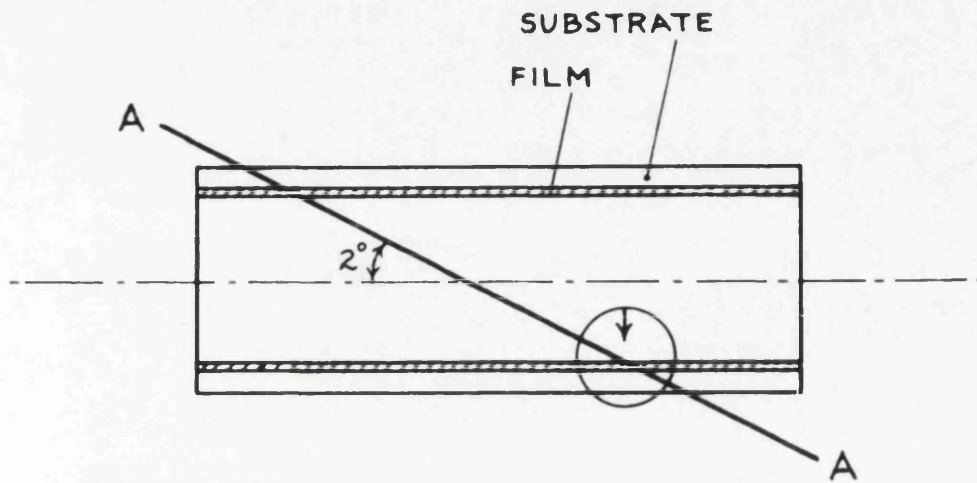


FIG. 4.1 METHOD OF MEASURING THICKNESS OF FILM 44

grooves, and by the fact that the  $2^{\circ}$  bevel angle is only approximate. Furthermore, the assumptions on density may not be correct. In this respect it should be noted that Hlawiczka and Ross (1968) have made Talysurf thickness measurements on sputtered niobium films which also indicated that films were thicker than would be expected from the weight of niobium deposited.

#### 4.2 Macrodefects and grain size

The term "macrodefects" in the context of the thesis is used to describe imperfections in films other than impurities and dislocations, and which are of a size much greater than the coherence length. The defects to be described are of the order of microns in size, i.e. comparable with film thickness. Preliminary examination under optical microscope of tantalum films on quartz revealed the presence of holes in the films. Fig. 4.2 (a) is a photograph of what can be described as a "pinhole" about  $8 \mu\text{m}$  diameter in a  $1 \mu\text{m}$  thick film. When such defects were first found it was decided to undertake a detailed study of the nature and number, if any, of similar defects in the much thicker films which had been sputtered onto metallic substrates.

To locate holes which go right through a film it is necessary to use illumination from the back, which means that a film on copper or stainless steel must be removed from its substrate. Preferential etching was employed to dissolve away the copper or stainless steel

from small pieces cut out of film cylinders. For copper substrates the etch consisted simply of dilute nitric acid, which could remove all of the substrate in about 30 min. To dissolve stainless steel a mixture of 1 part conc.  $\text{HNO}_3$  plus 3 parts conc.  $\text{HCl}$  plus 3 parts water was used, an etch which required about 20 hours to completely dissolve the substrate. Great care was taken to avoid as far as possible introducing flaws while etching and handling the pieces of film. The etchants were of such a strength that the reaction proceeded slowly, without bubbling which could have damaged the film. Neither tantalum nor niobium are themselves affected by the above etchants (Miller, 1959)

#### Microscope photographs

Sputtered films from 3  $\mu\text{m}$  to 18  $\mu\text{m}$  thick have been examined under optical microscope with illumination on both front and back. Intense lighting from the back, with little or no front illumination, revealed whether or not there were holes through the film in the area under examination. Thus the presence or absence of pinhole defects could be established beyond doubt. Defects in various sizes and numbers were found in all specimens examined. In fig. 4.2 (b) to (e) are photographs showing macroscopic imperfections in some of the films; they are in order of increasing thickness. The photographs were taken with simultaneous illumination on back and front, the light from the back revealing holes right through as small white areas, and front illumination showing the general nature of the

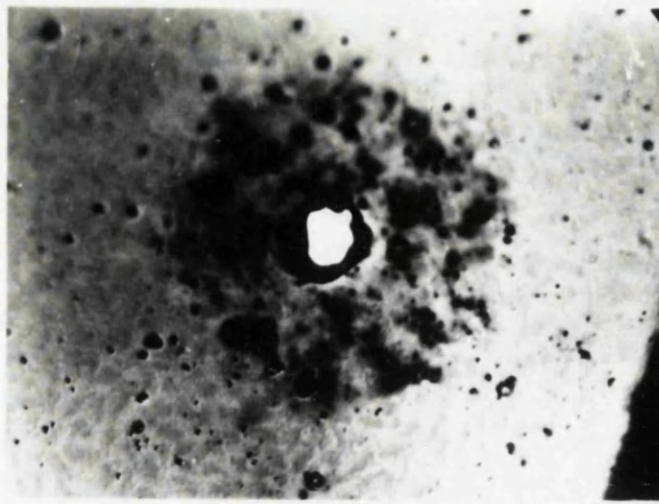
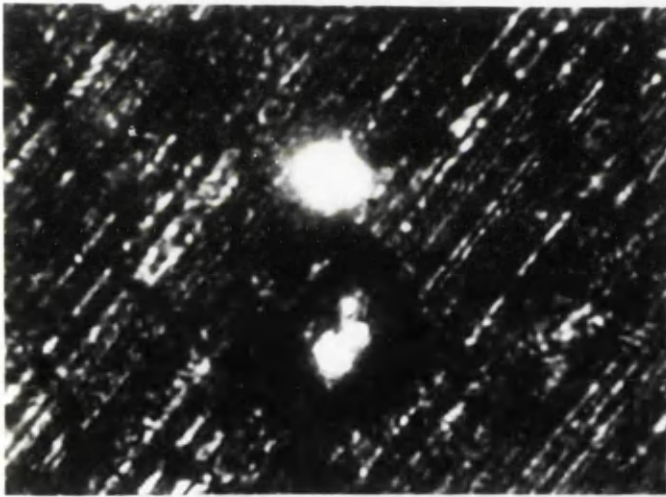
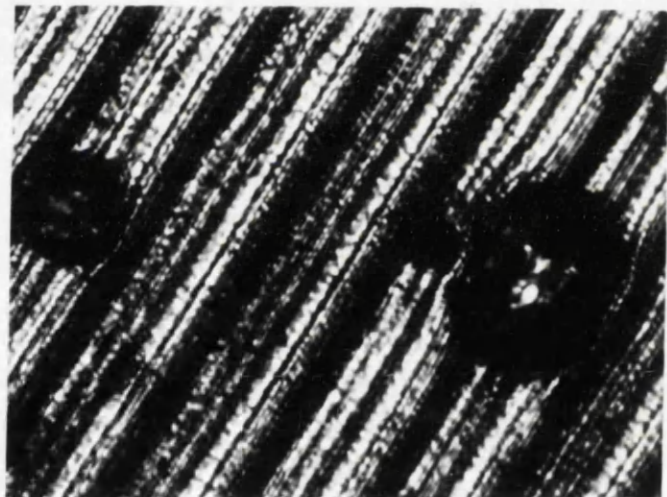
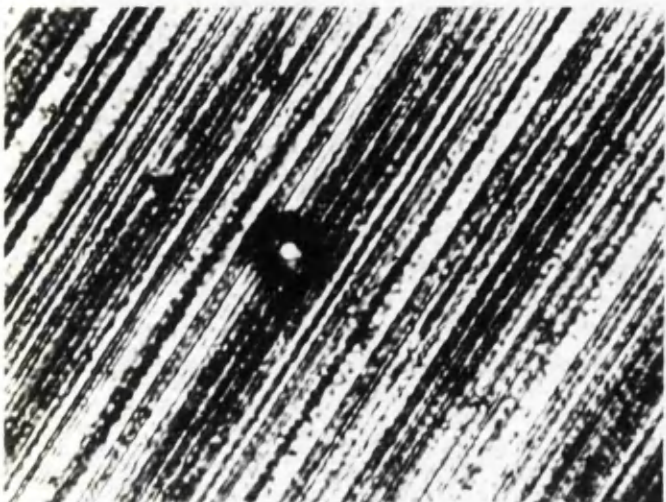
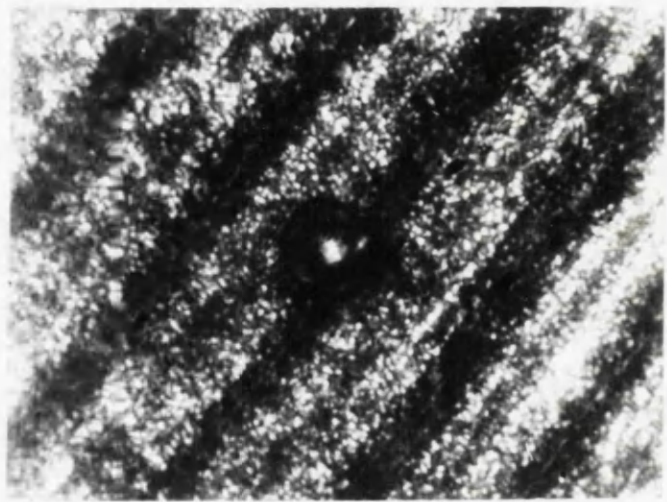
(a) 1  $\mu\text{m}$  Ta FILM(b) 6.5  $\mu\text{m}$  Nb FILM(c) 8.2  $\mu\text{m}$  Ta FILM(d) 10.3  $\mu\text{m}$  Nb FILM(e) 18.1  $\mu\text{m}$  Nb FILM

FIG. 4.2 MICROSCOPE PHOTOGRAPHS OF IMPERFECTIONS IN SOME SPUTTERED FILMS.  
ALL FRAMES: 1CM  $\equiv$  14  $\mu\text{m}$ .

film surface.

- (b) 6.5  $\mu\text{m}$  niobium film on copper. There is one hole about 9  $\mu\text{m}$  diameter plus several smaller holes close together and surrounded by a dark area about 25  $\mu\text{m}$  in diameter. The dark area is most probably a depression or hollow in the film surface, with holes right through at the centre where the film is thinnest.
- (c) shows two defects in a 8.2  $\mu\text{m}$  tantalum film on copper. The regular lines across the film are due to replication of machining marks on the substrate, which in this case are rather pronounced. (The machining marks on this film can also be seen clearly in fig. 4.1 ). The larger dark circular area again seems to be a hollow about 28  $\mu\text{m}$  diameter with a number of pinholes at the centre. However, no holes through the film could be detected in the smaller dark area.
- (d) 10.3  $\mu\text{m}$  thick niobium film on polished stainless steel. The photograph is of one defect, consisting of a pinhole about 2  $\mu\text{m}$  diameter

at the centre of a depression which is roughly  $11\mu\text{m}$  across.

- (e) The final photograph is an imperfection on the surface of an  $18.1\mu\text{m}$  niobium film deposited on copper ; it again appears to be a hollow about  $15\mu\text{m}$  diameter. However, there are no holes at the centre of the hollow. In fact, no holes going right through could be located in this film.

For the sake of clarity the most obvious flaws have been selected for photographs. In general the depressions and pinholes varied widely in size, many being much smaller than those in fig. 4.2. Note that holes will appear larger than they actually are because of diffraction at the edges of light coming through the hole. The number of such defects was found to be very roughly of the order of 3 per  $\text{cm}^2$ , tending to increase with thinner films. Not all defects have associated with them holes right through the film, but holes right through were found in all specimens except the thickest ( $18.1\mu\text{m}$ )

#### The origin of macrodefects

In view of precautions taken in handling films it is most unlikely that flaws were introduced after deposition ; therefore pinhole type defects must be formed during film growth. The fact

that defects occur in a film deposited on a polished substrate to more or less the same extent as in a film on a machined substrate is evidence that machining marks and other irregularities in the shape of substrate surface play no part. Pinholes have always been a problem in thin film manufacture (Scharnhorst, 1969), but explanations for their occurrence are few. The consensus of opinion with respect to films prepared above room temperature is that these holes are caused by minute particles electrostatically bound to the substrate surface (Holland 1956, Jorgenson and Wehner 1963).

Fig. 4.3 illustrates how such surface contamination can cause the formation of defects like those described above. Suppose an airborne particle of contaminating material lands on the substrate at (a) while the substrate is being dried after final cleaning, or while it is being mounted. When the substrate is preheated the particle may spread out, resulting in a roughly circular dirty area as at (b) which could be several microns in diameter. During film growth this area may tend to repel tantalum or niobium atoms so that nucleation does not occur there, with the consequence that a hole is left in the film, (c). Fig. 4.3 (d), (e) and (f) illustrate the development of the defect as the film grows thicker. Eventually, when thick enough, the hole is bridge by the growing film as at (g). Although purely speculative, this explanation is

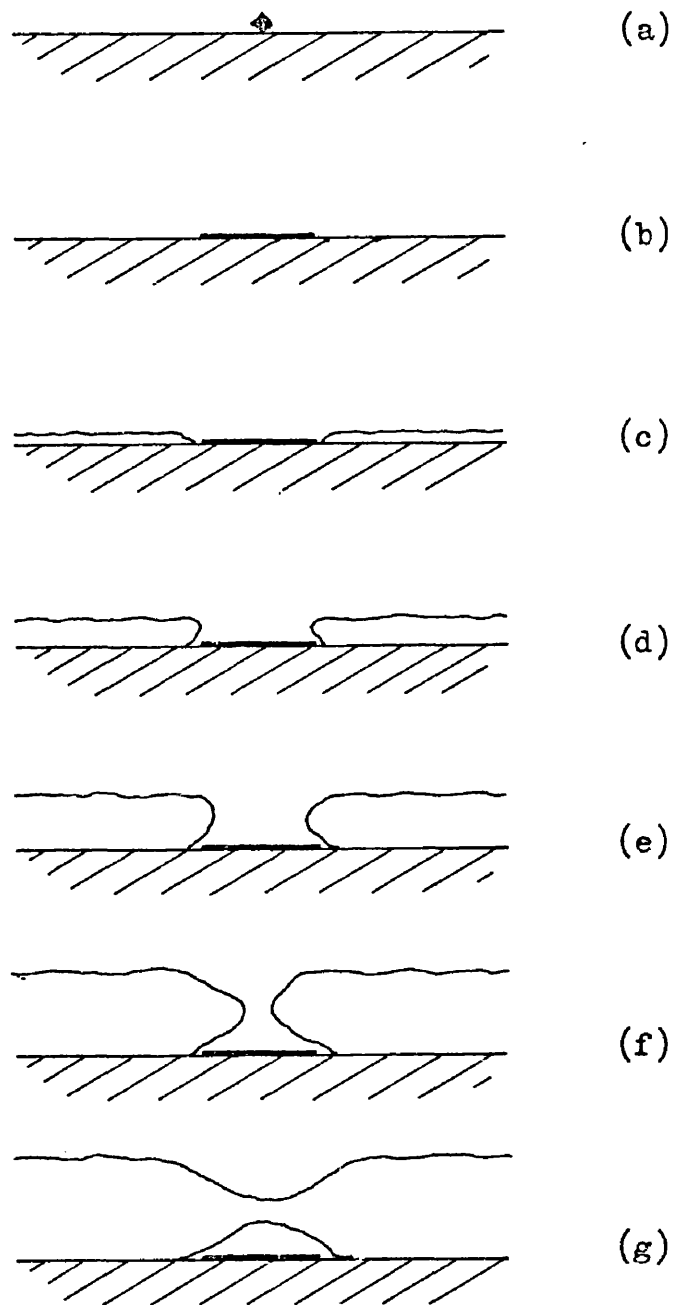


Fig. 4.3 Stages in the growth of a film, illustrating how contamination of the substrate may cause a defect.

reasonable in that defects observed are of the form suggested by fig. 4.3, i.e. hollows in the film surface with holes right through at the centre, the holes being absent in the thickest film.

The first step in preventing formation of pinhole defects is to exercise greater care in keeping the substrate clean before deposition. However, it is doubtful if contamination by airborne matter can be completely eliminated (Jorgenson and Wehner, 1963). A further cleaning process is possible after the substrate is mounted in the vacuum chamber by subjecting it to ionic bombardment in a glow discharge (Holland, 1956), a method which could be quite readily adopted with the unit described in chapter 3 by making the outer earthed cylinder the cathode. A similar cleaning effect is achieved with some of the more sophisticated sputtering methods mentioned in chapter 3, such as asymmetric a.c. sputtering or using a system with biased substrate. Techniques like these would perhaps remove residual substrate contamination. Even if the substrate is perfectly clean pinholes may still be formed. Scharnhorst (1969) has studied pinholes in tin films, the formation of which seems to be unrelated to particulate matter on the surface.

I have dealt with the subject of macrodefects at some length because, as will become evident later, their presence profoundly affects the manner of flux penetration into films. Of particular significance is the fact that holes become filled over if the film

is allowed to grow to a thickness of between 10 and 18  $\mu\text{m}$ . The effect of defects on flux penetration properties will be discussed in chapter 6.

### Grain size

Grain size of thick sputtered films is just large enough to be visible by optical microscope. The granular structure on the surface can be seen in all photographs in fig. 4.2 except (a), and is clearest in the 18.1  $\mu\text{m}$  film (e) where individual grains are visible. They indicate a grain size of the order of 1  $\mu\text{m}$ . Similar grain size was observed in all thick tantalum and niobium films on metallic substrates. M.J. Witcomb (private communication) has examined some niobium films by electron microscopy. His investigations indicate a somewhat smaller grain size within the film — in the range 0.05  $\mu\text{m}$  to 0.3  $\mu\text{m}$  diameter.

### 4.3 Surface topography

In addition to the effect of macroscopic imperfections, the shape and structure of the film surface over the relatively large areas where there are no defects can be a factor which determines the manner of flux penetration. To obtain a quantitative measure of surface roughness, surface profile traces have been taken on some of the specimens using a Talysurf machine at the University of Strathclyde. Talysurf traces are reproduced in fig. 4.4. All traces were taken in an axial direction on the inside surfaces of cylinders.

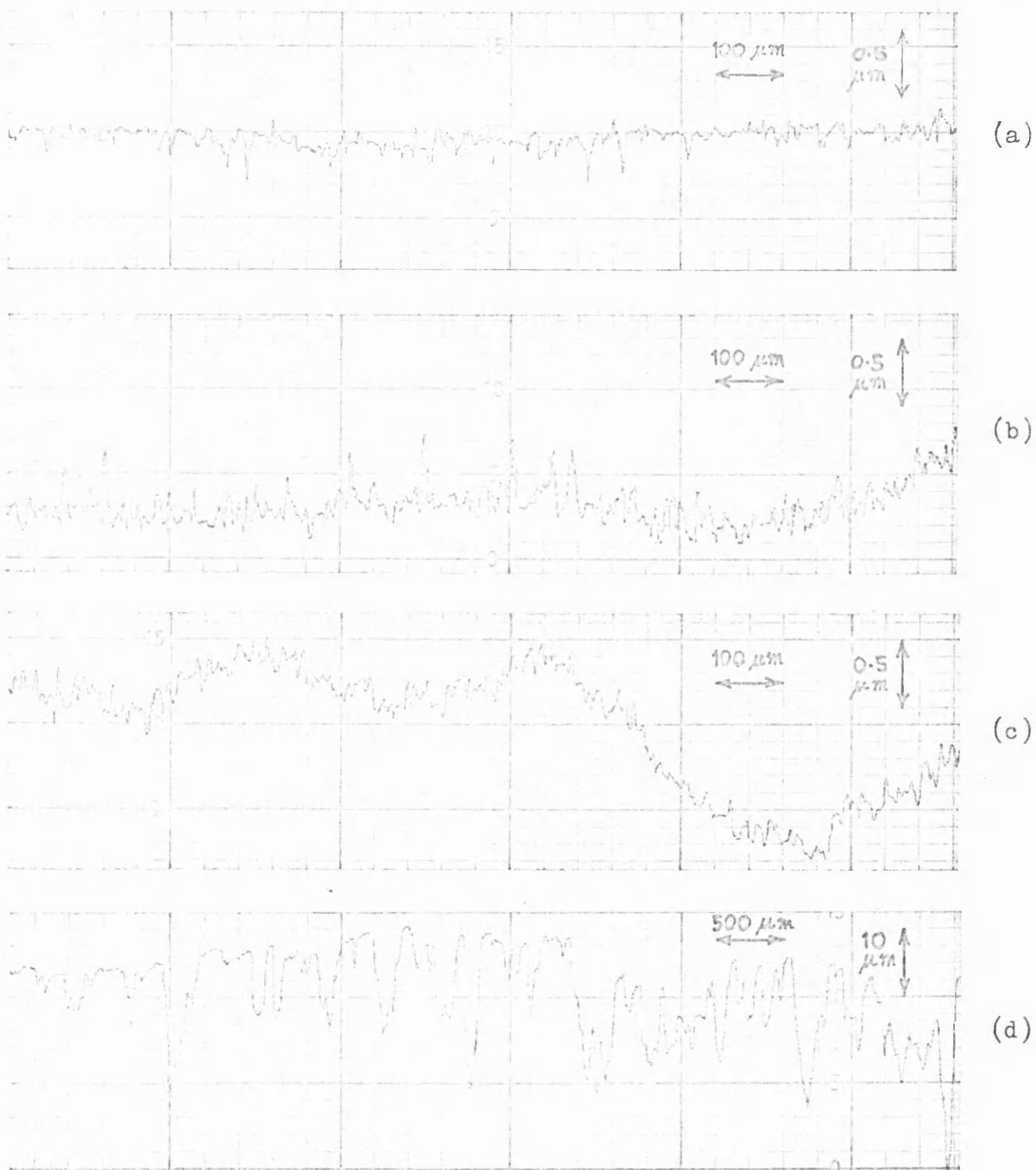


Fig. 4.4 Talysurf profile traces

- (a) Polished stainless steel substrate.
- (b) Film 50, Nb 16.1  $\mu\text{m}$ , deposited on polished substrate.
- (c) Film 47, Nb 19.4  $\mu\text{m}$ , deposited on substrate with smooth but not polished surface.
- (d) As-machined Nb cylinder.

Profile (a) is from a stainless steel substrate with the surface polished to nearly a mirrorfinish ; (b) is the surface of a 16.1  $\mu\text{m}$  thick film deposited on a substrate similar to (a). The film surface is rougher than the substrate by very approximately 0.3  $\mu\text{m}$  peak-to-peak, due presumably to the granular nature of the film. Trace (c) is the surface of a 19.4  $\mu\text{m}$  film on a stainless steel substrate which had a smooth surface, but not highly polished. The microstructure is as in trace (b), but superimposed on this is a larger scale roughness which must be a reflection of the poorer substrate surface finish. The traces show no sign of the pinhole type defects of section 4.2. This is not surprising — as there are only about three such defects per  $\text{cm}^2$  the chances of the Talysurf probe passing over one are small.

Finally at (d) is a Talysurf profile of the as-machined niobium cylinder. The surface is very much rougher than any of the sputtered films, being approximately 10  $\mu\text{m}$  peak-to-peak. (Note the change of vertical and horizontal scales in (d)). The effect of surface roughness on losses will be discussed in chapter 5.

#### 4.4 Impurities and cold work

Superconductive properties of both tantalum and niobium are influenced strongly by microstructure. In this section I shall consider the effects of impurities and cold work, and their relationship to measured values of  $T_c$  and  $H_{c2}$ .

Tantalum

Seraphim et al (1961) have studied the effects of imperfections (microscopic) on the critical temperature of tantalum. Their results show that interstitial oxygen, nitrogen and hydrogen all affect  $T_c$  in the same manner, namely  $T_c$  decreases approximately linearly with increasing interstitial content, the constant of proportionality being  $\sim 0.45$  K per at.%. Seraphim et al interpret this as a mean free path effect. But they show that cold work, even to the extent of decreasing m.f.p. by a factor of ten, has negligible effect on  $T_c$ . Results of Seraphim et al will be used to estimate impurity content in tantalum films from  $T_c$  values.

Niobium

The effects of dissolved gases in niobium have been studied in some detail by De Sorbo (1963), whose findings can be summarized as follows :

(a) Below the solubility limit —

Interstitial oxygen solute decreases  $T_c$  linearly by  $\sim 0.93$  K per at.%;

Interstitial nitrogen solute decreases  $T_c$  linearly by  $\sim 0.45$  K per at.%;

Both oxygen and nitrogen interstitials increase the kappa value ( $\kappa_1 = H_{c2}/\sqrt{2} H_c$ ) linearly by/

linearly by 3.2 per at.% at 4.2 K;

The M-H curve remains nearly reversible.

(b) Above the solubility limit —

The solubility limit for oxygen is  $\sim 3.8$  at.%

and for nitrogen is  $\sim 0.33$  at.%.

When the solubility limit is exceeded the impurities precipitate as oxides or nitrides,  $T_c$  starts to increase and the M-H curve becomes very irreversible. The kappa value continues to increase.

(c) Hydrogen impurity has little effect on  $T_c$ .

#### Cold work in niobium

The effects in niobium of deformation by cold working have been studied by Narliker and Dew-Hughes (1966). Their experiments show that a moderate degree of deformation results in irreversibility but has little effect on  $H_{c2}$ . To apply their findings to the niobium films we require to estimate the amount of deformation, which is introduced by reason of the differential contraction between film and substrate. Using the figures in table 3.1, and applying them to the temperature range  $600^\circ\text{C}$  down to 100 K (below about 100 K coefficients of thermal expansion tend rapidly to zero — Rose-Innes, 1964), the differential contraction results in at most  $\sim 1\%$  deformation when the substrate is copper and  $\sim 0.5\%$  when the substrate is stainless steel.

The article by Narlikar and Dew-Hughes indicates that 1% deformation will have negligible effect on  $H_{c2}$  — and hence on  $\kappa$  — and will introduce only a small degree of irreversibility. So it is not unreasonable to assume that measured  $T_c$  and  $H_{c2}$  values for niobium must be explained purely by the presence of impurities. This is supported by the fact that electron microscope investigations indicate the presence of very few dislocations in the sputtered niobium.

Before going on to measurement techniques to determine  $T_c$  and  $H_{c2}$  for films, the low temperature equipment will be described briefly.

#### 4.4.1 Cryogenic system

A standard silvered double glass dewar assembly is used with liquid nitrogen in the space between inner and outer dewars to act as a heat shield. Most of the experiments on niobium were performed at 4.2 K, but for work on tantalum the temperature had to be lowered by reducing helium vapour pressure in the dewar. A large rotary pump was used in conjunction with a mechanical pressure controller. The pressure controller, whose construction and operation are described in detail by Easson (1967), is capable of maintaining constant bath temperature to within  $\pm 5$  mK for periods of an hour or more, and gives very fine control over bath temperature. Pressure is measured with a precision dial manometer calibrated directly in Kelvins and capable of temperature indication to within  $\pm 1$  mK above 3.5 K and  $\pm 5$  mK above 2.0 K.

#### 4.4.2 Measurement of critical temperature

##### Tantalum films

Two pairs of clips with gold contacts bearing on the film are positioned on the cylinder as shown in fig. 4.5 (inset), the film cylinder being immersed in liquid helium. One pair act as terminals for a d.c. transport current of 100 mA and the voltage drop is measured across the other pair with a d.c. microvoltmeter. When fully normal nearly all the transport current flows in the substrate, resulting in a very small voltage drop, typically 0.4  $\mu$ v for 100 mA in a copper substrate. To make it easier to observe such a small voltage on top of drifting thermal e.m.f.s the current is switched in direction at roughly two second intervals. To obtain temperatures above 4.2 K the dewar is sealed and pressure allowed to rise to the required level, a small heater being used to bring the liquid helium to boiling point before measurements are made.

Typical resistive transition curves are given in fig. 4.5;  $T_c$  is taken as the temperature at which  $R/R_n = 0.5$ . Using findings of Seraphim et al (1961) the total content of interstitial gaseous impurities has been estimated for tantalum films. Results for  $T_c$  and impurity content are given in table 4.1(a). As we are primarily interested in niobium the effects of impurities in tantalum will not be considered further.

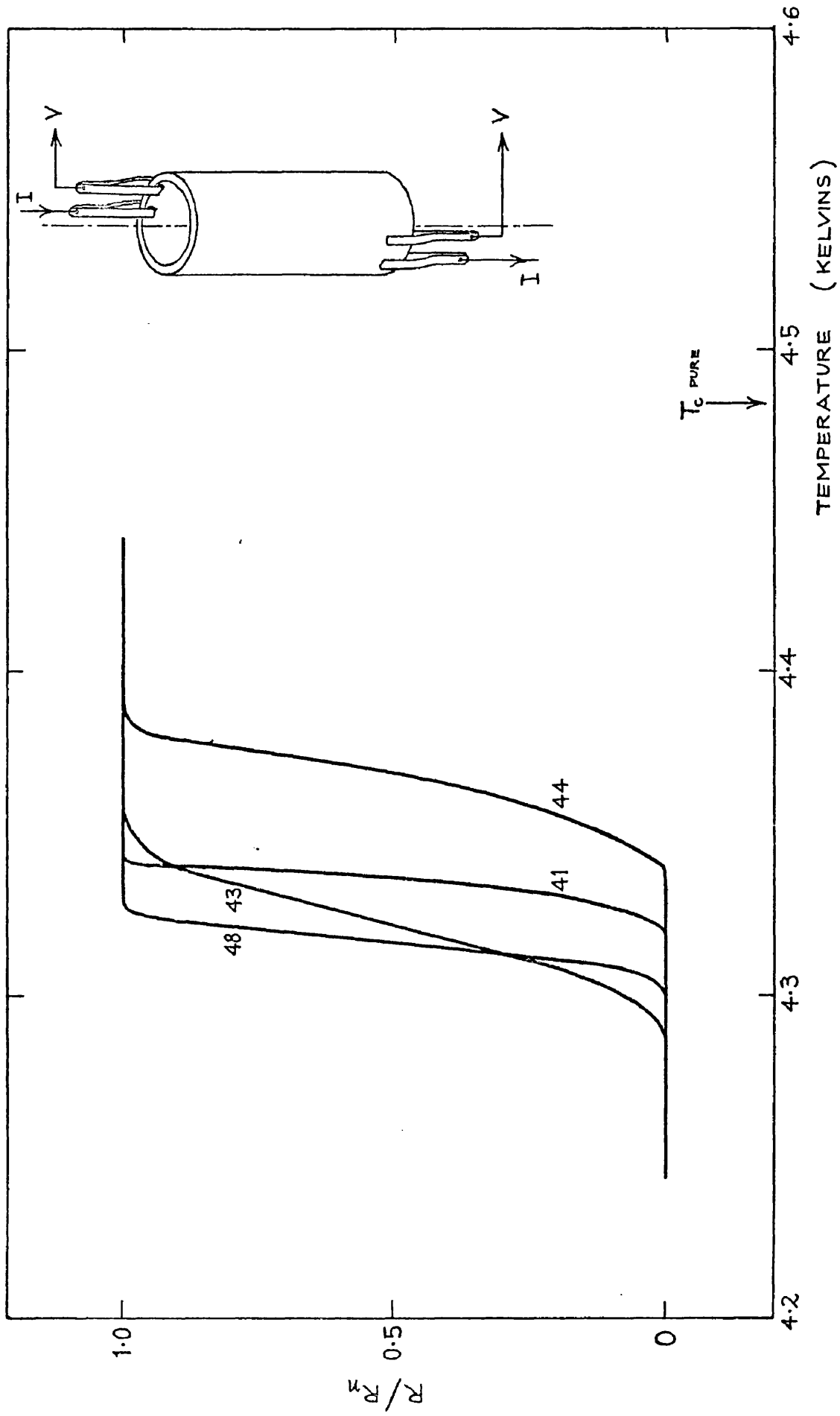


Fig. 4.5 Resistive transition curves for tantalum films.

Niobium films

Critical temperature measurements on niobium films require the cylinder to be placed in the cold gas above the helium bath, under which conditions thermal e.m.f.s at voltage contacts become so unpredictable that the above system cannot be used.  $T_c$  values of niobium films are obtained instead by measuring the temperature dependence of a.c. susceptibility of the cylinder as a whole to a very small a.c. field. The arrangement is illustrated in fig. 4.6. The a.c. solenoid is a single turn of wire carrying 20 mA r.m.s. at 50 Hz (the r.m.s. current in the film when superconducting is therefore  $\sim 20$  mA). The signal from the pickup coil is a maximum when the film is completely normal, and zero when it is sufficiently superconducting to screen the a.c. field completely. Temperature is measured with a calibrated germanium resistance thermometer positioned inside the cylinder as shown in the figure. The thermometer is mounted in a copper block in close contact with the film surface in an attempt to ensure thermal equilibrium with the film. Temperature is varied by moving the arrangement up or down very slowly in the cold gas in the dewar.

Transition curves have been obtained for the as-machined cylinder and for the two thickest niobium films (nos. 47 and 51). The a.c. susceptibility transition curves are quite reproducible, but unfortunately the values of  $T_c$  which they yield are not easily explained.

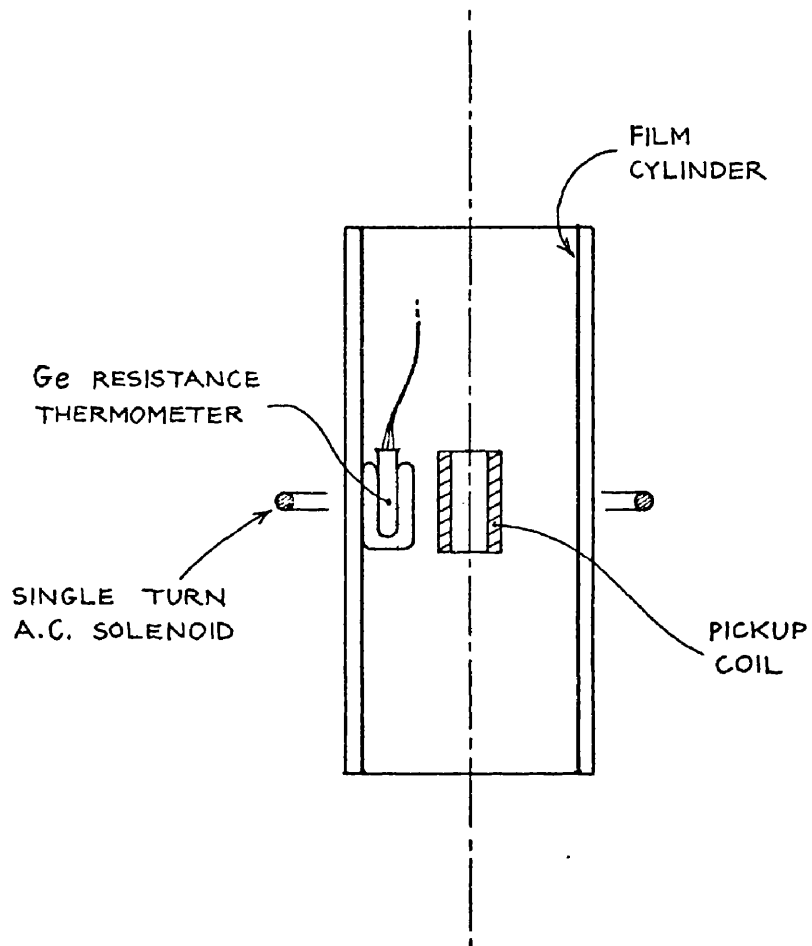


Fig. 4.6 System used to measure  $T_c$  and  $H_{c2}$  of niobium films.

Both films have a measured  $T_c$  about 0.5 K in excess of  $T_c$  for the as-machined niobium. According to De Sorbo (1963) a  $T_c$  in excess of the value for pure niobium indicates the presence of a second phase, i.e. precipitates of oxides or nitrides. Now the electron microscope studies undertaken by M.J.Witcomb (private communication) do not reveal the presence of precipitates in sputtered niobium, i.e. they suggest that gaseous impurities remain in solid solution, a fact which cannot be reconciled with  $T_c$  results.

The only obvious explanation is that the film and germanium thermometer were not in thermal equilibrium, in spite of the precautions taken. If this was so, it is clearly not possible to derive any information about impurity content. Since critical temperature measurements on niobium films did not yield the desired information they were not pursued further, attention being given instead to measurements of upper critical field. However, it should be noted that Ross (1968) measured  $T_c$  for his sputtered niobium films on quartz and found values consistently lower than  $T_c$  for the pure metal.

#### 4.4.3 Measurement of upper critical field

The method of measuring  $T_c$  for niobium films is also used to obtain a measure of  $H_{c2}$ . The film cylinder with single turn solenoid outside and pickup coil inside is immersed in a d.c. field produced by a superconducting solenoid. The solenoid is wound with

Nb-Zr wire in a rectangular cross-section winding, has a length of 78 mm and bore diameter of 41 mm, and can generate a field of up to 14 kOe at the centre of the bore. To measure  $H_{c2}$  the a.c. susceptibility was again observed, this time as a function of d.c. field. The following technique was used : D.C. field was increased until the film cylinder was driven completely normal, then decreased slowly while monitoring the pickup coil signal.  $H_{c2}$  was taken as that d.c. field level at which the very first sign of screening of the a.c. field appeared on the pickup signal.

Let us consider carefully just what is being measured. It should be noted first that the film will probably have a higher than average impurity content at the surface next to the substrate, where deposition begins, due to diffusion of impurities out of the substrate. The film layer next to the substrate may have a relatively high  $H_{c2}$  in which case it will be this layer that will first cause screening in a decreasing field. On the other hand, surface screening currents due to a surface sheath could flow on the inner film surface (they cannot flow on the surface next to the metallic substrate) up to a field  $H_{c3}$  greater than  $H_{c2}$ , in which case the inner surface layer may first cause screening in decreasing field. In either case it seems probable that the measure of critical field will be somewhat in excess of the value of  $H_{c2}$  for the bulk of the film. The method has been used, nonetheless, to give a rough measure of  $H_{c2}$  for niobium films at 4.2 K and for tantalum films at  $0.8 T_c$ .

Table 4.1 (a) gives results of  $H_{c2}$  measurements for two of the tantalum films, and the corresponding  $\kappa_1$  values,  $H_c$  being assumed equal to the value for pure material (included in the table for comparison).  $\kappa_1$  values are appreciably greater than for pure tantalum ; in fact the sputtered films are type II whereas pure tantalum is type I.

The results for niobium are utilised more fully as follows:

- (a) First  $T_c$  and  $H_c$  are assumed to have the values of pure bulk metal, namely 9.20 K and 1550 Oe at  $0.45 T_c$  (French, 1968).
- (b) Using equation 2.10, values of parameter  $\kappa_1$  are calculated.
- (c) From theoretical papers by Maki (1964, 66) which give the ratios  $\kappa_1/\kappa$  and  $\kappa_3/\kappa$  as function of temperature, values of  $\kappa_3$  are calculated. The assumption is made that the theory can be applied to non-ideal material.
- (d) Equation 2.9 defines  $\kappa_3$  in terms of the lower critical field  $H_{c1}$ . This equation only applies for  $\kappa \gg 1$  and short m.f.p. ( $\xi_0/l \gg 1$ ); to obtain  $H_{c1}$  we therefore use a modified expression derived by Tewordt and Newmann (1966) which defines  $H_{c1}$  as a function of  $\kappa_3$  for low values of  $\kappa$ .

- (e) Finally De Sorbo (1963) gives interstitial oxygen and nitrogen content in solution as a function of  $H_{c2}$ . His results are utilized to estimate impurity content of niobium films.

Experimental  $H_{c2}$  values and derived  $\kappa_1$ ,  $\kappa_3$ ,  $H_{c1}$  and impurity contents for sputtered niobium and the machined cylinder are listed in table 4.1 (b). Also included, for purposes of comparison, are some parameters for pure defect free niobium (from French, 1968). As explained above measured values of  $H_{c2}$  are probably rather high. If so, derived results for  $\kappa_1$ ,  $\kappa_3$  and impurity content will be higher, and  $H_{c1}$  lower, than the actual values for most of the film. It can, nevertheless, be concluded that due to the reduction of mean free path by impurities the kappa values of sputtered films are somewhat in excess of the pure niobium value, and critical field  $H_{c1}$  is lower than for pure niobium. The machined niobium cylinder has a higher measured upper critical field than any of the films. The apparent content of gaseous interstitials (based on De Sorbo's relationship between  $H_{c2}$  and impurity) is correspondingly high, although the bulk niobium must, in fact, be purer than the sputtered films. The high value of  $H_{c2}$  must in this case be the result of very severe cold work introduced by machining.

CHAPTER 5FLUX PENETRATION AND LOSSES

In this and the next chapter I shall describe the main experimental work and related results on the nature of flux penetration and dissipation. Chapter 5 is concerned mainly with experiments to measure flux penetration into film cylinders when an a.c. magnetic field is applied parallel to the film surface, and the average power dissipation associated with the process of penetration. The results are discussed and some comparisons made with other work on a.c. losses in niobium.

5.1 Preliminary measurements of screening field of short tantalum cylinders

First I shall deal briefly with some early work on the screening field of tantalum films sputtered onto the inside of short cylinders of quartz (i.d. 23 mm, length 12 mm). Such films could not be made more than  $\sim 1 \mu\text{m}$  thick. Screening field is measured with the arrangement shown in fig. 5.1(a), and is similar to the method used by London and Clarke (1964). A copper solenoid co-axial with the superconducting solenoid provides an a.c. field (50 Hz) superimposed on a d.c. field. A pickup coil is placed inside the thin film ring to measure the rate of change of flux  $\frac{d\phi_i}{dt}$  inside the ring. The coil

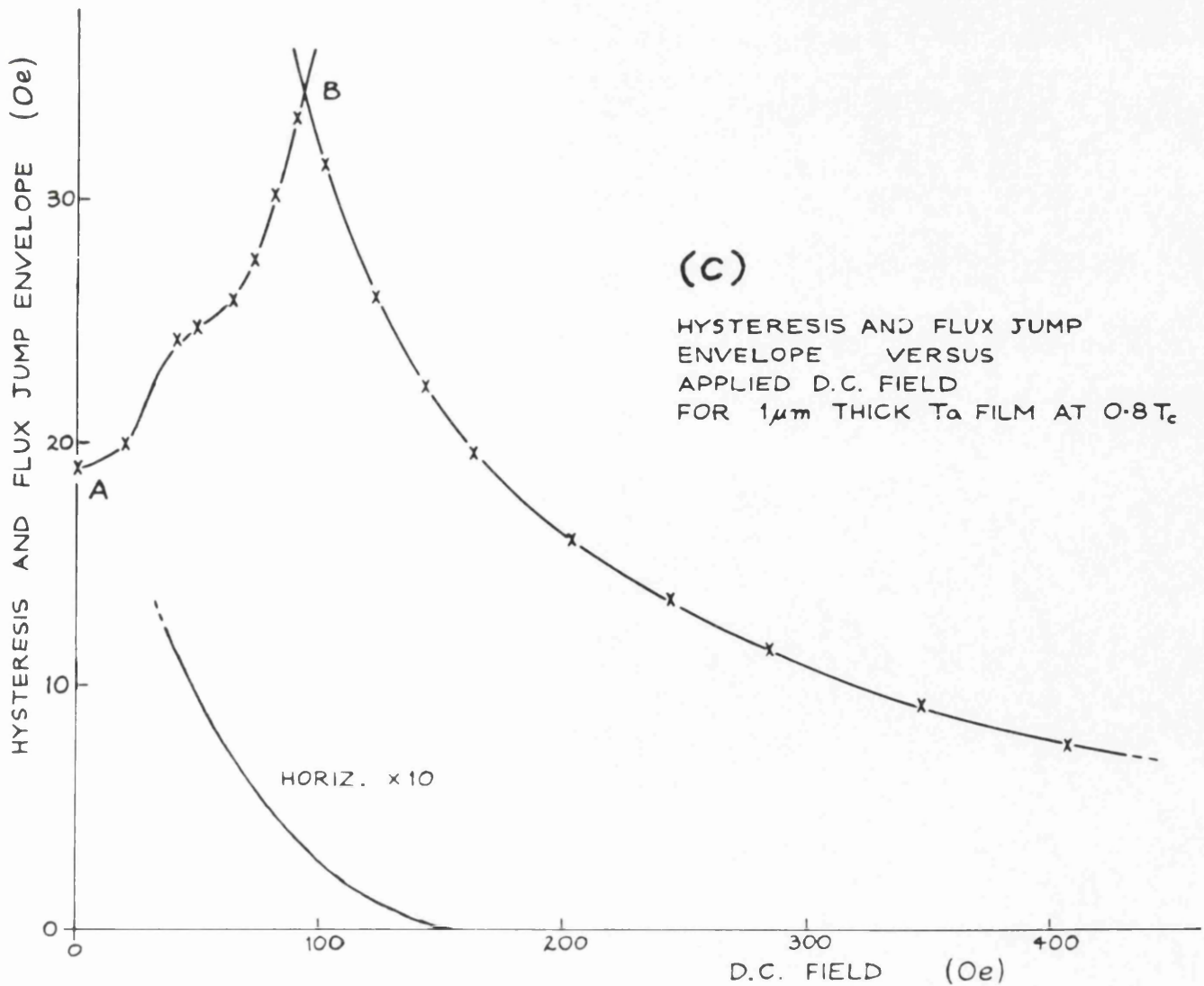
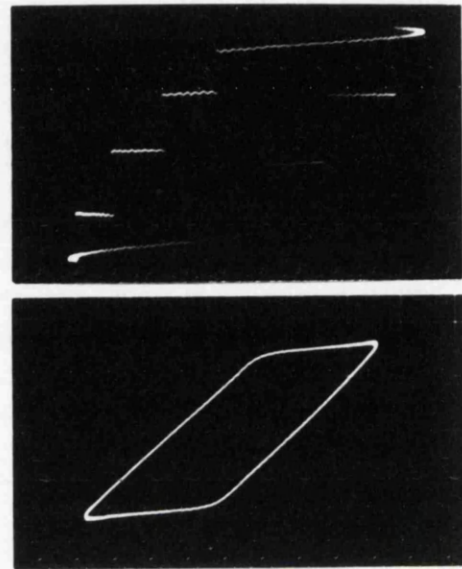
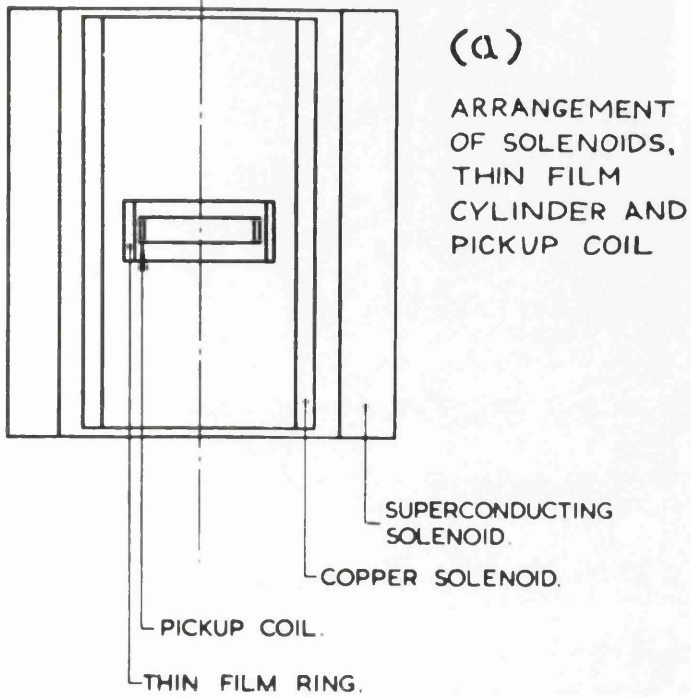


FIG. 5.1 MEASUREMENT OF SCREENING FIELD OF SHORT CYLINDERS

voltage is integrated in a simple RC circuit, enabling one to display the instantaneous a.c. component of flux  $\phi_i$  as the vertical deflection on an oscilloscope. The oscilloscope horizontal deflection is proportional to the a.c. solenoid current, and thus to the a.c. component of applied field. In this manner a hysteresis loop for the ring is displayed.

Typical loops are given in fig. 5.1(b). The screening field associated with the cylinder can be measured from such loops and plotted as a function of d.c. field as at 5.1(c). At low d.c. field levels where screening field tends to be large, flux penetrates into the cylinder bore in large jumps, which can be seen in the upper hysteresis loop. This is the manner of flux penetration from A to B on the graph, the curve between A and B being the size of flux jump envelope as a function of d.c. field. At higher d.c. field levels, above B, flux penetrates smoothly through the film as shown by the lower loop, and hysteresis decreases with increasing field until it becomes zero, in the case illustrated at 1600 Oe.

Similar results have been obtained for other thin tantalum films on quartz which did not peel or craze. Such behaviour in thin film superconducting cylinders has been observed by others, for example Hlawiczka and Ross (1968), London and Clarke (1964), McEvoy (1964). It had been hoped to relate screening properties to a critical state model. But this is not feasible because firstly only very thin ( $\sim 1 \mu\text{m}$ ) films can be deposited on quartz and even these do not behave

consistently, and secondly the inevitable large degree of fringing and field distortion at the cylinder ends makes it impossible to be sure of the manner in which flux penetrates through the film. When it became possible to deposit thick films on long metallic substrate cylinders these experiments were not pursued further. However, they served as a useful introduction to the kind of problems involved in attempting to measure flux penetration into a film in a parallel field.

## 5.2 Flux penetration and losses — experimental methods

The techniques to be described in the remainder of this chapter and the next apply to the relatively thick sputtered niobium and tantalum cylinders listed in table 4.1 and to the as-machined niobium cylinder. As explained in the introduction, in order to approximate to conditions in a co-axial a.c. cable system, it is necessary to apply an a.c. field to one side of the film only ( the side away from the substrate) and to eliminate end effects. The arrangement used is illustrated in fig. 5.2. The photographs in fig. 5.3 show details of construction of solenoid and pickup coils and their positions relative to each other and the film cylinder.

### The a.c. solenoid

A solenoid of pure niobium wire is placed co-axially inside the cylinder. As long as the film screens the field completely the

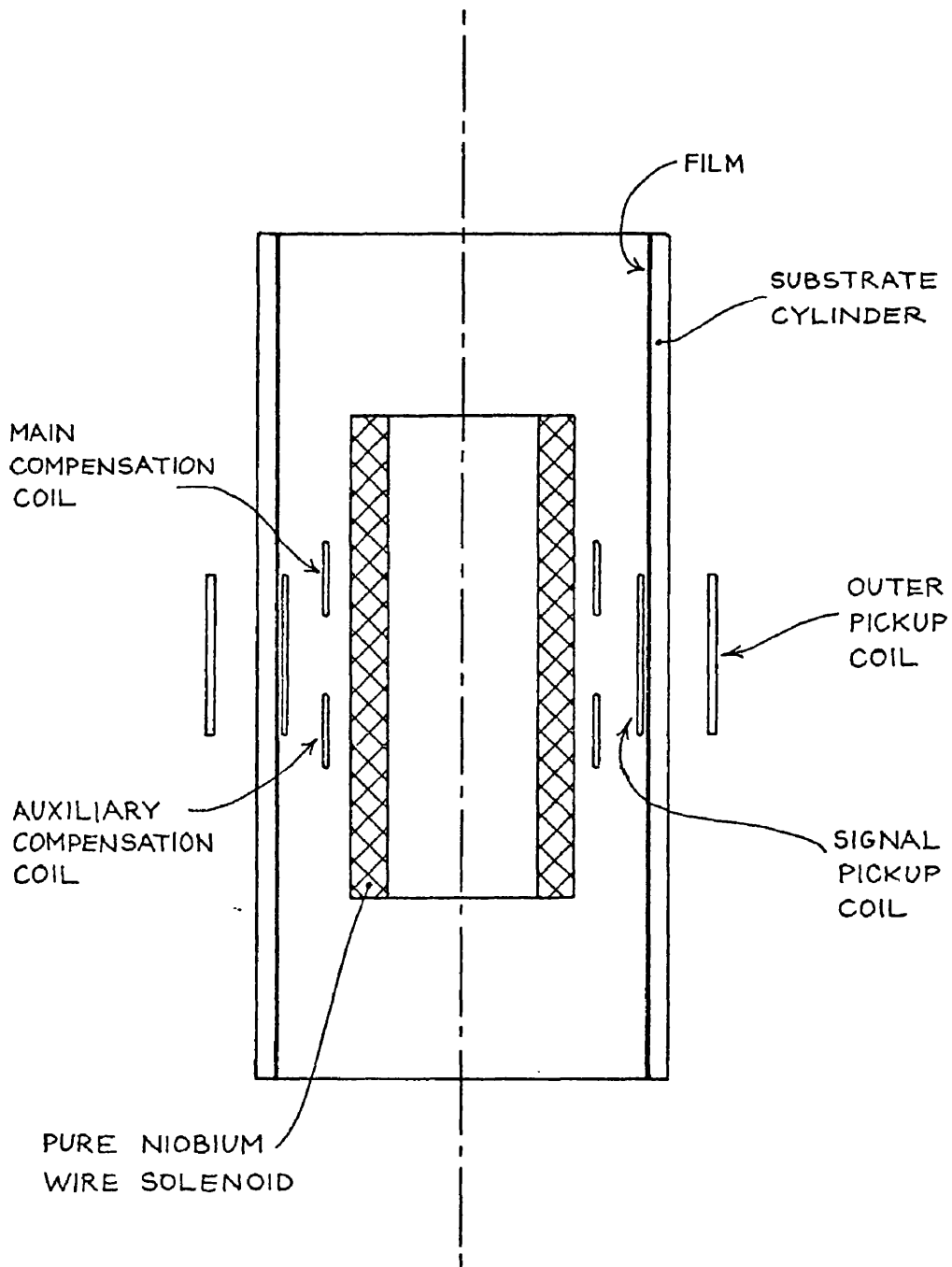


Fig. 5.2 Sectional view of assembly for observing flux penetration into films.

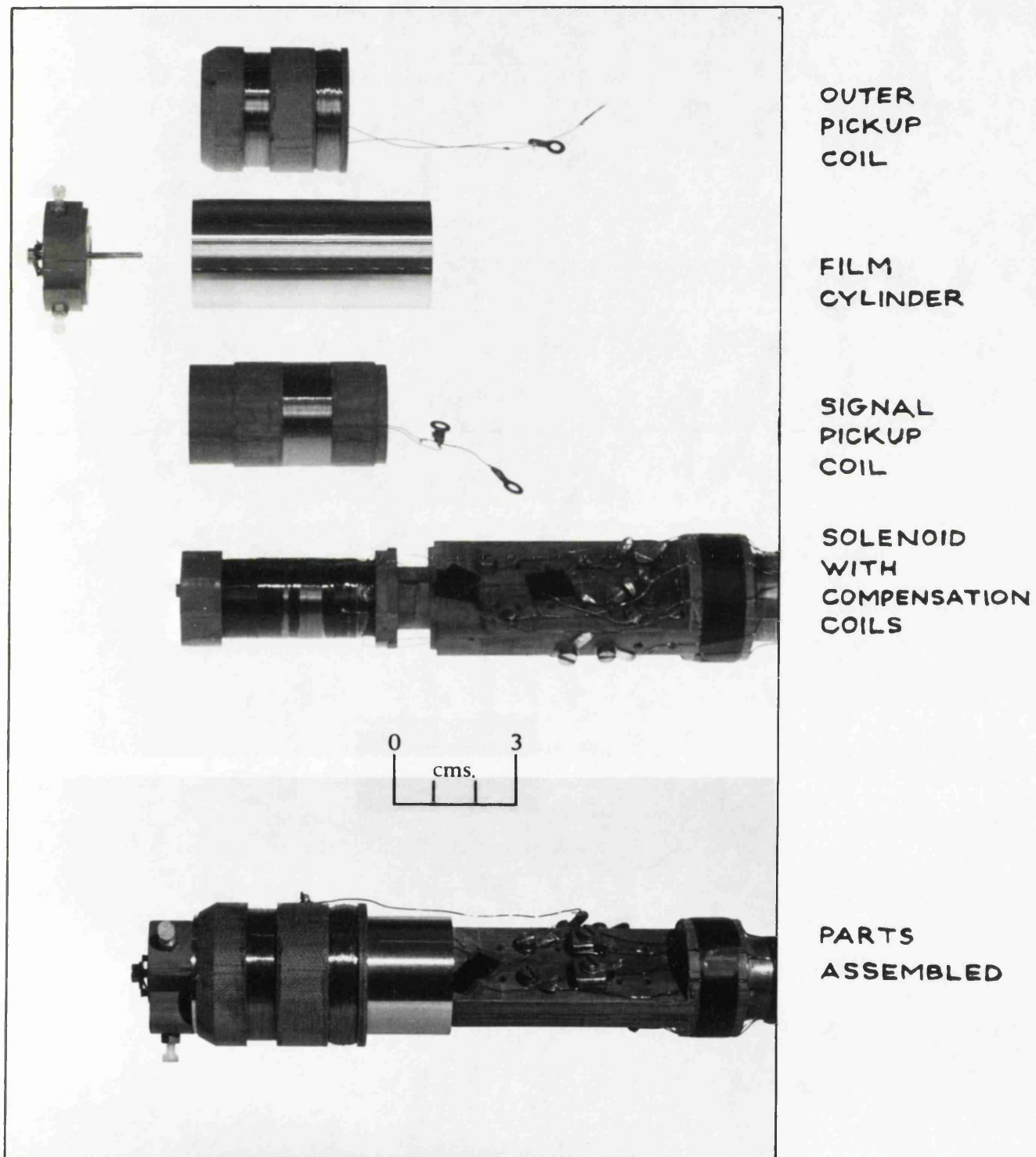


FIG. 5-3 APPARATUS FOR OBSERVING FLUX  
PENETRATION INTO FILMS.

field return path is confined to the annular space between solenoid and film, and since the solenoid is shorter than the cylinder end effects are not present. An experiment described in chapter 6 verifies that flux penetration is confined to the central region of the cylinder. The niobium solenoid can generate a peak a.c. field of 1330 Oe before going normal.

It is fed from 50 Hz mains via a variac, step-down transformer, ammeter and series L-C circuit tuned to 50 Hz. The tuned circuit, consisting of a bank of capacitors and a large liquid nitrogen cooled solenoid, gives an overall Q-factor of 19, and serves to reduce harmonics from the mains which would otherwise interfere with the observation and proper compensation of flux penetration waveforms. The solenoid was calibrated by placing a pickup coil with accurately known dimensions and turns in the annular space and observing the output when the a.c. field was sufficiently low that no flux penetration into the film occurred. The calibration factor determined in this way is 760 Oe peak in annular space per amp r.m.s. solenoid current.

#### Pickup coils

To monitor flux penetration into the film a system is used which is basically similar to that employed by Easson and Hlawiczka (1967). A pickup coil, referred to as the signal coil and consisting of a single layer of about 180 turns, is placed as shown in the figure

very close to the film surface in the middle of the region where field is applied. The voltage from the signal coil consists of two components ; there is a sinusoidal component in phase with field due to the finite thickness of the pickup coil wire and the small gap between coil and film — this will be termed the direct pickup voltage ; there is a non-sinusoidal component due to flux penetration into the film itself — this is termed the penetration voltage. To observe the waveform of flux penetration into the film a compensation system (Easson and Hlawiczka 1967, Buchhold 1963) must be used to eliminate the direct pickup voltage.

Compensation coils are placed in the annular space as shown in the diagram, and are positioned some distance from the film surface as compared with the signal coil so that the compensation voltage is a true replica of applied field waveform. The main compensation coil is put in series opposition with the signal coil and is wound with sufficient turns to cancel most of the direct pickup voltage. The nearly-compensated signal is put in series with the voltage from the auxiliary compensation coil which has first been passed through a simple variable attenuation and phase shift circuit. This is shown more clearly in the block diagram in fig. 5.4. By adjusting attenuation and phase settings of the compensation circuit the small remaining direct pickup component can be eliminated, leaving only the flux penetration signal. One would expect only the amplitude of the auxiliary compensation to require adjustment since it should

be in phase with the direct pickup voltage. But in practice small phase shifts do occur, presumably due to leads and circuitry, so that slight phase adjustment is necessary. The criteria adopted to determine when the signal is properly compensated are discussed in section 5.4. Finally, a pickup coil is placed round the outside of the film cylinder to detect the onset of flux penetration right through to the outside.

### 5.3 The loss measuring system

First, a note on notation. The sinusoidal 50 Hz field in the annular space will be referred to as  $H$ , with peak value  $H_m$ . i.e.

$$H = H(t) = H_m \sin \omega t \quad (5.1)$$

The peak field at which non-linear flux penetration into the film is first detected will be called  $H_{m1}$ , and the field at which flux penetration right through the film to the outside occurs will be  $H_{m2}$ . The total flux which has penetrated irreversibly (that is, excluding flux penetration to the London penetration depth) into the film is termed  $\phi(t)$ , or simply  $\phi$ , and has peak value  $\phi_m$ . The voltage from the signal pickup coil,  $e_1(t)$ , when properly compensated is proportional to  $d\phi/dt$ , thus

$$e_1(t) = n \frac{d\phi}{dt} \quad (5.2)$$

where  $n$  is number of turns on signal coil. The instantaneous energy

dissipation in the film is  $P(t)$ , the mean value per unit area of film surface being represented by  $\bar{P}$ .

Now, the instantaneous rate of flow of energy into the specimen can be derived from Poynting's energy flow vector (Easson and Hlawiczka 1967). The rate of energy flow at any instant is given by

$$\frac{dW}{dt} = \frac{1}{4\pi} (\underline{E} \times \underline{H}) \quad \text{in c.g.s. units per unit surface area of sample,}$$

where  $\underline{E} \times \underline{H}$  is the Poynting vector. In the simple slab geometry with  $\underline{E}$  and  $\underline{H}$  mutually perpendicular

$$\left| \frac{dW}{dt} \right| = \frac{1}{4\pi} EH \quad .$$

The electric field  $E$  is caused by the rate of change of flux at the sample surface, thus

$$E = - \frac{1}{b} \cdot \frac{d\phi}{dt}$$

where  $b$  is the length of the perimeter of the sample, in this case the circumference of the inside of the film. Hence

$$\left| \frac{dW}{dt} \right| = \frac{1}{4\pi b} H \frac{d\phi}{dt} \quad .$$

The power loss in one cycle is obtained by integrating over a cycle,

$$\begin{aligned}\bar{P} \text{ (one cycle)} &= \frac{1}{4\pi b} \oint H \frac{d\phi}{dt} dt \\ &= \frac{1}{4\pi b} \oint H \cdot d\phi \quad .\end{aligned} \quad (5.3)$$

This is equivalent to saying that the area of the  $\phi$  versus  $H$  hysteresis loop gives power loss per cycle. The mean dissipation at frequency  $f$  is then

$$\bar{P} = \frac{f}{4\pi b} \oint H(t) \cdot \frac{d\phi(t)}{dt} \cdot dt \quad \text{per unit area} \quad (5.4)$$

The quantities  $H(t)$  and  $d\phi(t)/dt$  are directly observable as applied field and compensated pickup voltage respectively. Mean dissipation can be measured directly by taking the time average of the product of these two quantities.

### Electronic wattmeter

The system used to perform this function is shown in block diagram form in fig. 5.4. The compensated voltage from signal pickup coil  $e_1$  is first fed to a Tektronix type RM 122 pre-amplifier which has noise level of 5  $\mu\text{v}$  r.m.s. (referred to input) and gain  $G$  of 100 or 1000. The amplified signal is applied to the input of a switched-gain amplifier. A signal proportional to  $H(t)$  is taken from across a 0.5 ohm resistor in series with the solenoid and applied to a second

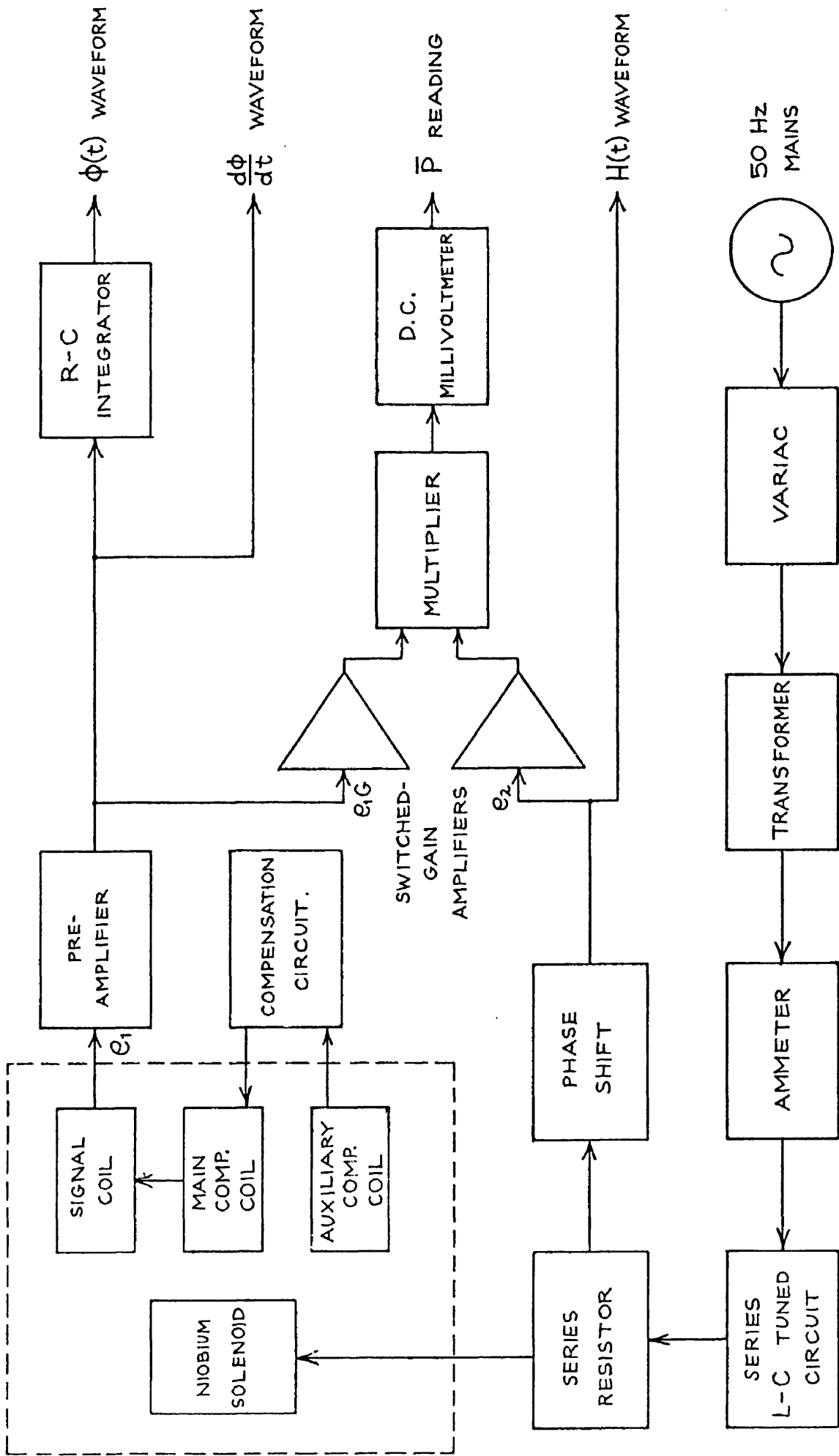


Fig. 5.4 Block diagram of system. The broken rectangle encloses parts immersed in liquid helium.

switched-gain amplifier. This signal, referred to as  $e_2(t)$ , should be in phase with  $H(t)$  and therefore in the correct phase relationship with  $e_1(t)$ ; in practice it is found that, as with the compensation system, a phase shift network is required in the  $e_2$  channel. Outputs from the switched-gain amplifiers are taken to a Fenlow type MC 101 analogue multiplier whose output is monitored on a d.c. millivoltmeter. In use the gains of the amplifiers preceding the multiplier are switched to settings which give maximum signal levels at the multiplier inputs without exceeding saturation limits. The frequency response of the  $e_1$  channel is limited at the low end by the pre-amplifier to 0.2 Hz, and at the high end by the multiplier to 30 kHz.

The d.c. millivoltmeter has a time constant much longer than 20 ms. Hence it gives a reading  $\bar{E}$  which is proportional to the time-average of the product  $Ge_1e_2$ . i.e.

$$\bar{E} \propto \int e_1 e_2 dt$$

$$\text{But } e_1(t) = -n \frac{d\phi(t)}{dt} \quad \text{and} \quad e_2(t) \propto H(t)$$

$$\bar{E} \propto \int H(t) \cdot \frac{d\phi(t)}{dt} dt$$

Thus from equation 5.4,  $\bar{E} \propto \bar{P}$ ; the voltmeter reading is a direct measure of mean energy dissipation in the film. Other quantities can also be observed by displaying on an oscilloscope signals at appropriate points in the system, as shown in the block diagram. The pre-amplifier output is the  $d\phi/dt$  signal, which can be integrated in a simple R-C

circuit with time constant of 0.2 seconds to give the  $\phi$  waveform.  $\phi$ -H loops are displayed by using the  $\phi$  signal as vertical deflection and a signal from the  $e_2$  channel as horizontal deflection on an oscilloscope.

### Calibration, sensitivity and accuracy

The electronic wattmeter was calibrated by passing a known 50 Hz current through the solenoid series resistor and applying a known 50 Hz voltage to the  $e_1$  channel at the input to the switched-gain amplifier, and adjusting their relative phase to give a maximum d.c. voltage reading  $\bar{E}$ , which occurred when they were in phase. By taking into account the signal coil turns  $n$ , the pre-amplifier gain  $G$ , the inside circumference of the film  $b$ , the solenoid calibration factor and the settings of the switched-gain amplifiers, an overall calibration factor was determined.

If the flux penetration waveform is properly compensated the system sensitivity should depend only on  $n$ ,  $b$  and the low frequency noise level at the pre-amplifier input. In practice, however, it was found that lack of accuracy limited the sensitivity through uncertainty about the precise degree of compensation required. On approaching the more sensitive settings of the wattmeter the reading became increasingly affected by very small changes in the degree of compensation, the limit being determined by the point at which the power loss reading was of the same order as the reading due to

uncertainty in adjusting compensation. This limit was found to correspond to a  $\bar{P}$  reading of about  $0.01 \mu\text{W}/\text{cm}^2$ , and loss measurements below  $0.1 \mu\text{W}/\text{cm}^2$  were of doubtful accuracy ; they only served to indicate general trends.

Accuracy was checked at high dissipation levels by comparing readings on the wattmeter with measured areas of corresponding  $\phi$ -H loops as displayed on an oscilloscope. Above  $0.2 \mu\text{W}/\text{cm}^2$ , measured losses by the two methods were within  $\pm 25\%$ , with agreement improving at higher loss levels.  $\pm 25\%$  may seem rather poor, but it should be noted that losses are measured over more than three orders of magnitude and vary steeply with applied field, so greater accuracy is not necessary.

#### 5.4 Penetration waveforms and compensation

Typical compensated  $d\phi/dt$  waveforms,  $\phi$  waveforms and  $\phi$  versus H hysteresis loops for flux penetration into some thick sputtered tantalum and niobium films are illustrated by the photographs of oscilloscope displays in fig. 5.6. For these photographs  $H_m < H_{m2}$ , i.e. there is no flux penetration through the film to the outside.

#### Compensation procedure

An explanation will now be given for the criteria used to determine the precise degree of compensation required to remove the direct pickup from the output of the signal coil so that waveforms

displayed are due only to flux penetration into the film. From detailed analysis of critical state models Easson and Hlawiczka (1967) show that at the turning points of applied magnetic field, i.e.  $\pm H_m$ ,  $d\phi/dt = 0$  and  $d^2\phi/dt^2 = 0$ . This is illustrated in fig. 5.5, which is reproduced from their article. It shows waveforms for  $\phi(t)$  and  $d\phi/dt$  derived from a simple Bean-London critical state model, and their relationship in time to the sinusoidal applied magnetic field. If it is assumed that experimental waveforms also possess these properties, then the two conditions can be used to determine correct compensation. The magnitude and phase of the sinusoidal signal from the auxiliary compensation coil are adjusted in the compensation circuit until the displayed  $d\phi/dt$  waveform satisfies the above conditions. Fig. 5.6(a) illustrates one half-cycle of a correctly compensated  $d\phi/dt$  waveform; the points at which  $\phi'$  and  $\phi''$  are both zero are easily located by sharp kinks which occur at the peaks of applied field.

The conditions  $\phi' = \phi'' = 0$  apply not only to critical state models, but to any model of flux penetration in which flux trapping occurs at  $\pm H_m$ . If sheath currents are present and there is a surface screening field such that no flux leaves the specimen until applied field is reduced from  $H_m$  to  $H_m - \Delta H$ , then  $d\phi/dt$  will remain equal to zero during this time. This feature, which can be seen in waveform (a), lends support to the compensation criteria.

But when we study the experimental waveforms for some of the other films difficulties arise. Consider the half-cycle  $d\phi/dt$  waveforms

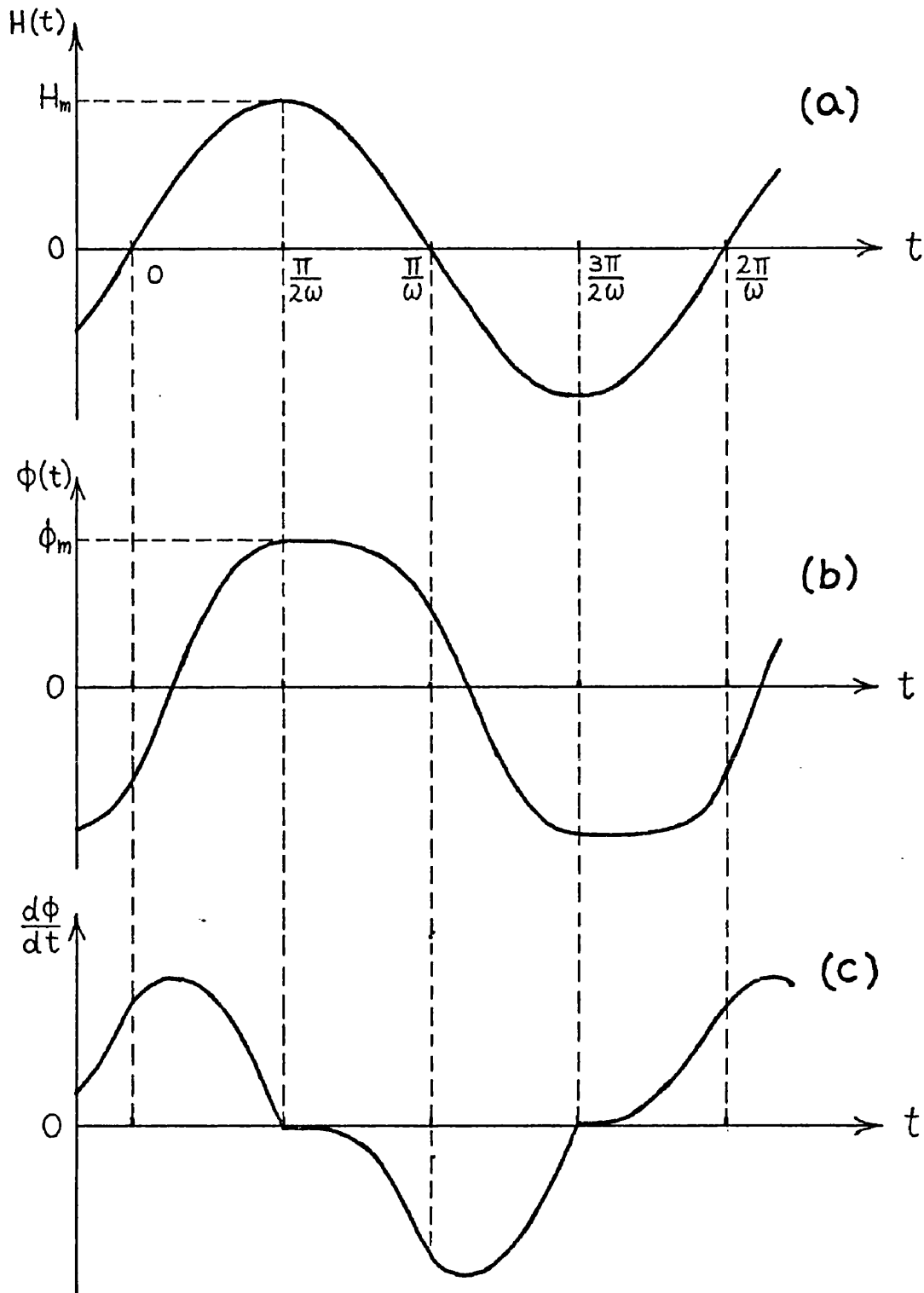
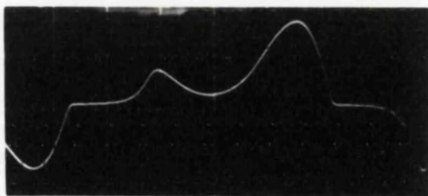


Fig. 5.5 Waveforms derived from the Bean-London critical state model. (From Easson and Hlawiczka, 1967.)

- (a) Applied field sinewave
- (b)  $\phi(t)$  waveform
- (c)  $d\phi/dt$  waveform

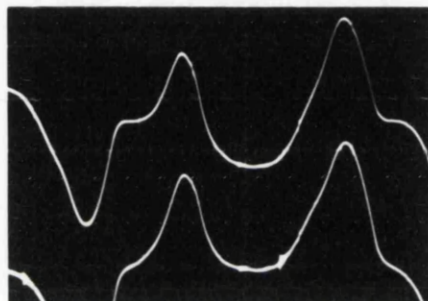
FILM 48 Ta 23.6  $\mu\text{m}$ .



(a)  $d\phi/dt$  WAVEFORM (HORIZ: 2ms/DIV.)  
AT 0.6  $T_c$ ,  $H_m = 340$  Oe.



(b)  $\phi$ -H LOOP  
AT 0.45  $T_c$ ,  $H_m = 500$  Oe.



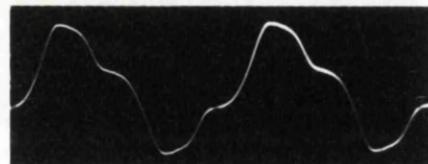
FILM 47 Nb 19.4  $\mu\text{m}$   $H_m = 980$  Oe.

(c)  $d\phi/dt$  WAVEFORMS (HORIZ: 2ms/DIV.)  
SHOWING TWO POSSIBLE  
COMPENSATION SETTINGS.

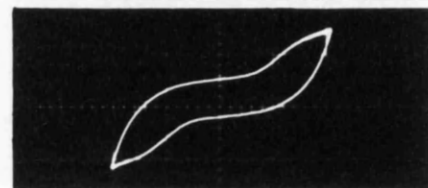


FILM 50 Nb 16.1  $\mu\text{m}$   $H_m = 980$  Oe.

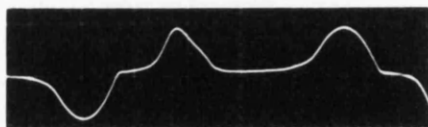
(d)  $d\phi/dt$  WAVEFORM (HORIZ: 5ms/DIV.)



(e)  $\phi$  WAVEFORM (HORIZ: 5ms/DIV.)

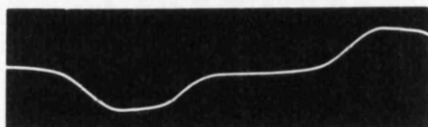


(f)  $\phi$ -H LOOP.

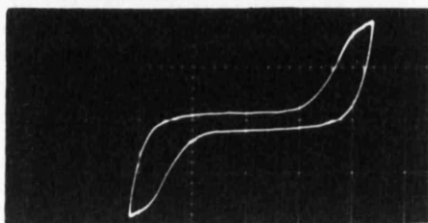


FILM 51 Nb 24.7  $\mu\text{m}$   $H_m = 1100$  Oe.

(g)  $d\phi/dt$  WAVEFORM (HORIZ: 2ms/DIV.)



(h)  $\phi$  WAVEFORM (HORIZ: 2ms/DIV.).



(j)  $\phi$ -H LOOP.

FIG. 5.6 SOME FLUX PENETRATION WAVEFORMS AND HYSTERESIS LOOPS FOR SPUTTERED Ta AND Nb FILMS. (ALL Nb FILMS AT 4.2 K).

in fig. 5.6(c) for a 19.4  $\mu\text{m}$  niobium film. If the criteria above are adopted for compensation the waveform appears as in the upper trace; this is an impossible situation in that it implies that  $d\phi/dt$  becomes negative (i.e. flux leaves the specimen) in an increasing applied field, and vice-versa. In this case it seems more correct to adjust compensation until the waveform is as in the lower trace;  $d\phi/dt$  is now positive or zero when H is increasing, negative or zero when H is decreasing, but implies that flux trapping does not occur at  $\pm H_m$ . When these difficulties arose it was decided to adopt another compensation procedure as follows : The applied field was increased to just below  $H_{m1}$  (just below the point at which flux penetration could be detected) and, with vertical sensitivity at a maximum, the compensation adjusted until the  $\phi$ -H display appeared as a horizontal straight line. Applied field was then increased to the desired level and waveforms or loops observed without further compensation adjustment. The remaining photographs in fig. 5.6, (b) and (d) to (j), were taken using this compensation method, as were all measurements of power loss.

#### Flux penetration into thinner films

Attempts have been made to observe flux penetration into and measure losses in most of the specimens listed in table 4.1. No results were obtained for any film thinner than 16  $\mu\text{m}$ . When an a.c. field is applied to the inner surface of such film cylinders it is found that no flux penetration into the film can be detected before

the occurrence of penetration through the film to the outside, i.e.  $H_{m2}$  is equal to  $H_{m1}$ . Experimental values of  $H_{m1}$  and  $H_{m2}$  are listed in table 5.1. For purposes of later comparisons  $H_{c1}$  values as derived in chapter 4 are included.

There is little point in taking results beyond the stage at which magnetic flux in the film penetrates through to the outside, as we then have no knowledge of the manner of flux distribution within the film. Therefore measurements of flux penetration and losses have been confined to the 23.6  $\mu\text{m}$  thick tantalum film, the three thickest niobium films (16.1, 19.4, 24.7  $\mu\text{m}$ ) and the as-machined niobium cylinder. Regarding the niobium cylinder machined from bulk, flux penetration into the specimen was found to begin at very low applied field, even at field levels approaching zero.  $H_{m2}$  was in excess of the solenoid maximum field. Comments on the significance of  $H_{m1}$ ,  $H_{m2}$ , flux penetration waveforms and hysteresis loops are reserved until section 5.6.

## 5.5 Results of loss and flux penetration measurements

Using the electronic wattmeter with the compensation procedure described above, measurements of mean power loss  $\bar{P}$  as a function of peak applied field  $H_m$  have been made on the three thickest niobium films, the machined niobium cylinder and the thickest tantalum film. The peak total flux  $\phi_m$  versus  $H_m$  has also been measured for these

Film	Thickness $\mu\text{m}$	$H_{c1}$ (from ch.4) Oe	$H_{m1}$ Oe	$H_{m2}$ Oe
43 Ta	4.1	-	260	= $H_{m1}$
48 Ta	23.6	-	160	380
45 Nb	6.5	410	250	= $H_{m1}$
49 Nb	10.3	540	840	= $H_{m1}$
50 Nb	16.1	450	530	1130
47 Nb	19.4	500	550	1060
51 Nb	24.7	480	640	1090
As-machined Nb	$\sim 250$	400	see text	$> 1330$

Table 5.1 Measured values of  $H_{m1}$  and  $H_{m2}$ .

Ta films, at  $0.6 T_c$ ; Nb films, at 4.2 K.

specimens. Measurements on niobium were at 4.2 K (corresponding to  $0.45 T_c$  if  $T_c$  is assumed to be 9.2 K) and for the tantalum film the temperature was 1.97 K, again equal to  $0.45 T_c$ . Niobium specimens will be discussed first. The results are presented in fig. 5.7. It will be noticed that  $\bar{P}$  and  $\phi_m$  graphs for niobium films have been extended into the region above  $H_{m2}$  where flux penetrates to the outside of the cylinder for part of each cycle. Only the 19.4  $\mu\text{m}$  thick film displays a change in behaviour at  $H_{m2}$ ; as this is one isolated result it may be co-incidental.

$\bar{P}$  versus  $H_m$  results will now be compared with Easson and Hlawiczka (1968), Rocher and Septfonds (1967) and Buchhold and Rhodenizer (1969), whose work, as mentioned in chapter 1, is sufficiently similar to enable comparisons to be drawn.

#### Comparison with Easson and Hlawiczka (1968)

Easson and Hlawiczka have measured losses in niobium slabs in a parallel a.c. field using an electronic wattmeter system similar to the above. They obtained  $\bar{P}$  as a function of  $H_m$  at 4.2 K in a 50 Hz field on specimens machined from bulk and on rolled foils, both materials having been subjected to various surface treatments. Their results are compared with present work in fig. 5.8(a). Easson and Hlawiczka measured surface profile of their specimens with a Talysurf and found the following for average peak-to-peak surface roughness :

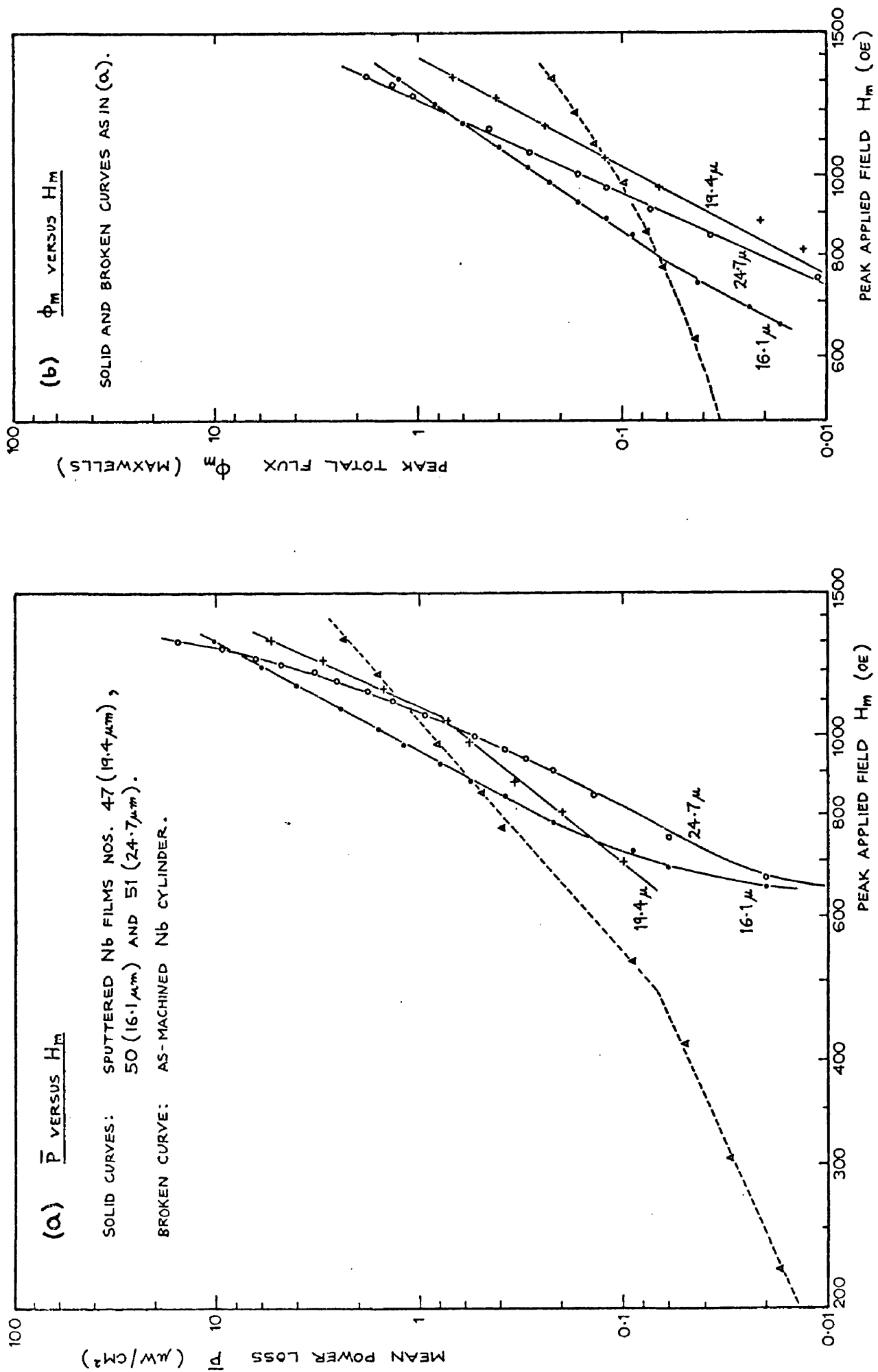


FIG. 5.7 RESULTS OF LOSS AND FLUX PENETRATION MEASUREMENTS.

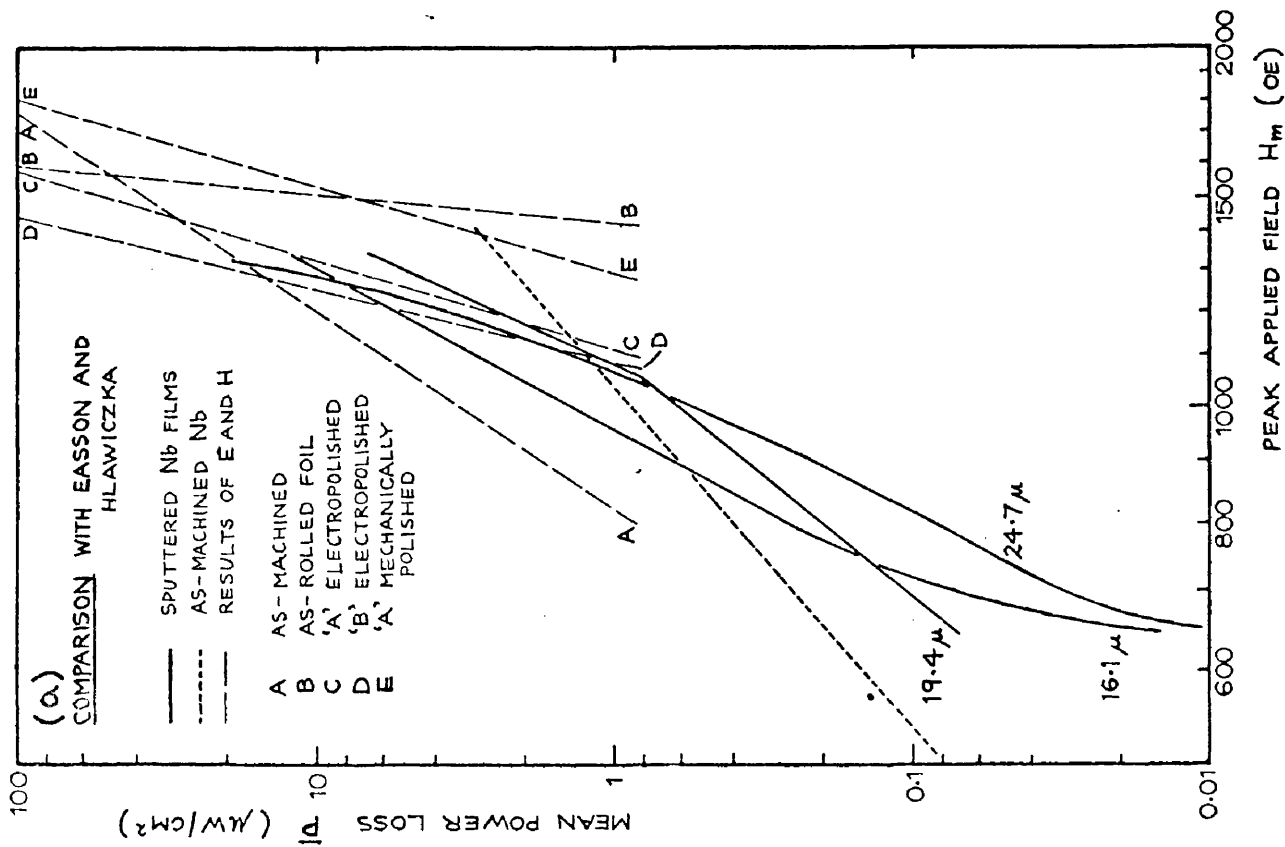
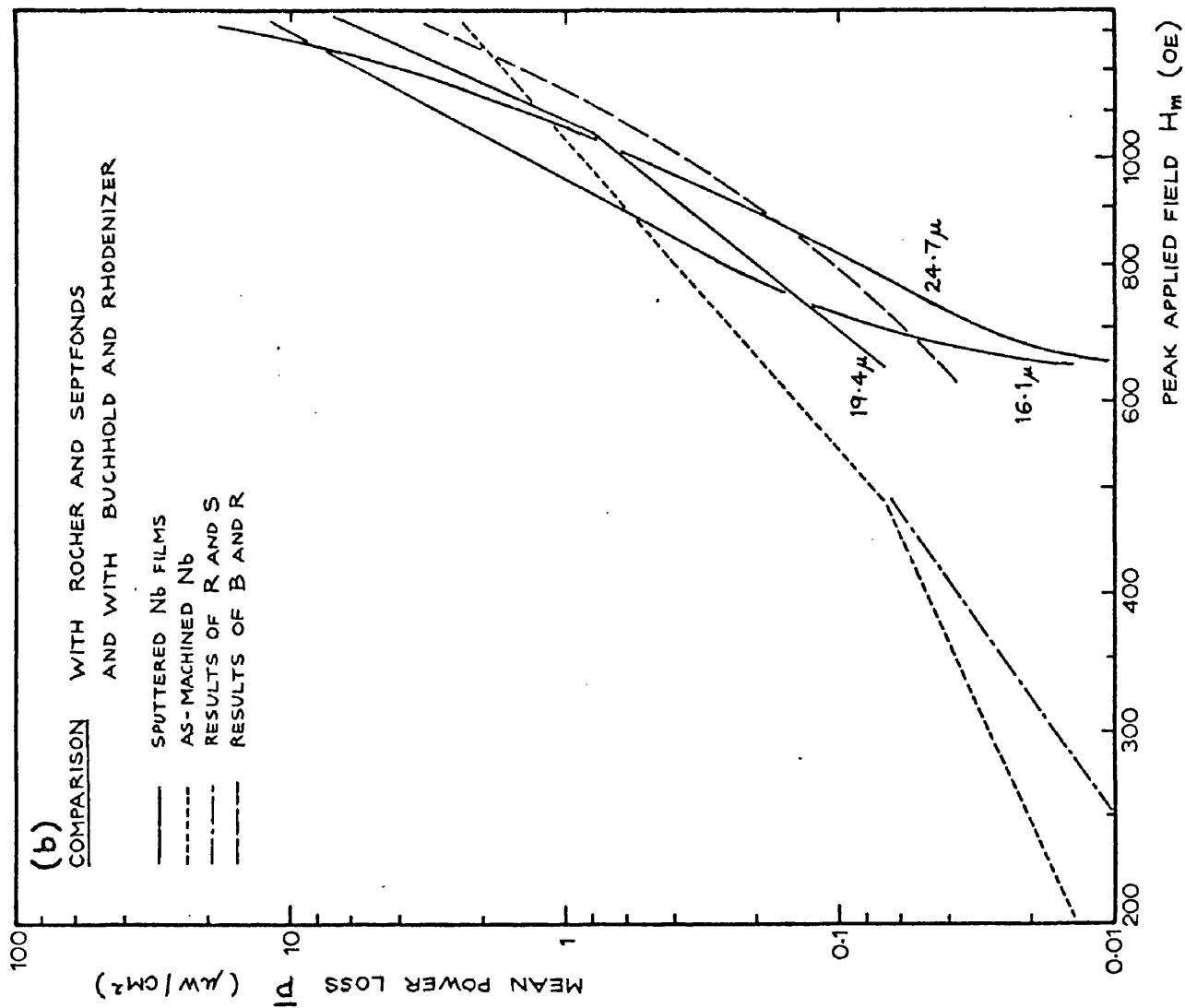


FIG. 5.8 COMPARISON OF LOSS MEASUREMENTS WITH OTHER WORK ON NIOBIUM.

As-machined niobium	~ 5 $\mu\text{m}$
As-machined or as-rolled, then electropolished	~ 5 $\mu\text{m}$
Mechanically polished	~ 0.3 $\mu\text{m}$
As-rolled	~ 0.3 $\mu\text{m}$

The Talysurf traces presented in chapter 4 indicate that sputtered niobium films have a surface finish comparable with mechanically polished or as-rolled material. However, in the range where results overlap, losses in the films occur at a lower field than in as-rolled or mechanically polished niobium. They are comparable with electropolished material, in spite of the much smoother surface of the films.

The work of Easson and Hlawiczka would seem to indicate that the smoother the surface, the higher the field at which losses begin and the more rapidly losses increase with field. The present studies seem to support this view. The 16.1  $\mu\text{m}$  and 24.7  $\mu\text{m}$  films were deposited on highly polished substrates (see fig. 4.4(a), (b)) while the 19.4  $\mu\text{m}$  thick film was deposited on a smooth but unpolished substrate (fig. 4.4(c)). Losses in the 19.4  $\mu\text{m}$  film begin at a lower field and increase, at least initially, less steeply than the other two films. Furthermore, the as-machined niobium cylinder has a rougher surface than the as-machined niobium studied by Easson and Hlawiczka (fig. 4.4(d)); on comparing these two it can be seen that losses in the rougher specimen begin at a very low field and increase

less steeply.

So far, the macrodefects discussed in section 4.2 have not been taken into consideration. It will become apparent from experiments to be described in chapter 6 that, as far as the initial stages of penetration and losses are concerned, pinhole type defects play a more significant part than overall surface roughness.

#### Comparison with Rocher and Septfonds (1967)

They measured losses in outgassed and electropolished niobium with resistance ratio of about 1000 at 4.2 K in a 1kHz field. They found that losses depended strongly on d.c. bias field and on any field present when the specimen was cooled — even the Earth's field being of significance in this respect. Comparisons have been made with their results on a specimen cooled in zero field and subjected to an a.c. field only. Fig. 5.8(b) shows how their results compare with the niobium cylinder machined from bulk. Note that results of Rocher and Septfonds have been adjusted by a factor of 20 to give equivalent losses at 50 Hz (they found mean dissipation to be linear with frequency). Rocher and Septfonds give no quantitative information on their specimen surfaces, but do conclude that surface roughness and trapped flux appear to be the main factors responsible for losses.

Comparison with Buchhold and Rhodenizer (1969)

Their loss measurements were performed on niobium samples with mechanically polished surfaces at 4.2 K in a 300 Hz field. They found losses to be very dependent on the rate of specimen cooling — when cooled slowly to helium temperature losses begin at a low field ; when cooled rapidly to 4.2 K losses begin at a much higher applied field and increase steeply with field. Buchhold and Rhodenizer explain this effect by metallurgical changes in the cold worked surface as the specimen is cooled ; slow cooling introduces surface deformation. In fig. 5.8(b) is reproduced their  $\bar{P}$  versus  $H_{in}$  curve (again corrected to 50 Hz) for a specimen which was cooled to 4.2 K in 30 minutes. This curve is comparable with the sputtered films.

All these results lead to one conclusion — that at low applied fields (near  $H_{c1}$ ) surface topography and surface structure are most important, possibly even the only factor, in determining the onset of losses in niobium under a.c. conditions and the rate at which losses increase with increasing applied field. For this reason it is difficult to compare one set of results with another without detailed knowledge of the specimen surface conditions in each case. Nevertheless the comparisons made above are useful in that they confirm that sputtered niobium behaves basically in the same manner as bulk material. A more detailed discussion of surface

effects is included in chapter 7.

### Losses in tantalum

The  $\bar{P}$  versus  $H_m$  curve for the 23.6  $\mu\text{m}$  tantalum film is given in fig. 5.9. On the same graph are reproduced results from W. I. Dunn (private communication) on an as-machined tantalum specimen at 2.5 K in a 50 Hz field. As with niobium the sputtered material displays behaviour which is qualitatively similar to bulk tantalum. The work on tantalum films was not pursued beyond this stage ; the remainder of this thesis is concerned with niobium only.

### 5.6 Discussion of results

Having discussed loss measurements let us now consider in more detail the significance of other results, particularly the manner of flux penetration into films. First a comment on the lower critical field. Values of  $H_{c1}$  as derived in chapter 4 are given along with  $H_{m1}$  in table 5.1. Except for the 6.45  $\mu\text{m}$  thick film and the as-machined cylinder,  $H_{c1}$  is less than  $H_{m1}$ . As explained earlier  $H_{c1}$  results are expected to be lower than the actual value of  $H_{c1}$  for most of the sputtered layer. Again it will emerge shortly that the lower critical field is not necessarily the main factor which determines the point of initiation of flux penetration into a specimen.

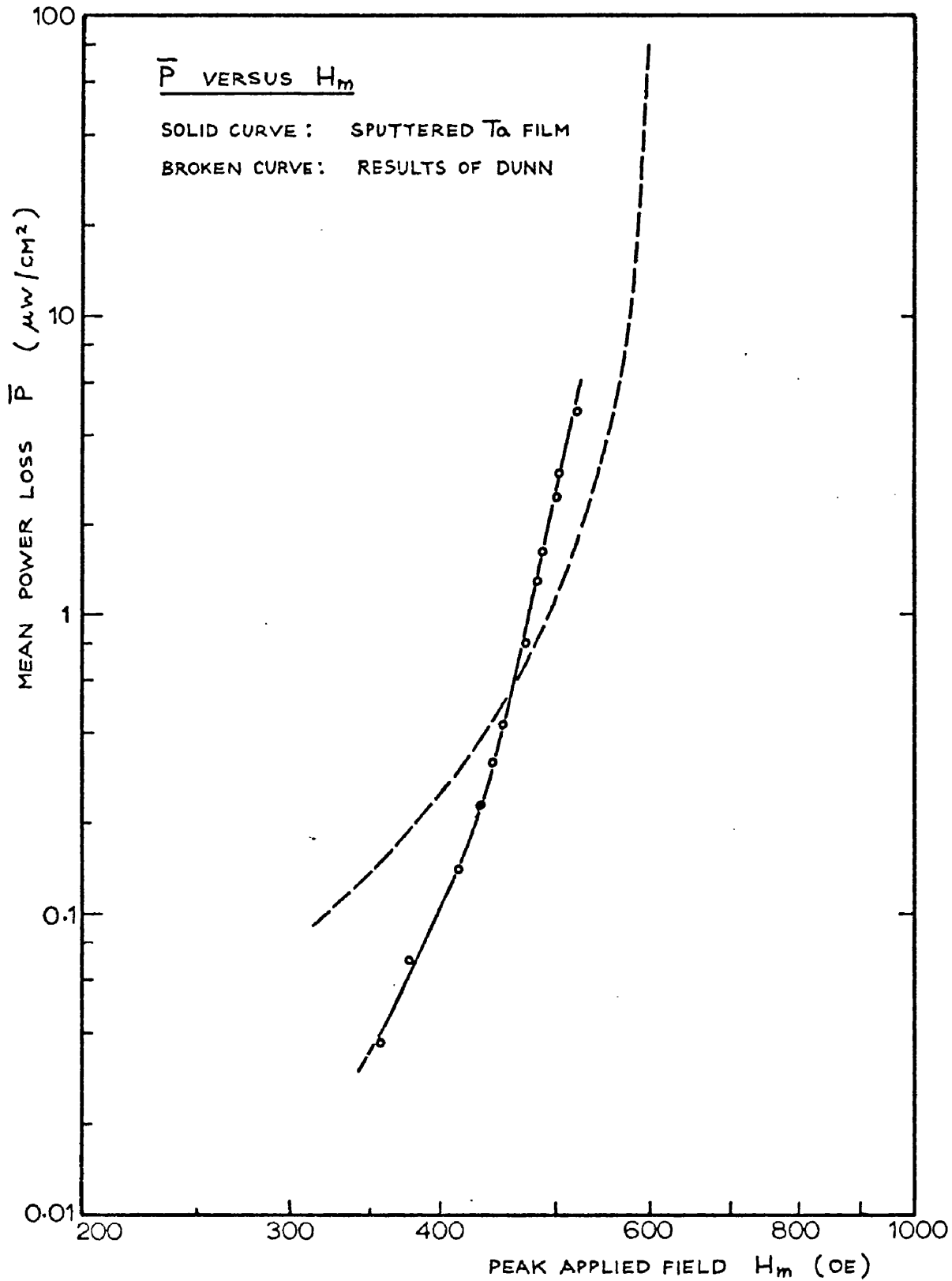


**FIG. 5.9** RESULTS OF LOSS MEASUREMENTS FOR A Ta FILM (NO. 48,  $23.6\mu\text{m}$ ) AND COMPARISON WITH DUNN (UNPUBLISHED).

### Comparisons with critical state model

I shall attempt to interpret results on the basis of the generalized critical state model of Dunn and Hlawiczka (1968). Their model is based on a hysteresis loop of the form shown in fig. 2.7. Two important features are the flat portions around the middle of the applied field cycle and the flat portions at the peaks of applied field. These are caused by flux trapping due to the lower critical field  $H_{cl}$ , and the presence of surface sheath currents which result in flux trapping over the range  $2\Delta H$  at  $\pm H_m$ . The experimental  $\phi - H$  loops reproduced in fig. 5.6 show, to varying degrees, more-or-less flat regions in the middle which suggest flux trapping for applied field roughly in the range  $-H_{cl} < H < H_{cl}$ . But the experimental loops do not have the flat portions at  $\pm H_m$ , which suggests that flux trapping due to surface sheath currents is not present, or at least not fully effective.

### A quantitative comparison

Consider now the total flux  $\phi_m$  which has penetrated into a film cylinder when the magnetic field is at a peak. The peak flux which has penetrated when applied field is  $H_{m2}$  will be designated  $\phi_{m2}$ .  $\phi_{m2}$  is therefore total flux in the film when the flux distribution is such that some flux has just started to penetrate through to the outside. According to the generalized critical state

model the flux distribution within the thickness of the film will be of the form shown in fig. 5.10. The effective applied field at the surface,  $H_e$ , on an increasing half cycle equals  $H = (H_{c1} + \Delta H)$ . The screening field  $\Delta H$  will be ignored and  $H_{c1}$  will be assumed equal to  $H_{m1}$ . The peak effective applied field at the surface  $H_{me}$  is therefore equal to  $H_{m2} - H_{m1}$ . The further assumptions will be made that within the film the flux gradient is constant (Bean-London model) and that flux is distributed uniformly round the circumference of the film cylinder. Having made these assumptions, and using measured values of  $H_{m2}$ ,  $H_{m1}$  and film thickness, it is possible to calculate the total flux  $\phi_{m2}$  which the critical state model predicts should be present within the film. Total flux in the film is directly proportional to area A and is given simply by

$$\phi_{m2} = \frac{1}{2} \cdot H_{me} \cdot w \cdot b \text{ Maxwells}$$

where  $H_{me}$  is in Oersted and w and b are film thickness and cylinder circumference respectively, in centimetres. In the table below are given calculated and experimental values of  $\phi_{m2}$  for the three thickest niobium films.

Film thickness w $\mu\text{m}$	$H_{me}$ (= $H_{m2} - H_{m1}$ ) Oe	Area A Gauss- $\mu\text{m}$	Calculated $\phi_{m2}$ Maxwells	Experimental $\phi_{m2}$ Maxwells
16.1	600	4830	3.5	0.55
19.4	510	4950	3.5	0.14
24.7	450	5500	4.0	0.35

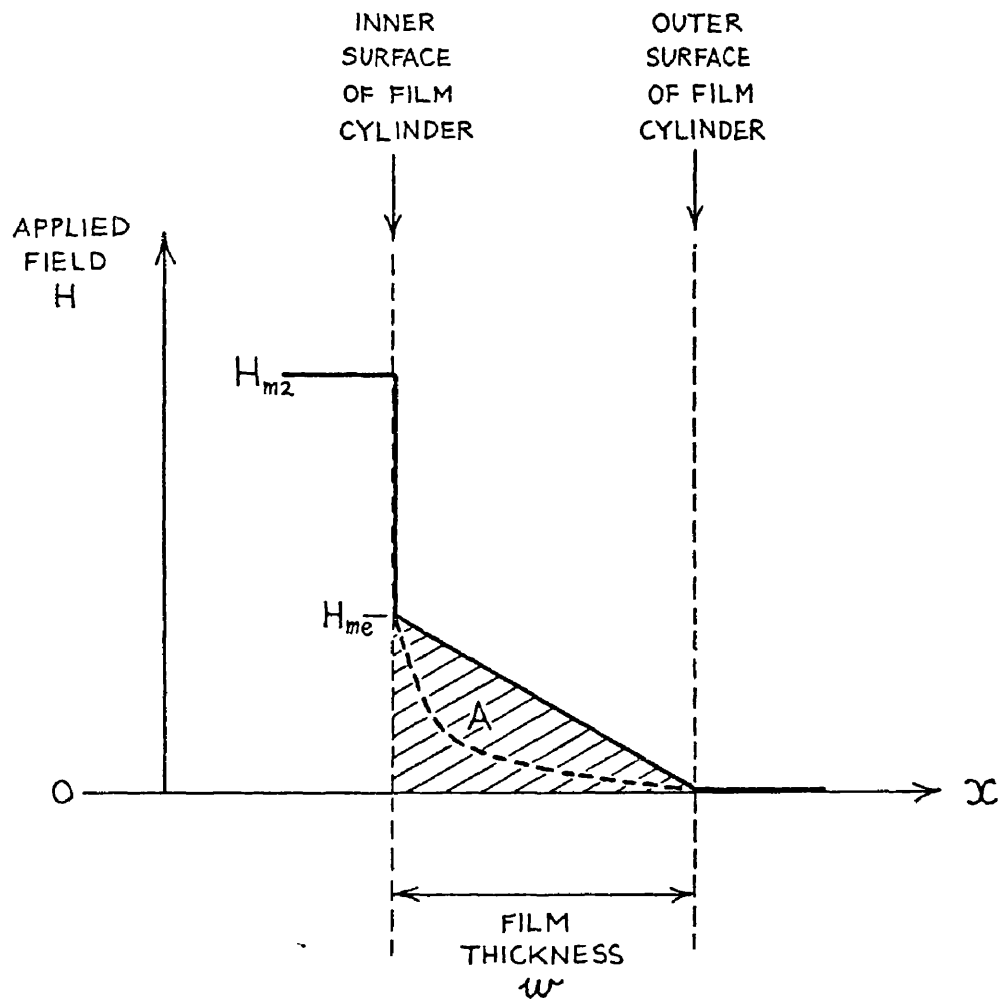


Fig. 5.10 Distribution of flux in film according to critical state model.

Measured results are lower than those calculated on the critical state basis by a factor of roughly ten. In defining the critical current as a function of field (see section 2.5) it is generally accepted that  $J_c$  is constant or a decreasing function of field ; hence the flux density gradient must be constant or increasing with distance in from the surface. So it is extremely unlikely that flux would distribute itself within the film in a manner such as shown by the broken line in fig. 5.10. Furthermore,  $H_{me}$  is not likely to be much less than  $H_{m2} - H_{m1}$ , certainly  $H_{me}$  is unlikely to be low enough to reduce area A by a factor of ten. Only one conclusion it seems can be drawn, namely that the assumption of uniform flux distribution in the film with respect to the circumferential direction is not correct. The calculations suggest that flux penetrates into only about 10% or less of the area of the film being monitored, that is the area under the signal pickup coil.

If the conclusion is correct that flux does not penetrate uniformly over the specimen surface when subjected to a uniform applied field, it clearly has very important implications about the nature of flux penetration. It is especially important to the present work which is concerned with the initial stages of penetration and dissipation. Therefore when this point was reached it was decided to perform some experiments to clarify the processes of flux penetration into and through sputtered cylinders.

CHAPTER 6LOCALIZED FLUX PENETRATION

Calculations at the end of the previous chapter suggest that flux does not penetrate evenly into the film surface, although the applied field is uniform. It was decided to carry out experiments to throw light on the large scale spatial distribution of flux penetration. The experiments consisted of placing pickup coils at various positions round the outside of the film cylinder, applying an a.c. field on the inside, and monitoring the signal from each coil.

The experimental findings presented here are only possible because magnetic field is applied to one side of a thin superconducting layer. The cylinder geometry can be contrasted with the more usual specimen arrangement of a rod in a parallel field, or the slab geometry used by Easson and Hlawiczka (1967) with field applied on both sides of the slab. With rod or slab geometry it would be very difficult to perform experiments to investigate the spatial variation of flux distribution, particularly if penetration is nearly all confined to a thin surface layer.

### 6.1 Variation of flux penetration with respect to axial direction

A test was first carried out to determine how penetration varied with position in an axial direction. This was done chiefly to

verify that flux penetration at the cylinder ends due to field fringing did not induce a signal in the signal pickup coil which was placed close to the film surface at the middle of the cylinder (see section 5.2). Two pickup coils are situated round the outside of the cylinder, one at the middle, the other near one end, as in fig. 6.1, and an a.c. magnetic field is applied to the inside using the niobium solenoid described in chapter 5. The pickup coil voltages are monitored simultaneously.

The experiment was carried out on film 44 (Ta, 8.2  $\mu\text{m}$ ). On increasing a.c. field inside the cylinder it was found that invariably a signal was obtained first from pickup coil A, there being an output from coil B only upon further increasing the field. This indicates that magnetic field penetration right through initiates at the centre of the cylinder, and not at the ends ; it is reasonable to assume that initiation of flux penetration into the film occurs in the same manner. It can thus be concluded that field fringing at cylinder ends does not interfere with the observation of penetration at the centre. This does not mean that fringing does not occur, but simply that the fringing field is weak enough to be trapped near the ends of the cylinder.

## 6.2 Variation of flux penetration with respect to circumferential direction

For this part of the investigation four small identical pickup

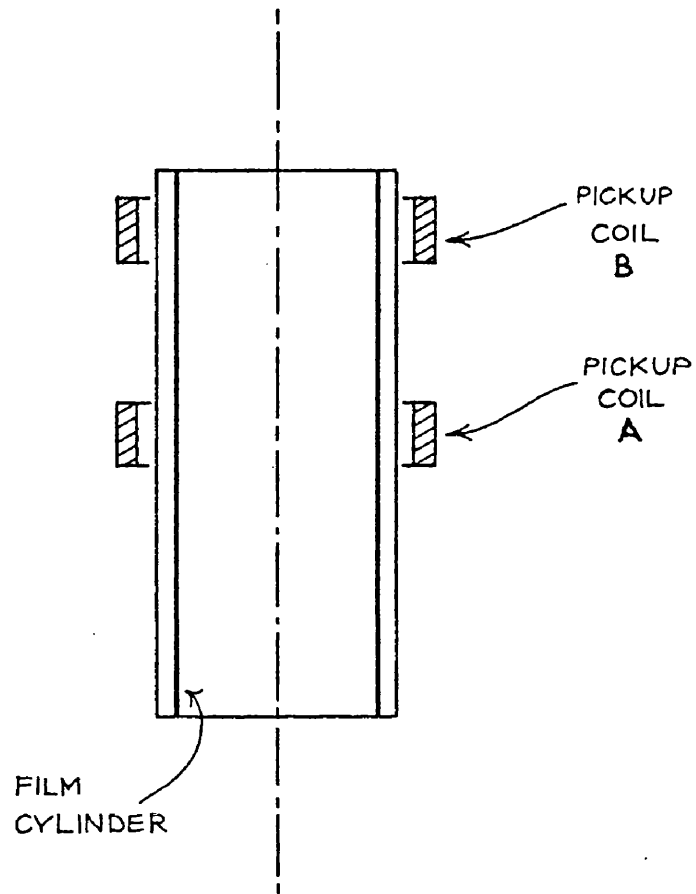


Fig. 6.1 Arrangement of pickup coils to monitor variation of flux penetration with respect to axial direction.

coils were wound, removed from their formers, flattened and curved slightly, and placed round the outside of a film cylinder at the centre position as shown in fig. 6.2. Each coil monitors flux penetrating to the outside over roughly one quadrant of the cylinder. An a.c. field is applied to the inside with the niobium solenoid as in previous experiments. The manner of penetration through to the outside was investigated at 4.2 K on three sputtered niobium cylinders, nos. 45, 49, and 47 (6.5, 10.3, 19.4  $\mu\text{m}$  thick respectively).

Results for film 45 will be discussed in detail. Upon increasing the a.c. magnetic field inside the cylinder, a signal was first detected from pickup coil B at  $H_m = 257$  Oe, and upon further increasing field a signal was obtained from coil A at  $H_m \cong 290$  Oe, from coil C at  $H_m \cong 310$  Oe and from coil D at  $H_m = 372$  Oe. The situation is made clearer by fig. 6.3, an oscilloscope photograph of the signal from each coil at  $H_m = 406$  Oe. Traces at more sensitive settings have a 50 Hz sinewave superimposed upon them ; this is due simply to fringing round the cylinder ends and should be ignored — we are only concerned with the non-sinusoidal peaks which indicate flux penetration through the film at the peaks of each cycle of field inside. The largest signal is from coil B, indicating that most of the flux reaching the outside penetrates through at a region beneath or near coil B. The peaks from coils A and C are much weaker but occupy the same portions of each cycle as coil B peaks, which suggests that signals from A and C are caused by flux

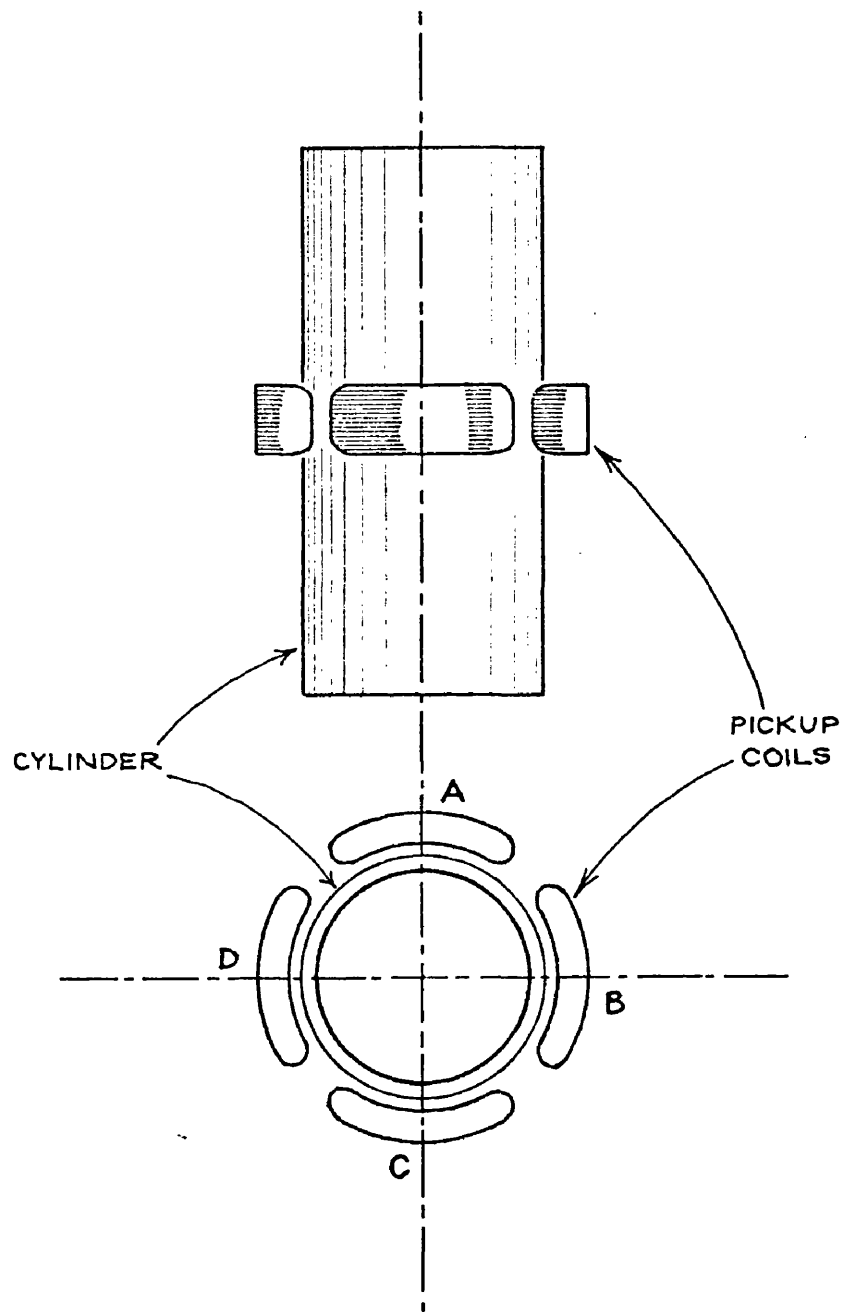


Fig. 6.2 Arrangement of pickup coils to monitor variation of flux penetration with respect to circumferential direction.

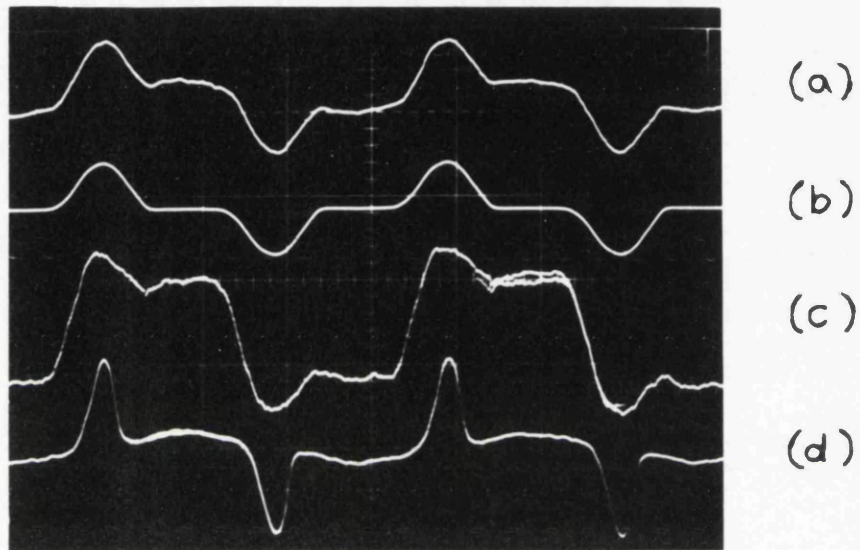


FIG. 6-3

PICKUP COIL SIGNALS AT 406 Oe PEAK  
APPLIED FIELD.      HORIZ : 5 ms/DIV.

- |     |         |        |             |
|-----|---------|--------|-------------|
| (a) | COIL A, | VERT : | 0.1 mV/DIV. |
| (b) | COIL B, | VERT : | 1 mV/DIV.   |
| (c) | COIL C, | VERT : | 0.1 mV/DIV. |
| (d) | COIL D, | VERT : | 0.2 mV/DIV. |

"spreading out" upon penetrating through the region under coil B. It should be noted that the onset of a signal from A or C was not clearly defined, whereas the signal from B first appeared as a sharp peak at a well defined value of  $H_m$ . The output from coil D has the form of sharp peaks which also appeared at a well defined field level, implying the initiation of a second region of flux penetration.

The mode of penetration of magnetic field through the film is therefore as follows : On increasing field no penetration occurs until  $H_m = 257$  Oe, at which point flux begins to come through at the peaks of each cycle over a region near pickup coil B. As  $H_m$  is increased further flux continues to penetrate near B but over an increasing portion of each half-cycle, and is sufficient to produce a signal in coils A and C also. When  $H_m = 372$  Oe a new area of flux penetration appears near coil D. It will again be assumed that the way in which flux penetrates through the film is a true indication of the manner of penetration into the film. The other two niobium films behaved in a similar fashion, although the  $H_m$  at which penetration signals appeared were different.

The above results confirm that it is incorrect to assume uniform flux penetration under conditions of uniform applied field. It would seem, rather, that magnetic flux must enter the specimen preferentially at local "weak spots" or "patches" on the surface,

as shown by the contours of constant flux density in fig. 6.4. The diagram is not meant to portray the actual size or shape of areas of penetration, it is purely to illustrate the concept.

### 6.3 Non-uniform penetration and macrodefects

At the end of chapter 2 the concept of a surface energy barrier was introduced. Bean and Livingston (1964) have shown theoretically that when a uniform parallel field is applied to a perfectly smooth surface of type II superconductor, flux penetration into the surface and the associated nucleation of flux lines may be delayed until a field  $H_s$  considerably in excess of  $H_{c1}$ . But surface irregularities may create local fields equal to  $H_s$  when average applied field is relatively low. It has been verified experimentally by De Blois and De Sorbo (1964) that a plane smooth surface **does indeed act as** a nucleation barrier, and that roughening the surface permits flux penetration near  $H_{c1}$ .

The pinholes and similar large scale defects described in chapter 4 will almost certainly act as irregularities at which localized flux penetration may take place. It is not that the surface barrier is necessarily weakened or absent at defects, but that their geometrical shape causes local field enhancement. If macroscopic imperfections in the films are of the form suggested in chapter 4 then applied field will be enhanced at the edges of the holes or depressions, and penetration will first occur there. A possible

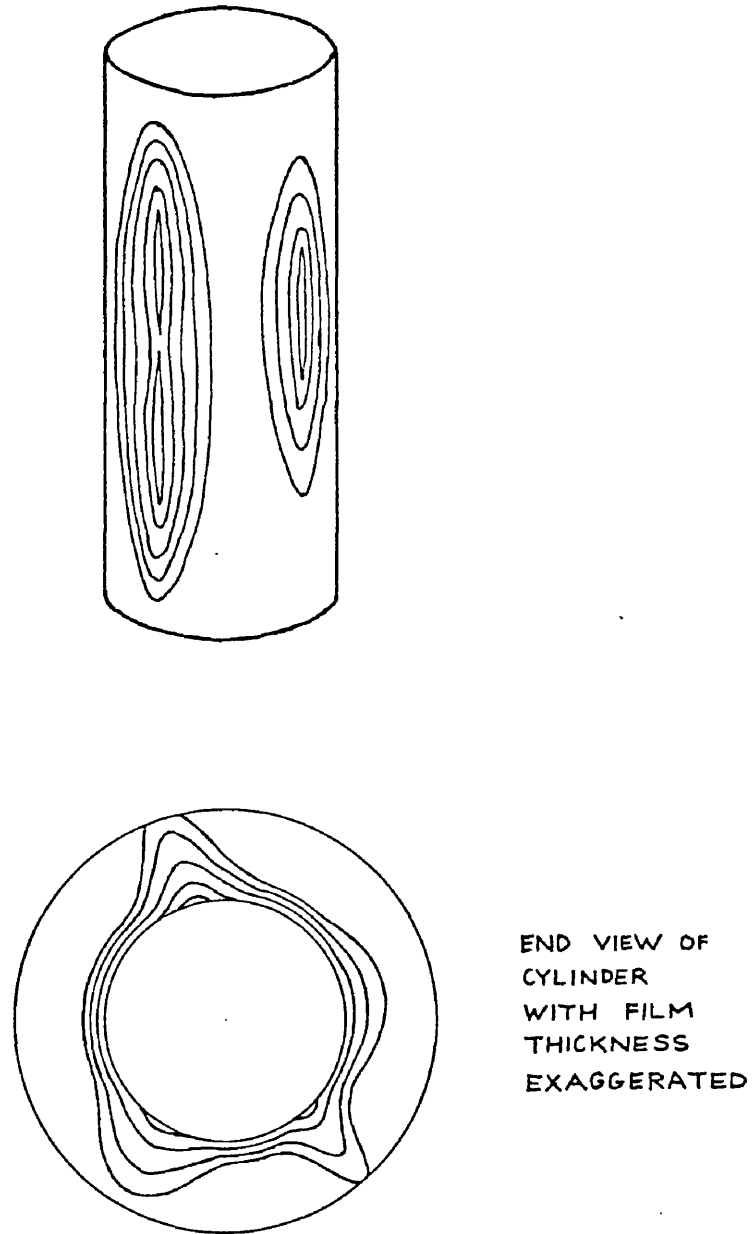


Fig. 6.4 Contours of constant flux density in a film cylinder, illustrating possible manner of non-uniform flux penetration.

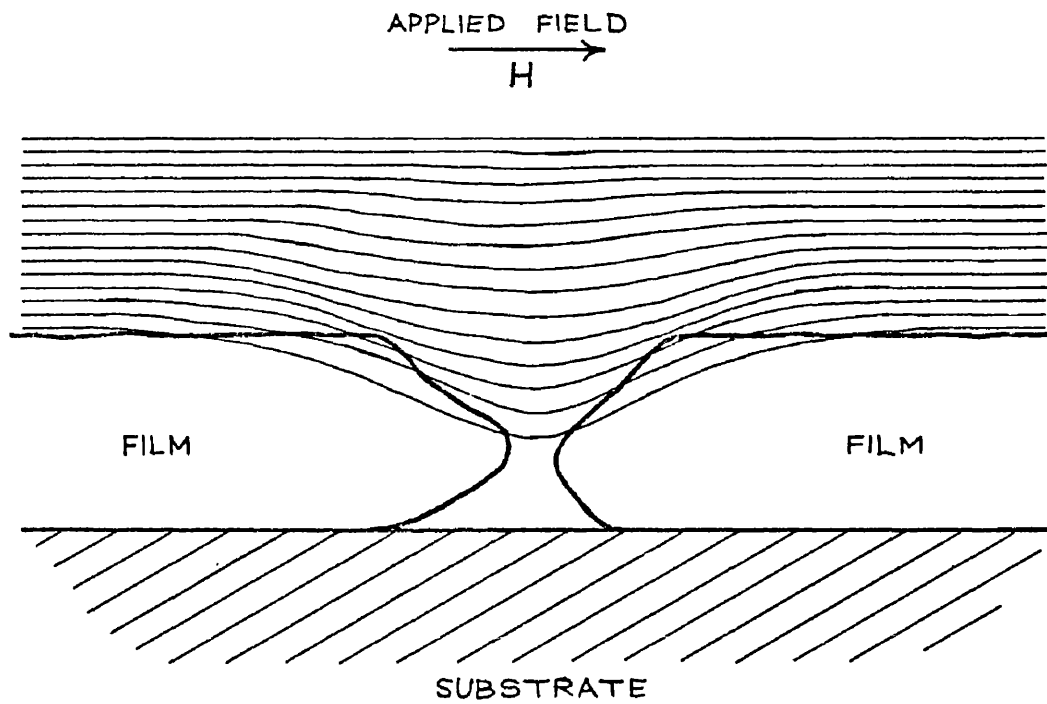


Fig. 6.5 Magnetic field streamlines at a macrodefect in a film, illustrating initiation of flux penetration.

manner of flux penetration at a defect is illustrated by fig. 6.5. Once flux lines have nucleated they will move according to the mechanisms described in chapter 2 until they become pinned, either within the body of the film or at the surface where they emerge. From the point of view of the experimental work it is possible that only very few of the defects dominate flux penetration behaviour of the whole cylinder ; e.g. the total measured flux  $\phi_m$  which has entered a film cylinder could be due to penetration at one defect.

There is no direct evidence that flux penetrates preferentially at the defects of section 4.2. However, there is no other obvious explanation for observed behaviour, and there is one piece of indirect evidence. Of films examined, those 10.3  $\mu\text{m}$  thick or less had pinholes going right through, and in all films 10.3  $\mu\text{m}$  thick or less penetration right through the cylinder to the outside takes place as soon as penetration into the film begins (i.e.  $H_{m2} = H_{m1}$ ). On the other hand, no holes could be found in the 18.1  $\mu\text{m}$  film (i.e. the film was continuous, although there were **macrodefects** on the surface), and for all films greater than 16.1  $\mu\text{m}$  thick flux does not appear at the outer surface until peak field is increased above the level which causes penetration into the film (i.e.  $H_{m2} > H_{m1}$ ). It would be desirable if this correlation could be confirmed by studying more specimens ; nevertheless it does lend support to the proposition that the defects are the point of initiation of flux penetration.

The relevance of these findings on the detailed manner of magnetic field penetration will be discussed in the next chapter.

CHAPTER 7DISCUSSION AND CONCLUSIONS

It has been demonstrated that magnetic flux penetrates non-uniformly into the film surface, most probably because of macroscopic defects in the film. The effect must obviously dominate the field screening properties of the sputtered cylinders, and the implications of localized flux penetration must be borne in mind when considering results presented in chapter 5. One thing is quite clear — that critical state models cannot be used to explain properties of films with macrodefects. In view of the manner of flux penetration a qualitative approach only is possible.

7.1 Effect of surface on penetration and losses

Before discussing the sputtered films it will be helpful to consider various effects which can take place at the surface of a superconductor, and which influence magnetization. Broadly speaking, three surface effects can be distinguished, although it is probable that in an actual specimen any separately identifiable surface phenomena are in fact inter-related.

(a) Energy barrier

First, there is the surface energy barrier of Bean and Livingston

(1964), De Blois and De Sorbo (1964) and others. This has been dealt with already in section 2.5, where it was explained that flux line nucleation and penetration into a type II superconductor may be delayed until the applied field is increased to a level  $H_s$  in excess of  $H_{cl}$ .

(b) Surface topography

The second factor which must be considered is the detailed surface shape, i.e. surface topography or roughness. The geometrical shape of a rough surface can cause localized field enhancement, so that at peaks on the surface the effective field is greater than the average applied field. A rough surface would thus be expected to reduce the field for initiation of flux penetration below the above mentioned value  $H_s$ , and may even permit some penetration below  $H_{cl}$ . Unless the material is almost completely free of microdefects it is likely that flux trapping will occur on or near a rough surface. Flippen (1967) has performed experiments on niobium which demonstrate that magnetic behaviour associated with the surface is explained by flux trapping at defects on or near the surface, which results in hysteresis. There has been very little work on the quantitative relationship between surface topography and flux penetration. It is probable that both the actual and relative values of vertical and horizontal components of roughness and their "spatial bandwidth" are of significance.

(c) Surface microstructure

The third factor which will influence behaviour at the surface is microscopic structure of the surface itself and the layer immediately below. The amount of impurities and deformation and their distribution with respect to distance perpendicular to the surface will affect specimen magnetization. Consider the effect of heavily cold working a surface, by polishing for instance. The high dislocation density will reduce mean free path and hence  $H_{cl}$  at the surface, permitting flux penetration into the surface layer to begin at a lower field. But by reason of the deformation the surface layer can now support a high critical surface current which may screen the bulk of the specimen to a field level in excess of the bulk  $H_{cl}$ .

The magnetization curves in fig. 7.1 explain this effect more clearly. The diagram shows the reversible M-H curve for a defect free type II specimen, and the virgin curve after the surface has been heavily deformed. The series of papers by Schweitzer, Bertman and Garber referred to in section 2.5 present experimental work on hysteresis in type II superconductors in which results are explained by critical surface currents. Theoretical and experimental studies by Fink and Barnes (1965) and Barnes and Fink (1966) have also shown that persistent currents can be induced in a multiply connected surface sheath, and that the magnitude of critical sheath current is extremely sensitive to surface state of the specimen.

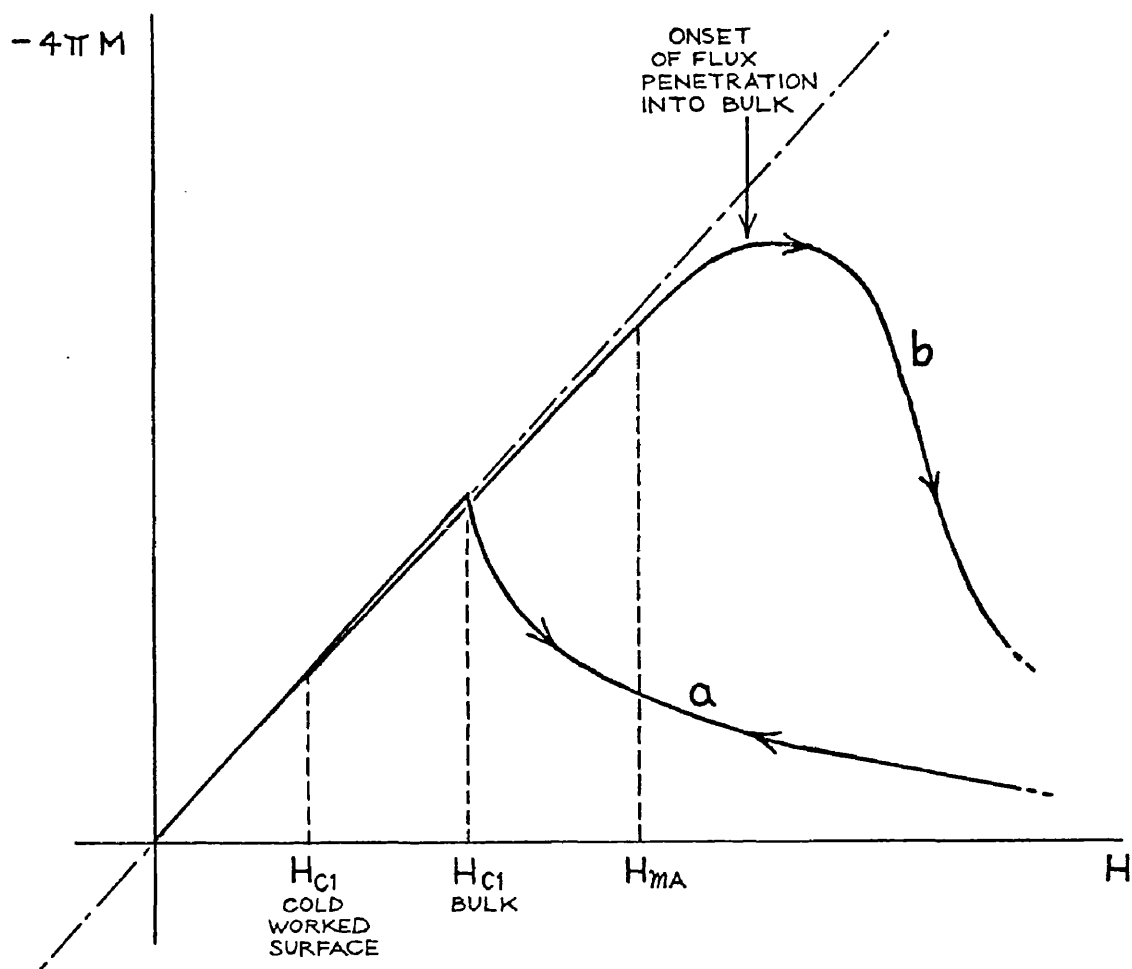


Fig. 7.1 Magnetization curves for a type II specimen.

- (a) Defect free.
- (b) With cold worked surface layer.

Now the region of the magnetization curve below  $H_{c1}$  in a type II superconductor (or below  $H_c$  in type I) is called the Meissner State. Screening of the bulk of a specimen by induced surface currents, so that flux does not enter the bulk until a field in excess of  $H_{c1}$  ( or  $H_c$  in the case of type I), has been termed by Seebold (1969) the enhanced Meissner State. Seebold has discussed the possibility of utilizing the effect in superconductors for a.c. applications. Although dissipation must occur in the very irreversible surface layer, it is possible that losses at a given field level, such as at  $H_{mA}$  in fig. 7.1, may be lower in a specimen with a severely cold worked surface than in one which is relatively pure and strain free throughout.

The three surface phenomena described above have the common feature that flux trapping occurs at or near the surface, with consequent hysteresis in magnetization and power dissipation. The surface effects (b) and (c) can be illustrated from the loss measurements of Easson and Hlawiczka (1968) which are included in fig. 5.8 (a). First, for as-machined niobium losses begin at a low applied field and increase relatively slowly with increasing  $H_m$ . Electropolishing does not improve surface roughness much (see section 5.5), but presumably does remove the cold worked material introduced by machining. Losses now begin at higher  $H_m$  and increase more rapidly with field, so that at higher field levels they exceed losses in as-machined material.

Mechanically polished and as-rolled specimens have much improved surface smoothness with an associated heavily cold worked layer (although as-rolled foils will be cold worked right through). The enhanced Meissner effect now comes into play. Although penetration into the surface must begin at a relatively low applied field, losses are below the detection limit (which for measurements of Eason and Hlawiczka was  $1 \mu\text{W}/\text{cm}^2$ ) until an  $H_m$  level appreciably in excess of that for electropolished material ; losses then increase very steeply with field. Since the as-machined specimen has a cold worked surface layer it might also be expected to exhibit the enhanced Meissner effect ; presumably in this case surface roughness dominates as far as penetration and losses are concerned. These comments help to make the point that the degree of surface deformation, the surface topography, and their inter-relation, affect the onset of losses and the manner in which they increase with peak applied field.

## 7.2 Surface effects and sputtered films

What is the significance of the surface phenomena discussed above as regards magnetization properties of sputtered niobium films ? The surface energy barrier (a) may be of significance as far as films are concerned ; there is no way of determining from results presented in this thesis whether or not it is an important factor. As the films have been subjected to at most 1% deformation, the effects of cold work on the surface layer will be negligible (see section 4.4).

Therefore (c), the enhanced Meissner effect, probably plays no part in determining the manner of flux penetration into the films.

It is most likely that surface topography, discussed under (b), is the factor which to a large extent determines behaviour of the sputtered films. As has been explained in section 6.3 pinholes and similar large scale defects will act as irregularities at which localized flux penetration may take place, the process being illustrated in fig. 6.5. The macrodefects behave as local "rough" areas on the surface which, by reason of their shape, cause localized field enhancement. Hence the applied field for initial penetration is less than  $H_s$  (if there is a surface energy barrier effect), and possibly less than  $H_{cl}$ .

Now macrodefects are present to the extent of approximately 3 per  $\text{cm}^2$ ; there must therefore be relatively large areas of film between defects where the surface is relatively smooth, as shown by the Talysurf traces of fig. 4.4. It is reasonable to assume that at such areas the applied field does not enter irreversibly, but rather penetrates reversibly to the London depth only. In chapter 5 results of loss measurements are presented as mean dissipation per unit area of film surface. However, since on the above assumption irreversible penetration occurs only over a small fraction of the surface — perhaps something like 1% to 10% of the film area to which field is applied — loss results can be considered to apply only to such a fraction. Then loss per unit area where power is actually dissipated will be greater by one or two orders of magnitude than the  $\bar{P}$  values indicated by

fig. 5.7 (a).

In section 6.3 I touched on the actual mechanism of power dissipation. When flux lines have nucleated and entered at a defect they will move in accordance with the mechanisms of vortex motion described in section 2.4 until they become pinned, either within the body of the film or at the points where they emerge from the surface. As explained in section 2.4 pinning is caused by microscopic structural defects which, through local changes in superconducting parameters, produce localized regions where flux lines may have higher or lower free energy. A flux line will be pinned at a local free energy minimum. Energy loss as heat results from viscous flow of flux lines between pinning centres.

If the explanations of film behaviour in this section are valid it appears that macrodefects (pinholes and depressions) provide regions of easy flux line nucleation and penetration, and microdefects (dislocations, impurities, etc.) act as pinning sites for flux vortices once they have nucleated.

It is clear from the foregoing discussion that magnetic behaviour of the sputtered films is dominated by the relatively large pinhole defects and depressions described in section 4.2. To improve the field screening properties the most important step is to eliminate macrodefects. Means of achieving this have been considered in chapter 4.

It should be noted that if there were no pinholes there would be no need to make the films more than a few penetration depths in thickness, say  $\sim 1 \mu\text{m}$ . If macroscopic defects could be eliminated what remaining surface finish would be required? It is very unlikely that a practical system would be designed to operate in the surface energy barrier region above  $H_{c1}$  as this region is unstable; so the surface would only have to be smooth enough to prevent appreciable penetration below  $H_{c1}$ . Although Easson and Hlawiczka (1968) do relate the onset of losses to the surface finish, their results are qualitative, and are somewhat confused by the effects of cold work which are also present. So just what constitutes an acceptable surface is not at all clear — further experimental work on this point would be desirable.

If large scale defects are eliminated and the surface is sufficiently smooth the films should be loss free up to  $H_{c1}$ , or just below  $H_{c1}$ . To attain high  $H_{c1}$  the niobium deposit must be as pure and strain free as possible. This, however, raises the possibility of utilizing the enhanced Meissner State as described in section 7.1. It is probably impracticable to do so, since an extreme degree of deformation would be required, more than could be readily introduced into the surface of a sputtered deposit. Thus the statement that the aim is as pure and strain free a niobium film as possible is still valid. Improvements in film preparation which could help in achieving this aim are discussed in section 7.4.

### 7.3 Relation of results to a practical cable system

To put the work on sputtered niobium into perspective, I shall briefly consider its significance from the viewpoint of a superconducting a.c. power transmission cable. Numerous feasibility studies of cable systems have been undertaken (Cairns et al, 1969, lists a number of references), and a certain amount of experimental work on conductors for superconducting cables has been carried out (Rogers et al, 1969). In the introductory chapter it was explained that a practical arrangement would consist of a twin tube conductor assembly, or a multi-tube assembly, or an all coaxial conductor assembly. Whichever is used, the field is present on only one side of the superconducting layer. I shall confine my remarks to the twin coaxial tube assembly shown in fig. 1.3, and assume operation at 4.2 K.

It is obviously most important to attain as high a surface screening current density as possible in the conductor tubes, and maximum screening current density depends on the field  $H_m$  at which losses become significant. A significant loss level must therefore be defined. Power loss in a superconducting cable under normal operating conditions of  $1 \mu\text{W}/\text{cm}^2$  or less is preferred, while  $10 \mu\text{W}/\text{cm}^2$  is considered to be an upper limit (Taylor, 1969). If  $1 \mu\text{W}/\text{cm}^2$  is taken as an acceptable loss level, the two thickest sputtered niobium films ( $19.4 \mu\text{m}$  and  $24.7 \mu\text{m}$  thick) could be used

with peak surface field  $H_m$  of just over 1000 Oe at 4.2 K.

Now there are indications that a 2000 MVA superconducting cable could be competitive with conventional underground cables, and that such a cable could be operated at an interphase voltage of 33 kV (Taylor, 1969). The current per phase is then 35 kA r.m.s. or 50 kA peak, so the peak current carried by one inner conductor tube is 25 kA. If the current carrying layers were to consist of sputtered niobium having loss behaviour similar to the thickest films prepared as described in chapter 3, then as shown above the maximum surface field would be  $\sim 1000$  Oe peak. The corresponding surface current is 80 A/mm, which gives an inner conductor diameter of 100 mm. If the niobium film was pure and defect free the cable could be operated at a peak surface field of 1400 Oe, just below  $H_{c1}$  for pure material, which would require an inner conductor diameter of only 71 mm.

#### 7.4 Suggestions for further work

Future studies along the lines of work presented here should have the following aims:

- To eliminate pinholes and associated large scale defects;
- To study effects of surface topography on flux penetration and losses ;

To determine the applicability or otherwise of critical state models in predicting the manner of flux penetration ;

To prepare films of higher purity — either by sputtering or by other methods.

Suggestions for avoiding the occurrence of macrodefects have been given in section 4.2, where the point was made that it is most important to exclude as far as possible particulate matter such as dust from the sputtering system. Clean room facilities would no doubt help in this respect. It was also suggested that ion bombardment of the substrate — either before deposition or, by using a more sophisticated sputtering technique, during deposition — would perhaps remove any remaining contaminating matter. As has been mentioned, if macrodefects can be eliminated it should not be necessary to make the niobium deposit more than a few penetration depths in thickness.

If films can be prepared which are free of macroscopic defects it will then be possible to investigate the effect of surface roughness on the onset of flux penetration and losses and their field dependence. It should be possible to determine what is an acceptable surface finish for a given application. When defects which provide points of flux line nucleation and penetration have been completely eliminated, then upon increasing applied field above  $H_{c1}$

the magnetic field should penetrate uniformly into the sputtered layer. Under such conditions it should be possible to determine whether or not the manner of flux penetration can be explained by a critical state model. Specifically, one could measure the total flux which has penetrated into the film when the flux distribution is such that it has just reached the outer surface of the film cylinder, as shown in fig. 5.10. As explained in section 5.6 this quantity is designated  $\phi_{m2}$ , and the associated peak applied field is  $H_{m2}$ . By determining  $\phi_{m2}$  and  $H_{m2}$  as a function of film thickness it should be possible to derive the shape of the flux density profile within the film.

It is clearly desirable to attempt to improve film purity so that the lower critical field  $H_{c1}$  approaches the value for pure, defect free niobium. The precautions suggested in section 4.2 to eliminate dust particles will to a certain extent reduce contamination from gases such as oxygen, nitrogen and hydrogen. Additional steps that could be taken to reduce the quantity of gaseous interstitial impurities in the niobium deposit are —

use a vacuum system capable of a lower ultimate pressure ;

bake out the system at a higher temperature and deposit the film with the substrate at a higher temperature ;

use purer argon for the sputtering atmosphere ;

alter sputtering conditions to give a factor deposition rate.

It would be worth investigating these possibilities in the course of any future work.

Finally, there are two methods of preparing niobium deposits other than sputtering which could be considered. The first has been used by Karasik et al (1968) and consists of precipitating niobium from  $\text{NbCl}_5$  in the vapour phase. Karasik et al used extremely pure  $\text{NbCl}_5$  and subjected the deposit to prolonged outgassing near the melting point at a pressure of  $5 \times 10^{-11}$  torr. They obtained very pure niobium which exhibited ideal type II behaviour. The second method is the electrolytic deposition technique of Mellors and Senderoff (1965) which was mentioned in chapter 3. They have obtained coherent, dense deposits of niobium by electrolysis of niobium salts dissolved in a bath of molten alkali fluorides. Meyerhoff (1969) claims that subsequent vacuum outgassing of the electroplated niobium for 100 hours at about  $2100^\circ\text{C}$  and at a pressure of  $10^{-8}$  torr results in an extremely pure product which shows almost complete magnetic reversibility and which also has a very smooth surface finish. The electroplating and heat treatment process has the advantage that it appears to have been developed to an advanced stage, having in fact already been used in some applications.

REFERENCES

- Abrikosov, A.A., (1957) Soviet Phys. JETP, 5, 1174.
- Altman, C., (1962) Trans. 9th National Vacuum Symposium, p.174,  
Pergamon Press, New York, 1963.
- Anderson, P.W., (1962) Phys. Rev. Letters, 9, 309
- Anderson, P.W., and Kim, Y.B., (1964) Rev. Mod. Phys., 36, 39.
- Asada, Y., and Nose, H., (1969) J. Phys. Soc. Japan, 26, 347.
- Bardeen, J., and Stephen, M.J., (1965) Phys. Rev., 140, A1197
- Barnes, L.J., and Fink, H.J., (1966) Phys. Rev., 149, 186.
- Bean, C.P., (1964) Rev. Mod. Phys., 36, 31.
- Bean, C.P., and Livingston, J.D., (1964) Phys. Rev., 12, 14.
- Berry, R.W., Hall, P.M., and Harris, M.T., (1968) "Thin Film  
Technology", van Nostrand, Princeton, N.J.
- Bertman, B., Schweitzer, D.G., and Lipschultz, F.P., (1966)  
Phys. Letters, 21, 260.
- Buchhold, T.A., (1963) Cryogenics, 3, 141.
- Buchhold, T.A., and Rhodenizer, R.L., (1969) IEEE Trans.  
Magnetics, MAG-5, 429.
- Budnick, J.I., (1960) Phys. Rev., 119, 1578.
- Cairns, D.N.H., Minors, R.H., Norris, W.T., and Swift, D.A.,  
(1969) Paper read at Conference on Low Temperatures  
and Electric Power, London, March 1969.
- Campbell, D.S., (1966) Proc. IERE-IEE conference on Applications  
of Thin Films in Electronic Engineering, London, July 1966,  
Supp. Vol., paper 35.
- De Blois, R.W., and De Sorbo, W., (1964) Phys. Rev. Letters, 12,  
499.
- De Sorbo, W., (1963) Phys. Rev., 132, 107.

- Dunn, W.I., and Hlawiczka, P., (1968) Brit. J. Appl. Phys. Ser. 2, 1, 1469.
- Easson, R.M., (1967) Ph.D. Thesis, University of Glasgow.
- Easson, R.M., and Hlawiczka, P., (1967) Brit. J. Appl. Phys., 18, 1237.
- Easson, R.M., and Hlawiczka, P., (1968) Brit. J. Appl. Phys. Ser. 2, 1, 1477.
- Fink, H.J., and Barnes, L.J., (1965) Phys. Rev. Letters, 15, 792.
- Flippen, R.B., (1967) Phys. Letters, 24A, 588.
- French, R.A., (1968) Cryogenics, 8, 301.
- Friedel, J., de Gennes, P.G., and Matricon, J., (1963) Appl. Phys. Letters, 2, 119.
- de Gennes, P.G., (1966) "Superconductivity of Metals and Alloys", Benjamin, New York.
- Gor'kov, L.P., (1959) Soviet Phys. JETP, 9, 1364.
- Green, I.M., and Hlawiczka, P., (1967) Proc. Instn. Elect. Engrs., 114, 1329.
- Hlawiczka, P., and Ross, J.M., (1968) Brit. J. Appl. Phys. Ser. 2, 1, 995.
- Holland, L., (1956) "Vacuum Deposition of Thin Films", Chapman and Hall, London.
- Irie, F., and Yamafuji, K., (1967) J. Phys. Soc. Japan, 23, 255.
- Jorgenson, G.V., and Wehner, G.K., (1963) Trans. 10th National Vacuum Symposium, p.388, Pergamon Press, New York, 1964.
- Joseph, A.S., and Tomasch, W.J., (1964) Phys. Rev. Letters, 12, 219.
- Karasik, V.R., et al (1968) JETP Letters, 8, 294.
- Kim, Y.B., Hempstead, C.F., and Strnad, A.R., (1962) Phys. Rev. Letters, 9, 306.
- Kim, Y.B., Hempstead, C.F., and Strnad, A.R., (1963a) Phys. Rev., 129, 528.
- Kim, Y.B., Hempstead, C.F., and Strnad, A.R., (1963b) Phys. Rev., 131, 2486.

- Kim, Y.B., Hempstead, C.F., and Strnad, A.R., (1964) Rev. Mod. Phys., 36, 43.
- Kim, Y.B., Hempstead, C.F., and Strnad, A.R., (1965) Phys. Rev., 139, A1163.
- Kusayanagi, E., and Yamafuji, K., (1969) Phys. Letters, 29A, 529.
- Livingston, J.D., and Schadler, H.W., (1964) General Electric Report No. 64-RL-3765M, Sept. 1964, Schenectady, N.Y.
- London, H., (1963) Phys. Letters, 6, 162.
- London, H., and Clarke, G.R., (1964) Rev. Mod. Phys., 36, 320.
- Lowell, J., (1965) Cryogenics, 5, 185.
- Lynton, E.A., (1964) "Superconductivity", Methuen, London.
- Maissel, L.I., (1962) Trans. 9th National Vacuum Symposium, p.169, Pergamon Press, New York, 1963.
- Maissel, L.I., (1966) "Physics of Thin Films", (Eds: G.Hass and R.E. Thun) vol. 3, p.61, Academic Press, New York.
- Maki, K., (1964) Physics, 1, 127.
- Maki, K., (1966) Phys. Rev., 148, 362.
- McEvoy, J.P., (1964) RCA Review, 25, 533.
- McEvoy, J.P., Jones, D.P., and Park, J.G., (1969) Phys. Rev. Letters, 22, 229.
- Mellors, G.W., and Senderoff, S., (1965) J. Electrochem. Soc., 112, 266.
- Meyerhoff, R.W., (1969) J. Appl. Phys., 40, 2011.
- Miller, G.L., (1959) "Tantalum and Niobium", Butterworths, London.
- Narlikar, A.V., and Dew-Hughes, D., (1966) J. Materials Sci., 1, 317.
- Neugebauer, C.A., and Ekvall, R.A., (1964) J. Appl. Phys., 35, 547.
- Newhouse, V.L., (1964) "Applied Superconductivity", Wiley, New York.
- Parks, R.D. (Editor), (1969) "Superconductivity", Dekker, New York.

- Rocher, Y.A., and Septfonds, J., (1967) *Cryogenics*, 7, 96.
- Rogers, E.C., Cave, E.C., and Grigsby, R., (1969) Paper read at Conference on Low Temperatures and Electric Power, London, March 1969.
- Rose-Innes, A.C., (1964) "Low Temperature Techniques", English Universities Press, London.
- Ross, J., (1968) Ph.D. Thesis, University of Glasgow.
- Saint-James, D., and de Gennes, P.G., (1963) *Phys. Letters*, 7, 306.
- Scharnhorst, P., (1969) *Surface Sci.*, 15, 380.
- Schweitzer, D.G., (1967) *Phys. Letters*, 24A, 718.
- Schweitzer, D.G., (1968) *Phys. Rev.*, 173, 461.
- Schweitzer, D.G., and Bertman, B., (1966 a) *Phys. Letters*, 20, 263.
- Schweitzer, D.G., and Bertman, B., (1966 b) *Phys. Letters*, 20, 339.
- Schweitzer, D.G., and Bertman, B., (1966 c) *Phys. Letters*, 22, 361.
- Schweitzer, D.G., and Garber, M., (1967 a) *Phys. Rev. Letters*, 18, 206.
- Schweitzer, D.G., and Garber, M., (1967 b) *Phys. Rev.*, 160, 348.
- Seebold, R.J.A., (1969) Ministry of Technology Contract, Final Report, Aug. 1969.
- Seraphim, D.P., Novick, D.T., and Budnick, J.I., (1961) *Acta Metallurgica*, 9, 446.
- Sosniak, J., (1968) *J. Appl. Phys.*, 39, 4157.
- Sosniak, J., and Hull, G.W., (1967) *J. Appl. Phys.*, 38, 4390.
- Taylor, M.T., (1969) Paper read at Conference on Low Temperatures and Electric Power, London, March 1969.
- Tewordt, L., and Neumann, L., (1966) *Z. Phys.*, 189, 55.
- Theuerer, H.C., and Hauser, J.J., (1964) *J. Appl. Phys.*, 35, 554.
- Tinkham, M., (1964) *Phys. Rev. Letters*, 13, 804.

van Vijfeijken, A.G., and Niessen, A.K., (1965) Philips Res. Rep.,  
20, 505.

Vinen, W.F., and Warren, A.C., (1967) Proc. Phys. Soc., 91, 409.

Vratny, F., (1967) J. Electrochem. Soc., 114, 505.

Vratny, F., and Harrington, D.J., (1965) J. Electrochem. Soc.,  
112, 484.

FLUX PENETRATION AND A.C. LOSSES  
IN SUPERCONDUCTING NIOBIUM  
AND TANTALUM FILMS

A Thesis

presented to the Faculty of Engineering  
of the University of Glasgow  
for the degree of

Doctor of Philosophy

by

Kenneth A.M. Arton, B.Sc.

May, 1970

v

SUMMARY

The penetration of magnetic flux into superconducting niobium and tantalum films, deposited by sputtering on the inside of cylindrical substrates, has been monitored under conditions of an a.c. magnetic field applied parallel to the film surface. The energy dissipation associated with irreversible flux motion in the film has been measured, and an attempt has been made to explain results on the basis of critical state models.

Niobium and tantalum films were prepared by sputtering with a d.c. glow discharge in an argon atmosphere. A cylindrical geometry was adopted to deposit films on the inner surface of cylindrical substrates, and the gettering action of the sputtered niobium or tantalum was utilized to obtain a pure deposit at the substrate. Films up to 1  $\mu\text{m}$  thick were deposited on quartz cylinders, and films from 3  $\mu\text{m}$  to 25  $\mu\text{m}$  thick were sputtered onto copper or stainless steel. To obtain a measure of purity the critical temperatures of tantalum films have been obtained,  $T_c$  values indicating a gaseous impurity content of typically 0.2 at.%.  $H_{c2}$  has been measured approximately for some thick niobium films, the results indicating kappa values of about 5, corresponding to about 1 at.% of dissolved gaseous impurities.

A 50 Hz a.c. field was applied to one side only of the film cylinders by means of a solenoid positioned co-axially inside, the solenoid being shorter than the cylinder to reduce the effects of field fringing at the ends. Flux penetration into the film was monitored with a pickup coil in close proximity to the film surface in conjunction with a compensation system to remove unwanted pickup. Losses in the film were measured by means of an electronic wattmeter technique. Mean power loss and peak flux penetration for niobium films from 16  $\mu\text{m}$  to 25  $\mu\text{m}$  thick have been obtained at 4.2 K as a function of peak applied field, and comparative measurements have been made on a thick sputtered tantalum film and on a specimen machined from bulk niobium. The results have been compared with other work on a.c. losses in niobium.

It was found that flux penetration and loss results cannot be readily explained by any critical state model. More detailed study of the manner of flux penetration revealed that the magnetic field penetrates preferentially at localized areas on the film surface, and that this behaviour dominates to such an extent that critical state concepts are not applicable. Examination of the films under optical microscope revealed the presence of relatively large scale defects (macrodefects) having a size of the order of several microns and being similar in structure to pinholes. It is concluded that such defects cause localized non-uniform flux penetration by acting as sites for flux line nucleation and penetration into the film.

Causes of macrodefects and means of eliminating them are discussed, and the work has been related to a possible practical superconducting a.c. power cable system.